TECHNICAL REPORT STANDARD TITLE PAGE

1. Report No.	2. Government Accession No.	3. Recipient's Catalog No.
FHWA/TX-86/ 37 +346-1F		

4. Title and Subtitle	5. Report Date
Roadside Concrete Barriers: Warrants and End Treatment	November 1985
	6. Performing Organization Code
7. Author(s)	8. Performing Organization Report No.
Dean L. Sicking and Hayes E. Ross, Jr.	Research Report 346-1F
9. Performing Organization Name and Address Texas Transportation Institute The Texas A&M University System College Station, Texas 77843	10. Work Unit No.
	11. Contract or Grant No. Study No. 2-8-83-346
12. Sponsoring Agency Name and Address Texas State Department of Highways and Public Transportation: Transportation Planning Division P. O. Box 5051 Austin, Texas 78763	13. Type of Report and Period Covered Final - September 1982 November 1985
	14. Sponsoring Agency Code

15. Supplementary Notes
Research performed in cooperation with DOT, FHWA.
Research Study Title: Concrete Safety Shaped Barrier for Roadside Application

16. Abstract

The primary emphasis of this research was the development of a low-maintenance end treatment to shield the end of a concrete safety shaped barrier. It consists of a series of energy-absorbing rubber cylinders that are reusable after an impact. The cylinders are supported by steel diaphragms, and the thrie-beam fender panels are used for redirection purposes. The design was shown to meet recommended impact performance standards through a series of full-scale crash tests. Further, costs and labor to restore the treatment after most impacts will be considerably less than any other operational end treatment.

Guidelines were also developed to identify roadway and traffic conditions where the concrete safety shaped barrier is warranted in lieu of standard W-beam roadside guardrail.

17. Key Words	18. Distribution Statement
End Treatment, Crash Cushion, Traffic Barrier, Concrete, Crash Test	No restriction. This document is available to the public through the National Technical Information Service 5285 Port Royal Road Springfield, Virginia 22161

19. Security Classif. (of this report)	20. Security Classif. (of this page)	21. No. of Pages	22. Price
Unclassified	Unclassified	192	

Form DOT F 1700.7 (8-69)

ROADSIDE CONCRETE BARRIERS:

WARRANTS AND END TREATMENT

by

Dean L. Sicking
Assistant Research Engineer

and

Hayes E. Ross, Jr.
Research Engineer

Research Report 346-1F
on
Research Study No. 2-8-83-346
Concrete Safety Shaped Barrier for Roadside Application

Sponsored by

Texas State Department of Highways and Public Transportation

in cooperation with

The U. S. Department of Transportation
Federal Highway Administration

November 1985

Texas Transportation Institute
The Texas A&M University System
College Station, Texas

METRIC CONVERSION FACTORS

Approximate Conversions to Metric Measures

Symbol	When You Know	Multiply by	To Find	Symbol
	LENGTH			
in	inches	*2.5	centimeters	cm
ft	feet	30	centimeters	cm
yd	yards	0.9	meters	m
mi	miles	1.6	kilometers	km
	AREA			
in^2	square inches	6.5	square centimeters	cm^2
ft^2	square feet	0.09	square meters	m^2
yd^2	square yards	0.8	square meters	m^2
mi^2	square miles	2.6	square kilometers	km^2
	acres	0.4	hectares	ha
	MASS (weight)			
oz	ounces	28	grams	g
lb	pounds	0.45	kilograms	kg
	short tons (2000 lb)	0.9	tonnes	t
	VOLUME			
tsp	teaspoons	5	milliliters	ml
Tbsp	tablespoons	15	milliliters	ml
fl oz	fluid ounces	30	milliliters	ml
c	cups	0.24	liters	l
pt	pints	0.47	liters	l
qt	quarts	0.95	liters	l
gal	gallons	3.8	liters	l
ft^3	cubic feet	0.03	cubic meters	m^3
yd^3	cubic yards	0.76	cubic meters	m^3
	TEMPERATURE (exact)			
°F	Fahrenheit temperature	5/9 (after subtracting 32)	Celsius temperature	°C

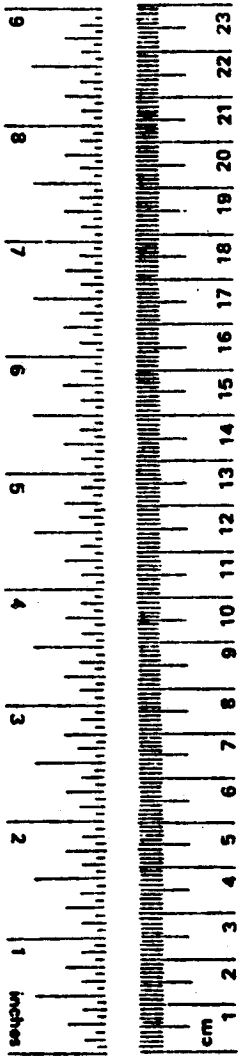

*1 in = 2.54 (exactly). For other exact conversions and more detailed tables, see NBS Misc. Publ. 286, Units of Weights and Measures, Price $2.25, SD Catalog No. C13.10:286.

Approximate Conversions from Metric Measures

Symbol	When You Know	Multiply by	To Find	Symbol
	LENGTH			
mm	millimeters	0.04	inches	in
cm	centimeters	0.4	inches	in
m	meters	3.3	feet	ft
m	meters	1.1	yards	yd
km	kilometers	0.6	miles	mi
	AREA			
cm^2	square centimeters	0.16	square inches	in^2
m^2	square meters	1.2	square yards	yd^2
km^2	square kilometers	0.4	square miles	mi^2
ha	hectares (10,000 m^2)	2.5	acres	
	MASS (weight)			
g	grams	0.035	ounces	oz
kg	kilograms	2.2	pounds	lb
t	tonnes (1000 kg)	1.1	short tons	
	VOLUME			
ml	milliliters	0.03	fluid ounces	fl oz
l	liters	2.1	pints	pt
l	liters	1.06	quarts	qt
l	liters	0.26	gallons	gal
m^3	cubic meters	35	cubic feet	ft^3
m^3	cubic meters	1.3	cubic yards	yd^3
	TEMPERATURE (exact)			
°C	Celsius temperature	9/5 (then add 32)	Fahrenheit temperature	°F

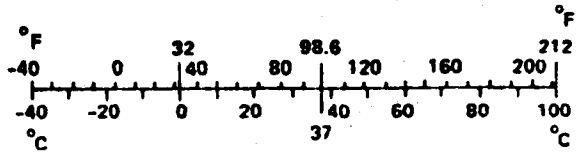

DISCLAIMER

The contents of this report reflect the views of the authors, who are responsible for the opinions, findings and conclusions presented herein. The contents do not necessarily reflect the official views or policies of the Texas State Department of Highways and Public Transportation or the Federal Highway Administration. This report does not constitute a standard, specification, or regulation.

KEY WORDS

End Treatment, Crash Cushion, Traffic Barrier, Concrete, Crash Test

ACKNOWLEDGMENTS

This research study was conducted under a cooperative program between the Texas Transportation Institute (TTI), the Texas State Department of Highways and Public Transportation (SDHPT), and the Federal Highway Administration (FHWA). Mr. Harold Cooner of the SDHPT worked closely with the researchers, and his comments and suggestions were appreciated.

ABSTRACT

The primary emphasis of this research was the development of a low-maintenance end treatment to shield the end of a concrete safety shaped barrier. It consists of a series of energy-absorbing rubber cylinders that are reusable after an impact. The cylinders are supported by steel diaphrams, and thrie-beam fender panels are used for redirection purposes. The design was shown to meet recommended impact performance standards through a series of full-scale crash tests. Costs and labor to restore the treatment after most impacts will be considerably less than any other operational end treatment.

Guidelines were also developed to identify roadway and traffic conditions where the concrete safety shaped barrier is warranted in lieu of standard W-beam roadside guardrail.

TABLE OF CONTENTS

		Page
I	INTRODUCTION	1
II	GUIDELINES FOR USE OF CONCRETE SAFETY SHAPED BARRIER	2
	A. CSSB Versus Metal Beam Barrier	2
	B. Foundation Requirements	13
III	DEVELOPMENT OF AN END TREATMENT	15
	A. Research Approach	15
	B. Lab Testing of Candidate Materials	15
	C. Design of Prototype Crash Cushion	25
IV	FULL-SCALE CRASH TESTS	40
	A. Preliminary Testing	40
	B. NCHRP 230 Compliance Testing	48
V	CONCLUSIONS & RECOMMENDATIONS	58
VI	REFERENCES	59

LIST OF FIGURES

FIGURE		PAGE
1.	BARRIER APPLICATION FOR DEVELOPMENT OF GUIDELINES FOR CONCRETE BARRIER USE ON THE ROADSIDE	3
2.	CSSB BARRIER IMPACT SEVERITY	6
3.	W-BEAM GUARDRAIL IMPACT SEVERITY	7
4.	LONGITUDINAL BARRIER REPAIR COSTS	8
5.	SOCIETAL COSTS VERSUS IMPACT SEVERITY	9
6.	GUIDELINES FOR CONCRETE BARRIER USE ON THE ROADSIDE	10
7.	GUIDELINES FOR END TREATMENT OF RIGID ROADSIDE BARRIERS	12
8.	CONCRETE BARRIER PLACEMENT RECOMMENDATIONS	14
9.	FOAM SAMPLES TESTED FOR USED IN LOW MAINTENANCE CRASH CUSHION END TREATMENT	16
10.	RUBBER SHAPES USED IN PRELIMINARY TESTING	17
11.	ULTRAVIOLET RADIATION TEST DEVICE	19
12.	SCALE MODEL DYNAMIC TEST FIXTURE	23
13.	IMPACT ENERGY ABSORBED BY FULL SCALE RUBBER CYLINDERS	28
14.	DYNAMIC TESTS OF FULL SCALE RUBBER CYLINDERS	31
15.	CONSTRUCTION DRAWINGS OF FINAL END TREATMENT DESIGN	33
16.	PHOTOGRAPHS OF PROTOTYPE LOW MAINTENANCE END TREATMENT	37
17.	TEST VEHICLE DAMAGE FROM TEST 1, 30 MPH IMPACT	41
18.	END TREATMENT AFTER TEST 1	42
19.	END TREATMENT AND TEST VEHICLE AFTER TEST 2, 40 MPH IMPACT	43
20.	VEHICLE DAMAGE AFTER TEST 3	44
21.	LOW MAINTENANCE END TREATMENT AFTER TEST 3	46
22.	SUMMARY OF TEST 3	47
23.	VEHICLE AND END TREATMENT DAMAGE AFTER TEST 4	49
24.	SUMMARY OF TEST 4	50
25.	SUMMARY OF TEST 5	51

LIST OF FIGURES
(CONTINUED)

FIGURE		PAGE
26.	TEST VEHICLE AND END TREATMENT AFTER TEST 5	53
27.	SUMMARY OF TEST 6	54
28.	LOW MAINTENANCE END TREATMENT AFTER TEST 6	55
29.	TEST VEHICLE DAMAGE AFTER TEST 6	57

LIST OF TABLES

TABLE		PAGE
1.	BARRIER BENEFIT/COST ANALYSIS DATA.	5
2.	END TREATMENT BENEFIT/COST ANALYSIS DATA.	11
3.	SCALE MODEL RUBBER CYLINDERS.	22
4.	TOTAL ENERGY ABSORBED BY MODEL RUBBER CYLINDERS	24
5.	ENERGY ATTRIBUTABLE TO INTERNAL DAMPING	26
6.	RATIO BETWEEN DAMPING AND STATIC ENERGY DISSIPATION	27
7.	MATERIAL SPECIFICATIONS FOR NATURAL RUBBER A.	30
8.	ENERGY ABSORPTION PROPERTIES OF FULL-SCALE RUBBER CYLINDERS	32
9.	PREDICTED OCCUPANT IMPACT VELOCITIES FOR 60 MPH HEAD-ON IMPACTS . .	39
10.	SUMMARY OF CRASH TEST RESULTS	45

I. INTRODUCTION

Maintenance of traffic barriers on heavily traveled freeways is a major problem for transportation agencies. Barriers are impacted frequently and require a large and costly maintenance effort. Repair of barriers on such facilities interrupts traffic flow, causing delays and increasing the potential for accidents that endanger both the motorists and repair crews. In recognition of these problems, highway engineers have successfully replaced many metal beam median barriers with the almost maintenance-free concrete safety shaped barrier (CSSB).

In recent years, interest in the use of the concrete barrier for roadside applications has grown. However, use of the CSSB for such applications introduces problems different from those present in median applications, including the determinination of how the rigid barrier should be terminated, where it should be used, and what type of foundation is necessary.

Foremost of the problems associated with the use of the CSSB on the roadside is the manner in which the barrier is terminated. When left exposed and untreated, the end of a rigid barrier is a severe hazard. Efforts to mitigate this problem have included the use of crash cushions, sloped ends, flared ends, ends buried in an earth berm or a backslope, and transitions to W-beam guardrail which is then terminated with a breakaway cable terminal or a turned-down end. All of these safety treatments present some safety and/or maintenance problems.

Although the crash cushion is probably the safest CSSB end treatment in use, crash cushion maintenance can be very costly. Existing crash cushions use expendable energy absorbing elements to attenuate head-on impacts. Every head-on impact destroys one or more of the energy absorbing elements. Labor and materials to replace damaged elements are costly, and for those end treatments that are impacted frequently, repair costs during the life of a crash cushion can be much greater than initial costs.

Another problem associated with the use of the CSSB on the roadside is the absence of objective guidelines for barrier selection and deployment. Most studies pertaining to the need for roadside barriers have been limited to the analysis of whether or not a barrier should be used, with little or no consideration for the type of barrier to be used. Although Calcote (1) did develop a procedure for determining the most beneficial roadside barrier to be used at any site, the analysis was limited to flexible barriers.

The study reported herein was undertaken to address (1) the development of guidelines for use of the CSSB on the roadside, and (2) the development of a low-maintenance end treatment for the CSSB.

II. GUIDELINES FOR USE OF CONCRETE SAFETY SHAPED BARRIER

A. CSSB Versus Metal Beam Barrier

Although the CSSB requires virtually no maintenance, metal beam guardrail has a lower initial cost and is generally less severe to impact than the CSSB. Therefore the metal beam roadside barrier is more cost beneficial at low traffic volumes due to the low impact frequency, and the CSSB is more cost beneficial at high traffic volumes. Currently a W-beam barrier on round wood posts is used for most roadside barrier applications in Texas. Thus, the primary objective of this phase of the study was to use a benefit/cost (B/C) analysis to determine conditions under which each barrier should be used on the roadside.

The B/C methodology compares the benefits derived from a safety improvement to the direct highway agency costs incurred as a result of the improvement. Benefits are measured in terms of reductions in societal costs due to decreases in the number and/or severity of accidents. Direct highway agency costs are comprised of initial, maintenance, and repair costs of a proposed improvement. A ratio between benefits and costs of an improvement is used to determine if the improvement is more cost-beneficial as shown below:

$$B/C_{2-1} = \frac{SC_1 - SC_2}{DC_2 - DC_1}$$

where:

B/C_{2-1} = benefit/cost ratio of alternative 1 compared to 2,

SC_i = societal cost of alternative i, and

DC_i = direct cost of alternative i.

Alternative 1 is the baseline option, i.e. the W-beam guardrail, and alternative 2 is the CSSB. The CSSB is preferred when the benefit/cost ratio becomes greater than 1.0. Note that this analysis is based on the assumption that a W-beam barrier is warranted.

Estimation of Benefits and Costs

Most benefits and some costs associated with a safety treatment must be estimated through predictions of accident frequency and severity. A comprehensive B/C algorithm utilizing an encroachment probability model was selected for use in this study (2). This model represents a significant improvement over most other B/C techniques in that accident severities are linked to predicted impact conditions, and impact conditions are estimated from real-world accident conditions. The reader should refer to Appendix IV for more detailed documentation of the B/C procedure.

The general approach to this study was to first study the benefits of barrier use without including the effects of the ends and to later evaluate available end treatments. Guidelines for barrier use were developed for a barrier application as shown in Figure 1. The 1000 ft. length was chosen

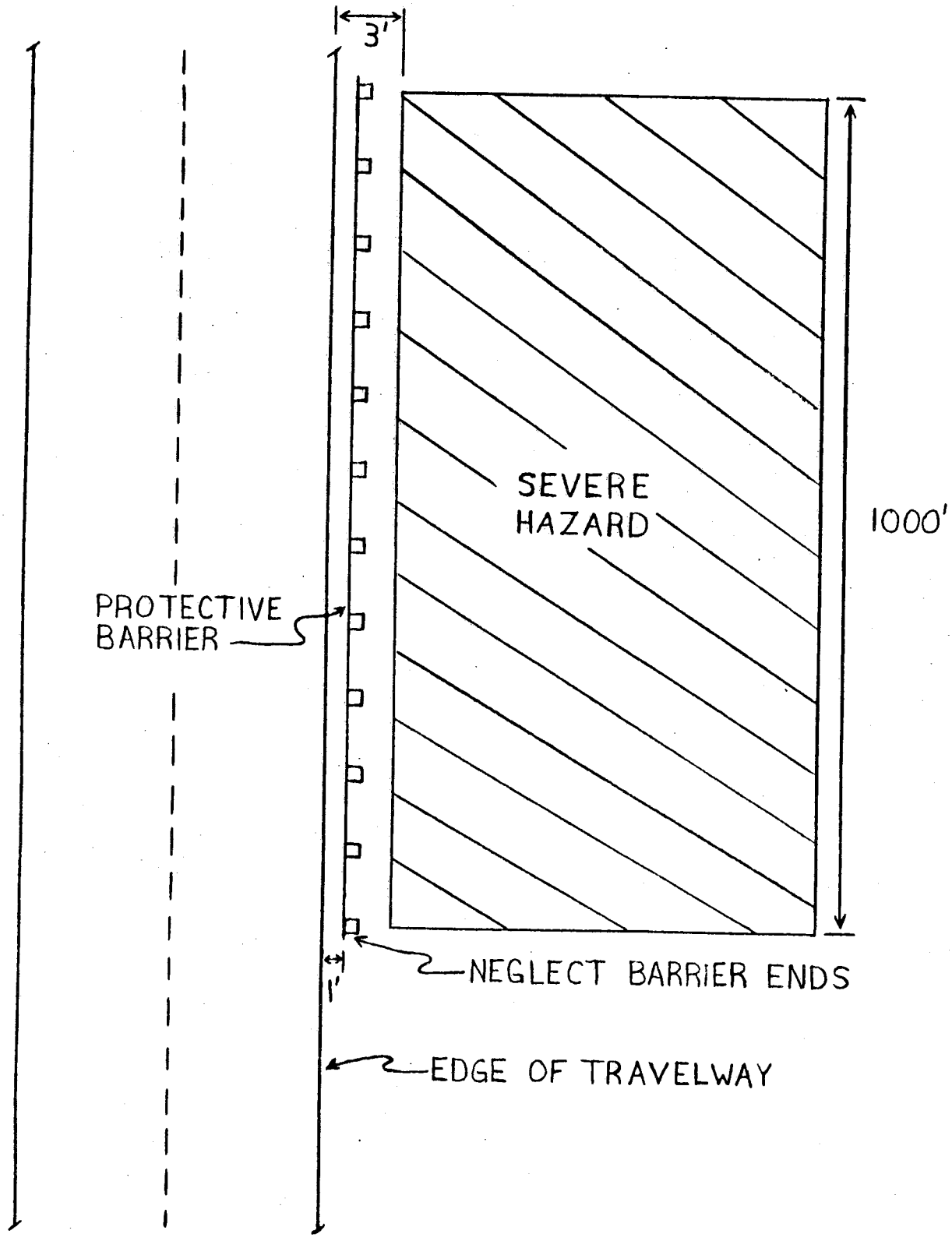

FIGURE 1 BARRIER APPLICATION FOR DEVELOPMENT OF GUIDELINES FOR CONCRETE BARRIER USE ON THE ROADSIDE

primarily for computational purposes and to eliminate the effects of barrier end treatments in the analysis. Therefore, this analysis is based on the assumption that the benefits and costs associated with a barrier system are relatively insensitive to the length of the barrier. A limited sensitivity analysis indicated that the this assumption is true for most reasonable barrier lengths. All other factors being the same, the CSSB tends to be slightly less cost beneficial as barrier length decreases. It should also be noted that the B/C analysis contained herein was conducted for freeway applications only and is not applicable to other types of highways.

The B/C algorithm requires input data regarding basic roadside feature dimensions and costs, severity of impact with roadside features, cost of repairing the features, and impact conditions under which safety devices can be expected to perform acceptably. Much of the necessary barrier cost data, shown in Table 1, was obtained from the Texas State Department of Highways and Public Transportation (SDHPT). Impact severity and repair cost data, shown in Figures 2, 3, and 4, was estimated from crash test data as described in references 2 and 3. A linear relationship was assumed between the severity index of an accident and the velocity of impact. Note that this does not imply a linear relationship between severity of impact and impact speed since, as shown in Figure 5, severity index is not linearly related to accident costs.

Guidelines for concrete safety shaped barrier use on the roadside are shown in Figure 6. This figure shows that CSSB use on the roadside is not cost beneficial until traffic volumes reach approximately 40,000 ADT. Therefore, it can be concluded that CSSB use on the roadside is cost beneficial only on urban freeways since rural freeways typically have larger barrier offsets and lower traffic volumes.

Note that barrier use guidelines shown in Figure 6 recommend the use of CSSB barriers as much as 30 feet from the traveled way. Earlier studies have discouraged the deployment of rigid barriers more than 15 feet from the traveled way. Early recommendations were based on expectations that impact angles would increase significantly as a barrier is moved further from the roadway. More recent accident studies indicate that changes in impact angle with barrier offset may not be as great as once believed (17) and that this question may merit further evaluation.

Three different barrier end treatments -- 1) transition to W-beam with "Texas Twist" terminal; 2) TREND, a proprietary terminal (18); and 3) a low maintenance rubber end treatment -- were then evaluated to determine traffic and site conditions where each system is most cost beneficial. Table 2 shows estimated cost, severity, and performance information for each of these end treatments. Data shown in Table 2 was obtained from supplier estimates and crash test results.

Guidelines for use of the three end treatments, shown in Figure 7, were then developed in a manner similar to guidelines for rigid barrier use on the roadside. As shown in this figure, the TREND first becomes cost beneficial at traffic volumes of 23000 ADT, and the higher cost rubber crash cushion terminal is not cost beneficial below 50000 ADT.

All traffic volumes shown in Figures 6 and 7 include traffic on both sides of the roadway, even though roadside barriers on urban freeways are

Table 1. Barrier Benefit/Cost Analysis Data

	W-Beam Guardrail	Concrete Barrier
Barrier Cost ($/ft)	12.50	27.50
Performance Level (kip-ft)		
2000 lb Vehicle	48	48
4500 lb Vehicle	97	97
12800 lb Vehicle	97	161
55000 lb Vehicle	97	200
Severity Index for Impacts Above P.L.	7.5	7.5
Barrier Life (years)	20	20
Discount Rate (%)	4	4
Functional Highway Class	Freeway	Freeway

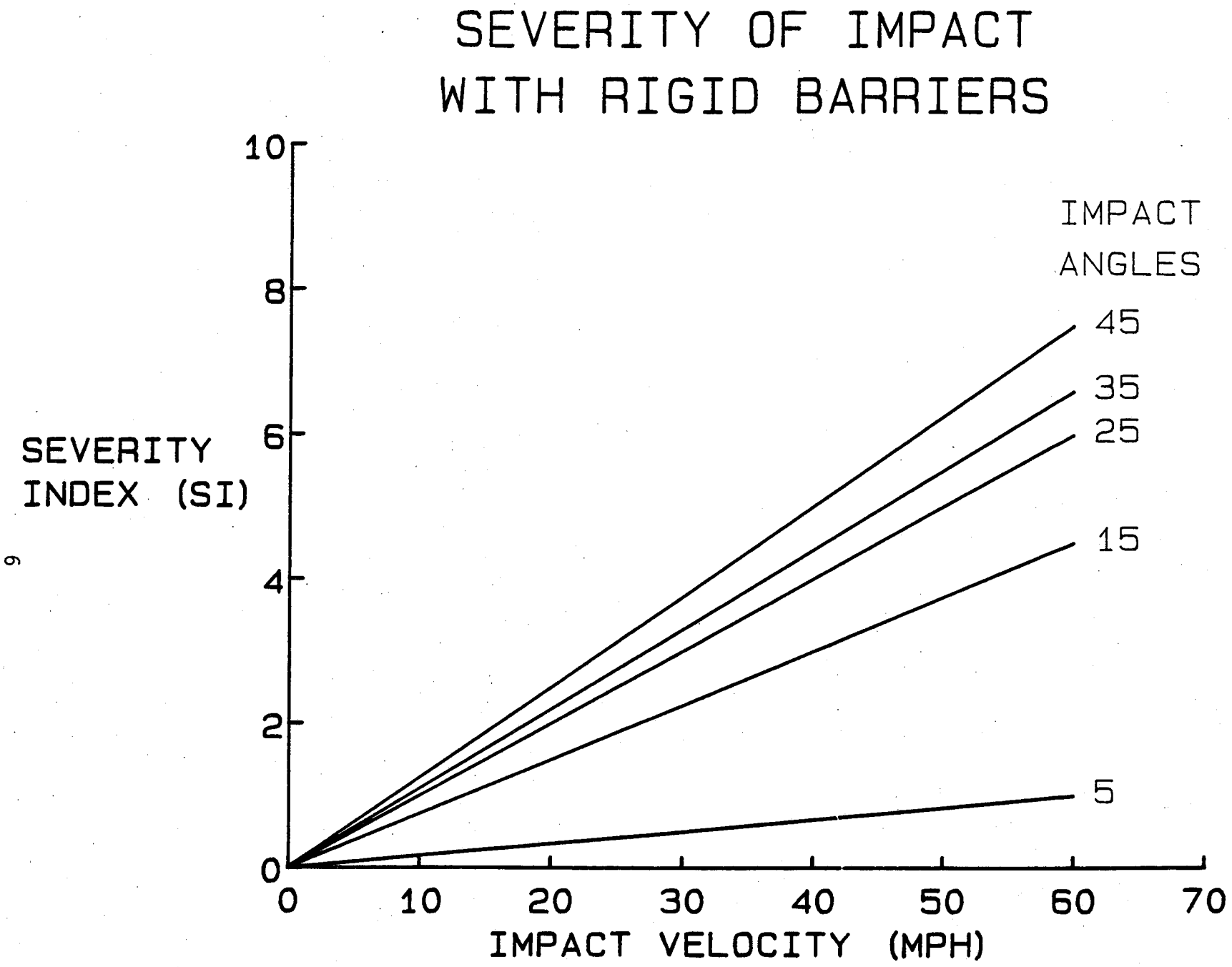

FIGURE 2. CSSB BARRIER IMPACT SEVERITY

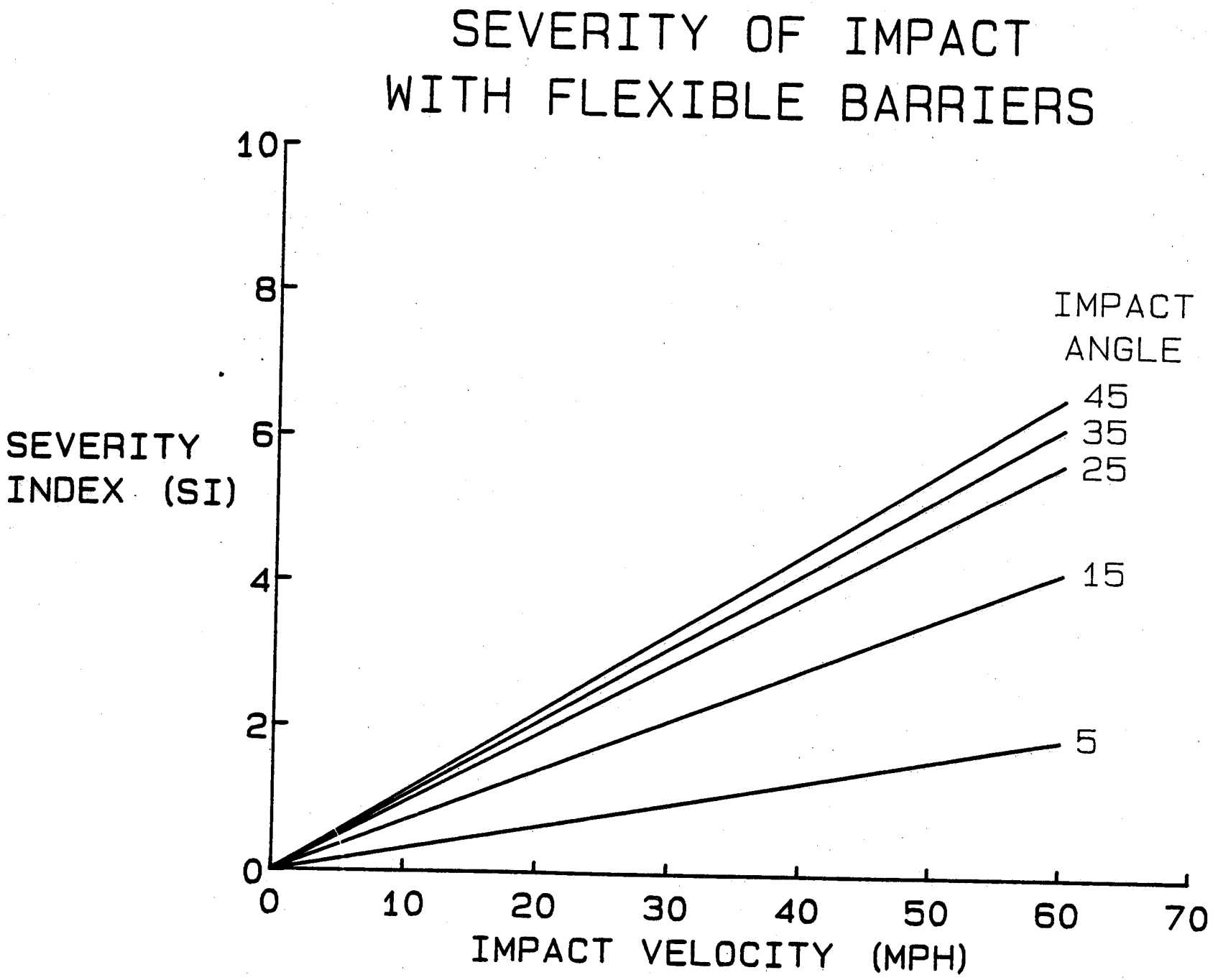

FIGURE 3. W-BEAM GUARDRAIL IMPACT SEVERITY

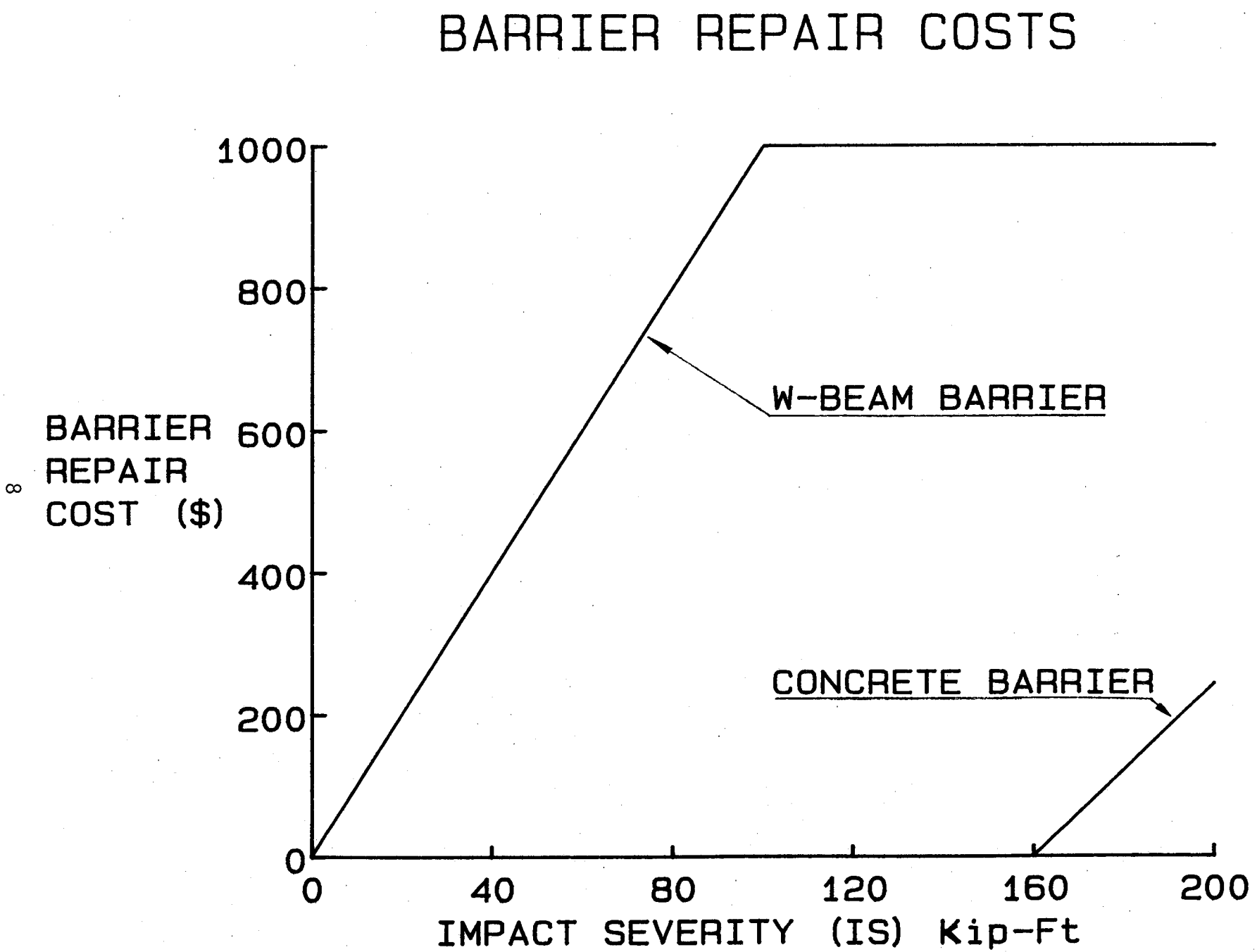

FIGURE 4 LONGITUDINAL BARRIER REPAIR COSTS

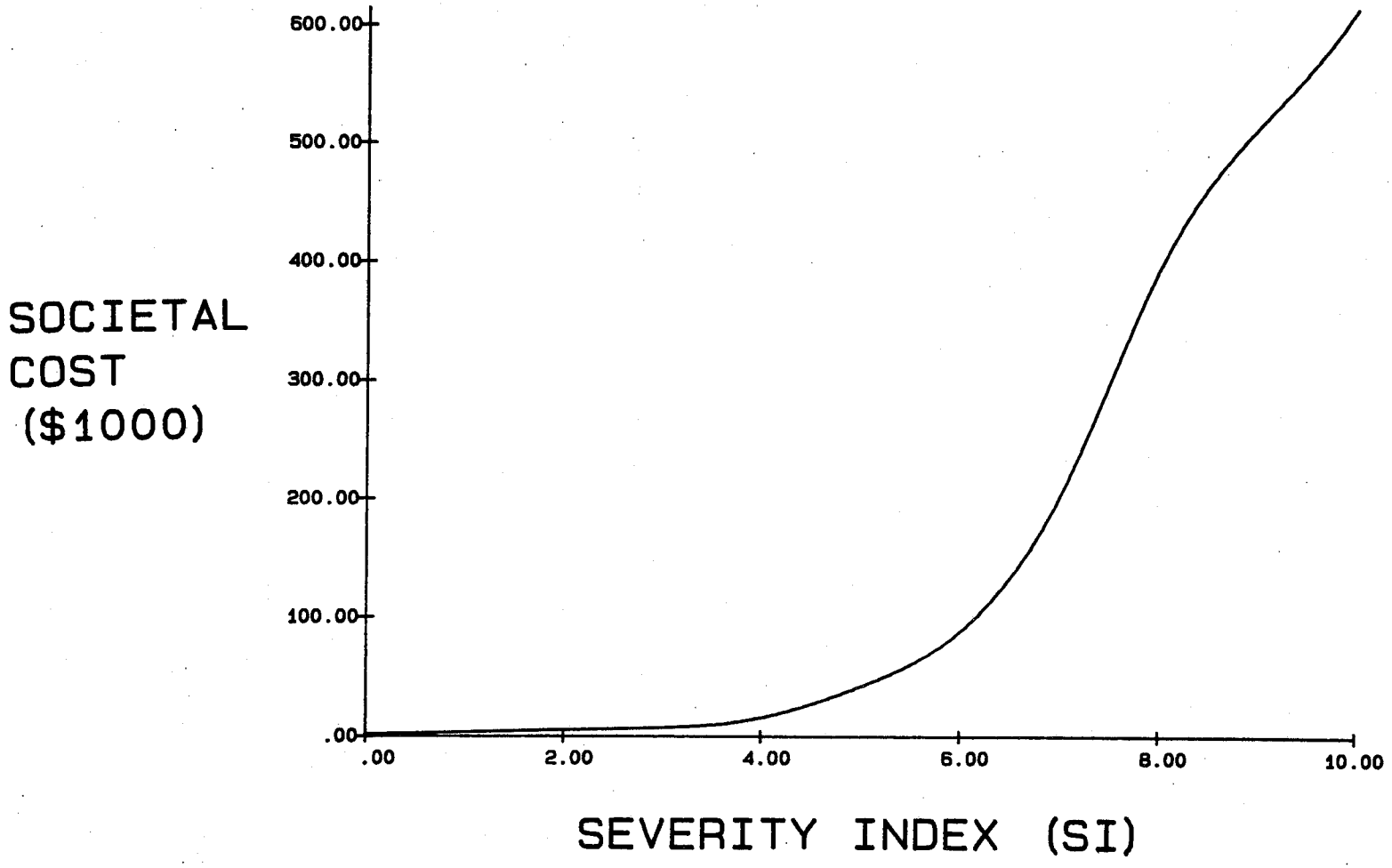

FIGURE 5 SOCIETAL COSTS VERSUS IMPACT SEVERITY

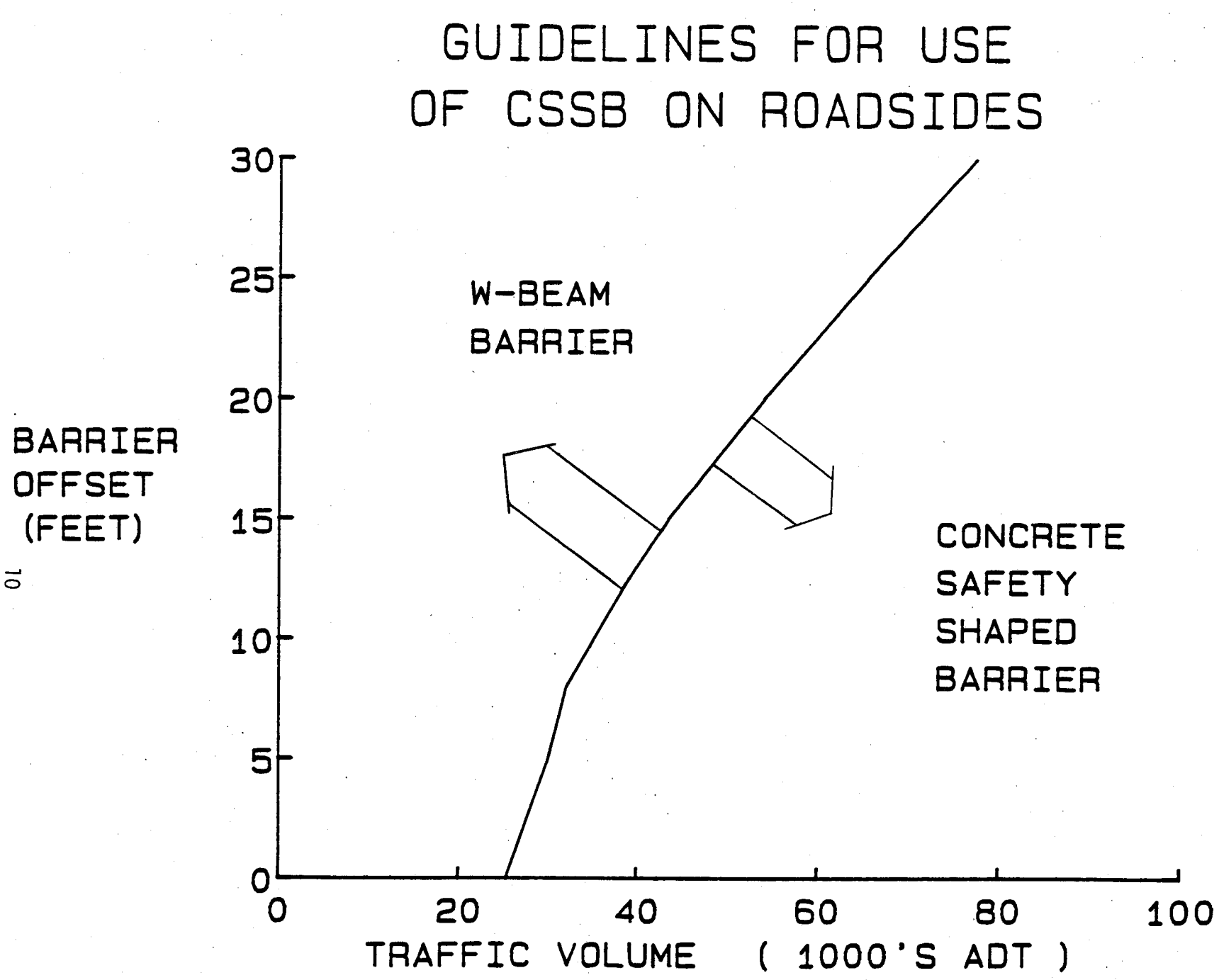

FIGURE 6 GUIDELINES FOR CONCRETE BARRIER USE ON THE ROADSIDE

Table 2. End Treatment Benefit/Cost Analysis Data

	Transition to W-Beam w/Texas Twist	TREND	Reusable Rubber Crash Cushion
Cost ($)	1000	5000	13000
Severity Index for Impacts			
Below Performance Level			
Side	Fig. 3	Fig. 3	Fig. 3
End (S.I./mph)	.11	.08	.08
Above Performance Level			
Side	7.5	7.5	7.5
End	7.5	7.5	7.4
Performance Level			
Side (I.S.,kip-ft)			
2000 lb Vehicle	48	48	48
4500 lb Vehicle	97	97	97
12800 lb Vehicle	97	97	97
55000 lb Vehicle	97	97	97
End (Total K.E.,kip-ft)			
2000 lb Vehicle	200	240	240
4500 lb Vehicle	540	540	540
12800 lb Vehicle	540	540	540
55000 lb Vehicle	540	540	540
Repair Cost ($/kip-ft)			
Side (I.S.)	Fig. 4	Fig. 4	5.0
End (Total K.E.)	2.0	2.3	0.30
Life of Treatment (years)	20	20	20
Discount Rate (%)	4	4	4
Functional Highway Class	Freeway	Freeway	Freeway

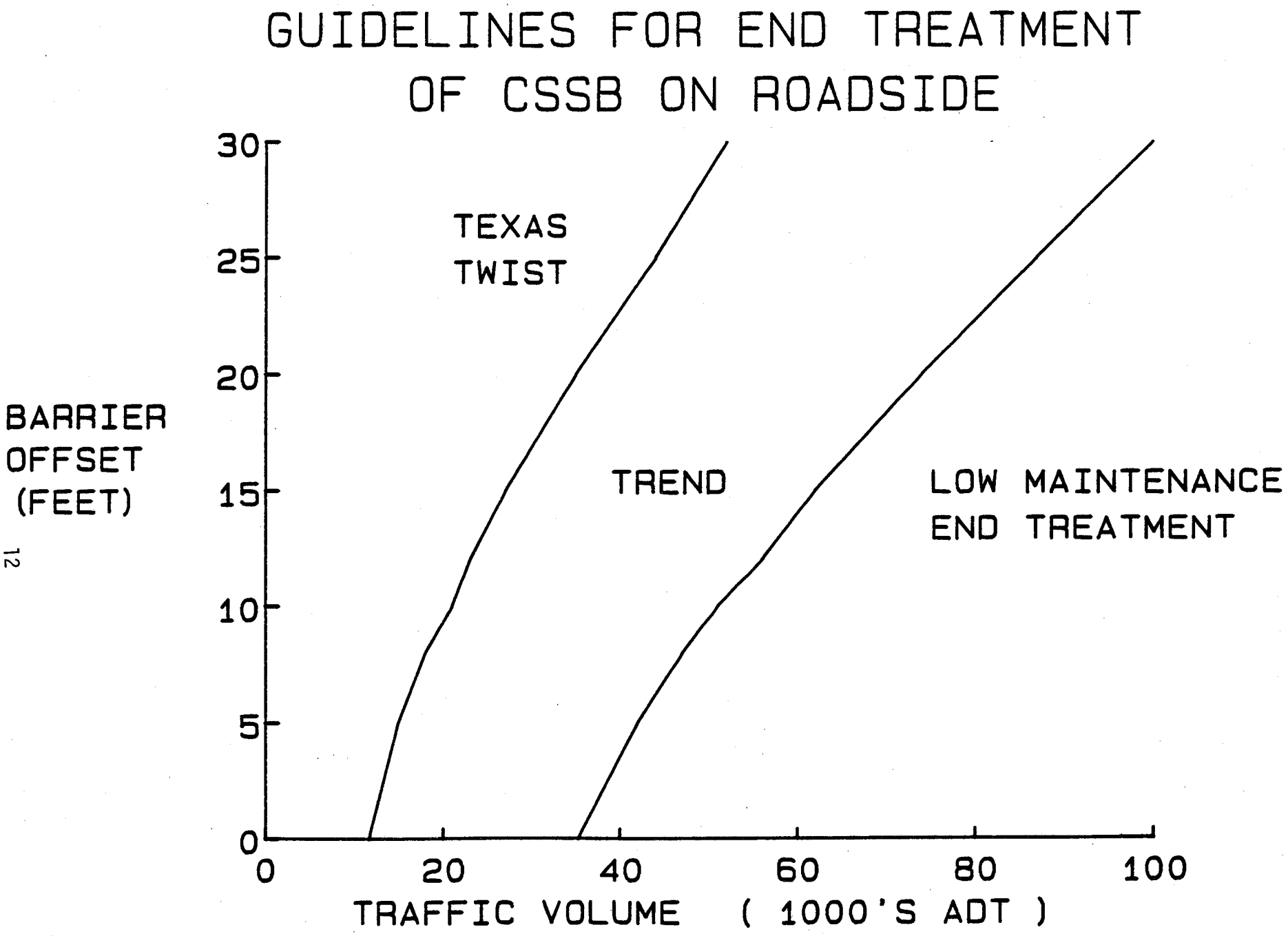

FIGURE 7. GUIDELINES FOR END TREATMENT OF RIGID ROADSIDE BARRIERS

generally only exposed to traffic traveling in one direction. Further, it should be noted that divisions drawn on Figures 6 and 7 mark lines where the benefit/cost ratio for an alternative first equals 1.0. An alternative should not be used when its benefit/cost ratio is less than 1.0. However, it does not follow that all improvements having a B/C greater than 1.0 can or should be implemented. When possible, benefit/cost analysis of all safety improvement programs contemplated by an agency within a given time and budget framework should be conducted and tabulated. Those improvements having higher B/C ratios should be given highest priority.

B. Foundation Requirements

An examination of foundation requirements for the CSSB showed that the barrier could be supported by a stabilized and well compacted soil, without appreciable barrier settlement. However, without any lateral restraint severe impacts would damage and/or move the barrier, whether it was a continuously reinforced design or a precast segemental design. There would also be a potential problem of maintaining the unpaved area between the edge of the paved roadway and the face of the barrier. Vegetation control would be difficult and erosion could create further problems. In an effort to eliminate these potential problems, it is the authors' recommendation that the barrier be supported in a manner similar to that shown in Figure 8.

Barrier/shoulder joints should be designed to prevent any lateral motion of the barrier. Lateral support elements should be designed such that any 10 ft segment of barrier can withstand the design impact force. Appendix G of reference 19 describes procedures for estimating impact loads on rigid barriers for design impact condition. For example, the design impact force from reference 19 corresponding to a full size automobile impacting at a speed of 60 mph and an angle of 25 degress is approximately 32,000 lb. Thus, lateral support elements attached to any 10 ft. segment of concrete barrier should be capable of resisting a 32,000 lb. lateral load. As an example, sufficient lateral restraint could be provided by 1-inch, 36 ksi steel dowels spaced on 5 ft. centers. Precast barrier segments can be developed in a similar manner by designing barrier anchorage and segment joints such that any 10 ft. segment of barrier can withstand the design load.

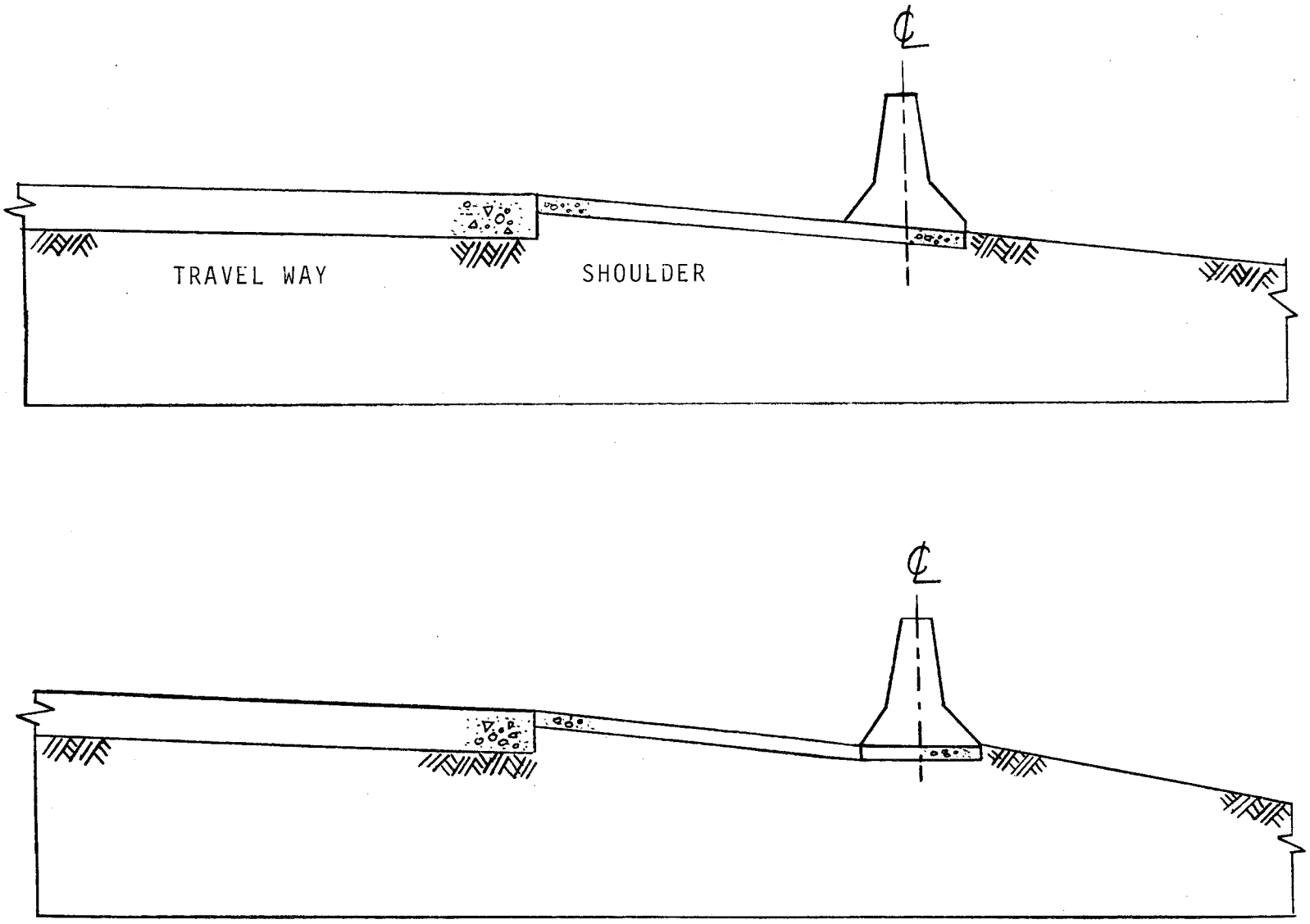

FIGURE 8 CONCRETE BARRIER PLACEMENT RECOMMENDATIONS

III. DEVELOPMENT OF AN END TREATMENT

A large portion of crash cushion maintenance cost is associated with the repair or replacement of damaged components. The most effective method of cutting repair costs is to limit component damage by eliminating sacrificial energy absorbing elements and strengthening other components. Maintenance costs can be cut further by reducing the size of the end treatment thereby reducing number of impacts on the cushion.

Many concrete barrier end treatments must be placed very close to the traveled way. If a cushion is to have application at such sites, it must be narrow ideally no wider than the standard concrete barrier. Narrow crash cushion end treatments must perform as a crash cushion when impacted head-on and as a longitudinal barrier when struck downstream. Therefore, the objective of this phase of the research was to design a low-maintenance crash cushion end treatment for concrete barriers that would (1) have no sacrificial energy absorbing elements, (2) have sufficient strength to withstand most impacts without damage to any components, (3) be approximately the same width as the standard CSSB, and (4) meet nationally recognized safety standards (4).

A. Research Approach

Conventional crash cushions attenuate vehicular impacts through the collapse or crushing of energy absorbing elements. The principal task in this phase of the study was to develop a method of allowing a cushion to absorb impact energy while it collapses without damaging any components. The initial phase of the study involved a search for and laboratory evaluations of materials or devices that could absorb large amounts of energy, without sustaining any damage, while undergoing large deformations at high strain rates. Another requirement of the attenuation method was that the ratio of energy absorbed by the cushion to the energy returned to the vehicle be low to prevent high-speed rebound of impacting vehicles.

Numerous chemical, plastic, and rubber companies were contacted during the search, and a large number of potential energy absorbing materials was located. Samples were obtained for all materials having the basic properties of interest, including Norsorex (5), Sorbothane (6), open and closed-cell polyurethane and polyethelene foams, and several natural and synthetic rubber compounds in various shapes. Spring manufacturers were also contacted regarding the potential use of steel springs as an energy absorbing device.

Sorbothane was eliminated at an early stage due to its high cost, and steel springs were eliminated due to the high ratio of energy absorbed to energy stored by the springs. Photos of the materials included in the evaluation process are shown in Figures 9 and 10. The second phase of the development involved the design of a prototype end treatment utilizing the material selected.

B. Lab Testing of Candidate Materials

Each of the candidate materials was subjected to a series of laboratory tests to determine its suitability for use in a crash cushion. Initially, preliminary high-speed compression tests were conducted to find any visual material damage that might occur during high-speed impacts. At this point all closed cell foam materials were eliminated from further consideration due to

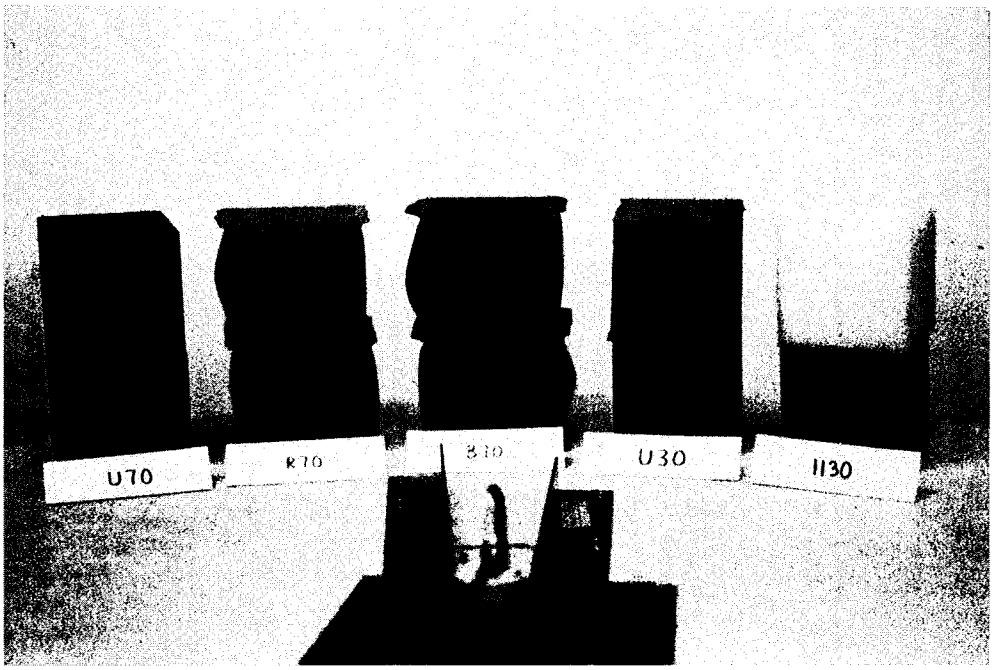

FIGURE 9 FOAM SAMPLES TESTED FOR USE IN LOW MAINTENANCE CRASH CUSHION END TREATMENT

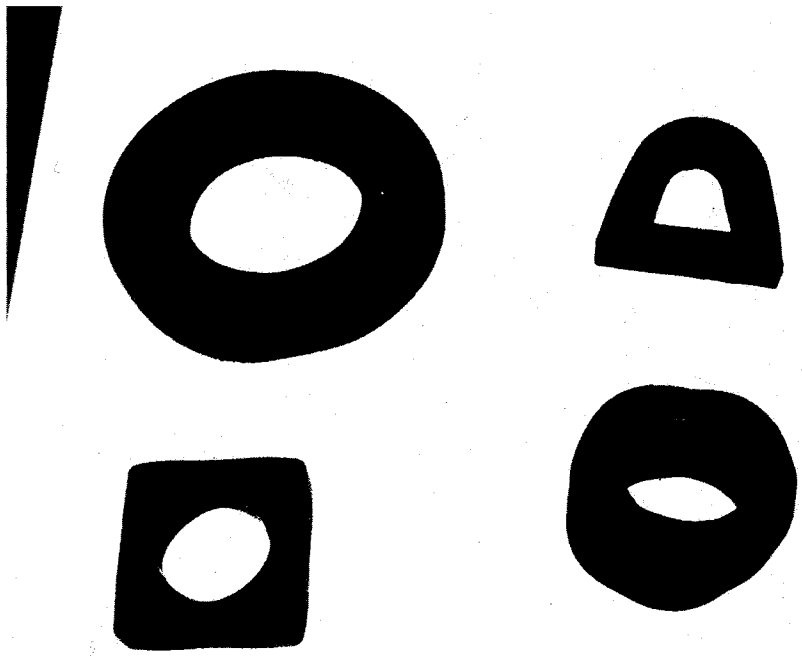

FIGURE 10 RUBBER SHAPES USED IN PRELIMINARY TESTING

the extensive damage resulting from a single compression test. Environmental testing was then conducted in conjunction with static load deflection testing to evaluate each material's resistance to environmental degradation. Finally, the remaining materials were subjected to numerous high- and low-speed compression scale model tests in an effort to predict dynamic response of full-scale impact attenuation devices.

Environmental Testing

After preliminary evaluation of all candidate materials, only Norsorex, open-cell polyurethane and polyethelene foams, and rubber compounds were considered to have the necessary properties. Although extensive environmental testing information was available for most of the rubber compounds under consideration, similar data for Norsorex and the foam materials was not available. Further, data for ultraviolet exposure and freeze-thaw tests of the rubber materials were not available. Therefore a limited testing program, involving ultraviolet exposure and freeze-thaw testing, was devised to examine the durability of the candidate materials.

Polyurethane and polyethelene foams are known to degrade rapidly under exposure to ultraviolet radiation. Therefore, two fiber reinforced vinyl materials were obtained to evaluate their potential for covering the foam to prevent deterioration. All materials under consideration, including covered and uncovered foams, were then exposed to high intensity ultraviolet radiation as shown in Figure 11. Each material sample was subjected to static compression testing at the start and periodically throughout the ultraviolet exposure test to detect any changes in the material's energy absorption characteristics. In addition, all samples were visually inspected and photographed periodically to document material changes. Samples of the foams and the vinyl coverings were placed outdoors in full summer sun to correlate ultraviolet testing to outdoor exposure. Samples placed outdoors were subjected to the same testing as those exposed to the high intensity ultraviolet lamp.

Ultraviolet exposure testing was conducted continuously for 44 days. As expected, uncovered polyurethane and polyethelene foams deteriorated rapidly during the ultraviolet radiation testing. However, covered samples of the same materials showed no signs of deterioration. Although vinyl materials used in the testing retained their tensile strength, both materials showed signs of reduced ductility and tear resistance after ultraviolet exposure. Norsorex and all rubber compounds tested showed no evidence of damage from exposure to ultraviolet radiation.

Samples exposed to the sun and those used in ultraviolet testing were compared both visually and through results of static compressive and tensile tests. This comparison showed that samples exposed to the high intensity lamp degraded approximately 15 times faster than samples placed in full summer sun. With a correlation factor of 15, 44 days of ultraviolet exposure would correspond to approximately 3.5 years of exposure to summer sunshine. Thus, vinyl covered foams can be expected to withstand 3.5 years of exposure to the sun with very little change in material properties. However, significant discoloration and embrittlement of the vinyl after the testing indicates that longer exposures could result in degradation of the vinyl's capacity to withstand impact loadings.

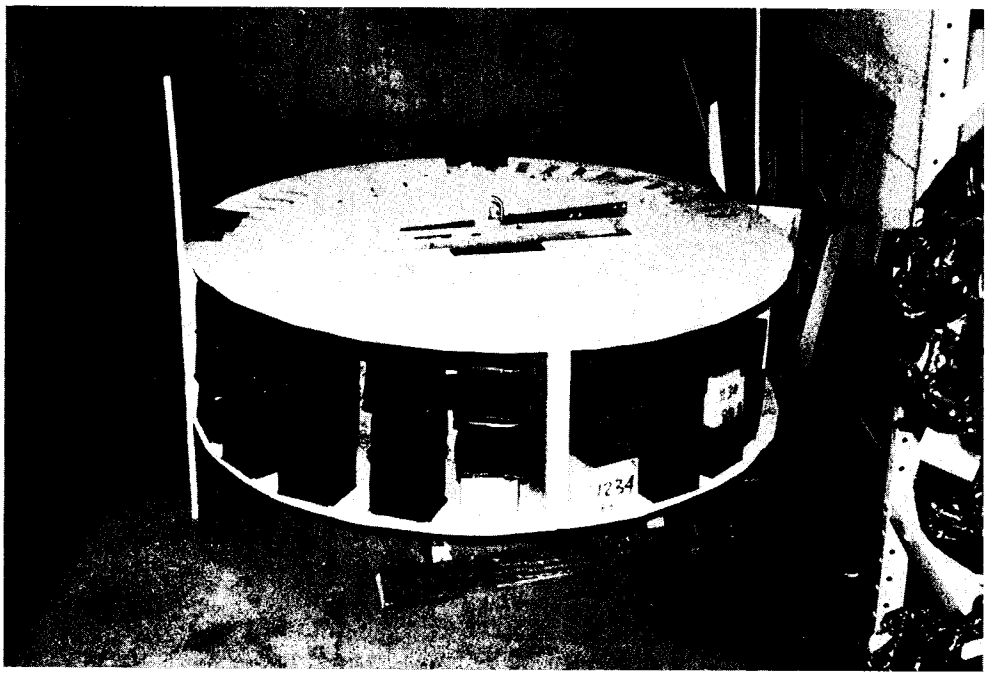

FIGURE 11 ULTRAVIOLET RADIATION TEST DEVICE

Freeze-thaw tests were also conducted on samples of the same materials used in the ultraviolet radiation testing. Test samples were moved every 12 hours between hot and cold environment chambers held at 140°F and 0°F, respectively. Static testing was again conducted periodically to observe any changes in stiffness of the materials. At the end of 44 complete cycles, all samples were carefully examined and photographed. No significant changes in stiffnesses were observed in any of the materials tested. However, visual inspection of Norsorex samples showed significant cracking of the outer walls of the cylinders. Therefore, Norsorex was eliminated from further consideration in this study.

Dynamic Testing

High-speed dynamic compression tests were conducted on the foam and rubber samples under various temperature and humidity conditions. Some rubber samples exhibited greatly increased stiffnesses, as much as 100 percent, when tested at temperatures well below freezing. Temperature effects on the stiffness of some of the other rubber samples and all foam samples were below 25 percent. However, some vinyl coverings on the open cell foam samples were damaged during low temperature dynamic testing. This damage appeared to be related to the manner in which the covers were attached to the foam samples rather than the vinyl itself since damage was limited to the seams in the vinyl. All samples tested at elevated temperatures exhibited a slightly reduced stiffness when compared to the tests conducted at ambient temperatures.

Open-cell foams tend to absorb water under high humidity conditions. Therefore all materials still under consideration were tested dynamically at 100% relative humidity. The objective of the test was to determine the effects of water retention on the stiffness and the energy absorbed by the material. From this standpoint all materials performed well with very little change in the stiffness or energy absorbed by the samples. However, both open-cell polyurethane and polyethelene foams showed signs of damage after the testing. Apparently the water captured in the material ruptured a significant number of material cells when impacted at high speeds. Subsequent testing of the samples exhibited a 10 to 20 percent permanent reduction in both the stiffness and energy absorbed by each sample. Thus, although open-cell polyethelene and polyurethane foams could probably be used in a crash cushion, rubber compounds were found to be much more durable and the foams were eliminated from further consideration.

Details of laboratory tests of the candidate materials, with the exception of the rubber compounds, are given in reference 16. Details of laboratory tests of the rubber materials are given in Appendix I.

As a result of laboratory testing of all candidate energy absorbing materials, rubber compounds were selected as the most promising attenuation material for use in a low maintenance crash cushion. However, the number of potential shapes of rubber energy absorbing devices is virtually limitless. Several different rubber shapes were included in the previous laboratory testing as shown in Figure 8. Of the shapes tested initially, the circular cylinder appeared to absorb the most energy per pound of rubber. Further, the circular rubber cylinder has been shown to absorb large amounts of energy and to be resistant to damage during impact loadings when used as ship and dock fenders (7,8). Therefore, a cylindrical rubber element was selected for use

as a reusable energy absorbing element.

Although the basic type and shape of energy absorbing medium had been chosen, the specific rubber compound and cylinder sizes were yet to be selected. The response of rubber cylinders to statically applied transverse loadings has been thoroughly studied both empirically and theoretically (7,8,9). These studies have shown that for any particular rubber compound the static stiffness of a cylinder is a function of the ratio between the outer diameter (D) and the wall thickness (t). Therefore the static stiffness of large rubber cylinders can be estimated by measuring the stiffness of scale model cylinders with similar D/t ratios.

Study of the dynamic response of rubber cylinders to transverse compression has been very limited. The nonlinear characteristics of rubber and the large strains associated with the collapse of a cylinder make finite element dynamic analysis of this phenomenon virtually impossible. Therefore, an empirical study of the dynamic force deflection characteristics of rubber cylinders was undertaken. One-fifth scale model cylinders in a variety of wall thicknesses and rubber compounds were obtained from Regal International of Corsicana, Texas (10). Table 3 shows the sizes and types of model cylinders tested. Figure 12 shows a photograph of the test setup used in the dynamic tests. Note that the test configuration allowed the sample to be compressed fully at a constant velocity. The scale model cylinders were tested in compression statically and at three different impact speeds (5, 30, and 75 ft/sec). Energy absorbed by each of the samples tested is shown in Table 4.

The energy absorbed by a rubber cylinder during a dynamic test has three sources, (1) inertia, (2) elastic stiffness, and (3) damping. Upon impact a portion of the rubber cylinder's mass begins to accelerate. When the cylinder is completely collapsed, approximately one half of the cylinder's mass has been accelerated to the the speed of the impact plate, while the other half is virtually stationary. The energy absorbed by the inertia of the cylinder can then be estimated from the impact velocity and the mass of the cylinder as shown below.

$$E_I = 1/4\ m\ V^2$$

where:

E_I = energy transferred to cylinder due to inertia (in.-lb),

m = mass of cylinder (lb-sec^2/in), and

V = velocity of impact plate (in/sec).

Energy absorbed due to the elastic stiffness of the specimen was measured from static testing. Energy attributable to internal damping within the specimen was then estimated from results of dynamic tests as shown below.

$$E_D = E_T - E_I - E_E$$

where:

E_D = energy attributable to internal damping (in-lb),

Table 3. Scale Model Rubber Cylinders

Sample No.	Wall Thickness (in.)	Hardness Durometer	Material Type
1	.30	50	N.R.-A
2	.30	60	N.R.-A
3	.30	70	N.R.-A
4	.30	80	N.R.-A
5	.45	50	N.R.-A
6	.45	60	N.R.-A
7	.45	70	N.R.-A
8	.45	80	N.R.-A
9	.60	50	N.R.-A
10	.60	60	N.R.-A
11	.60	70	N.R.-A
12	.60	80	N.R.-A
13	.30	85	Synthetic
14	.30	90	Synthetic
15	.45	85	Synthetic
16	.45	90	Synthetic
17	.60	85	Synthetic
18	.60	90	Synthetic
19	1.20	50	N.R.-A
20	1.20	60	Synthetic
21	1.20	85	Synthetic
22	1.20	90	Synthetic
23	.60	--	Neoprene
24	1.20	--	Neoprene
25	.31	80	N.R.-B
26	.44	80	N.R.-B
27	.63	80	N.R.-B
28	1.20	80	N.R.-B

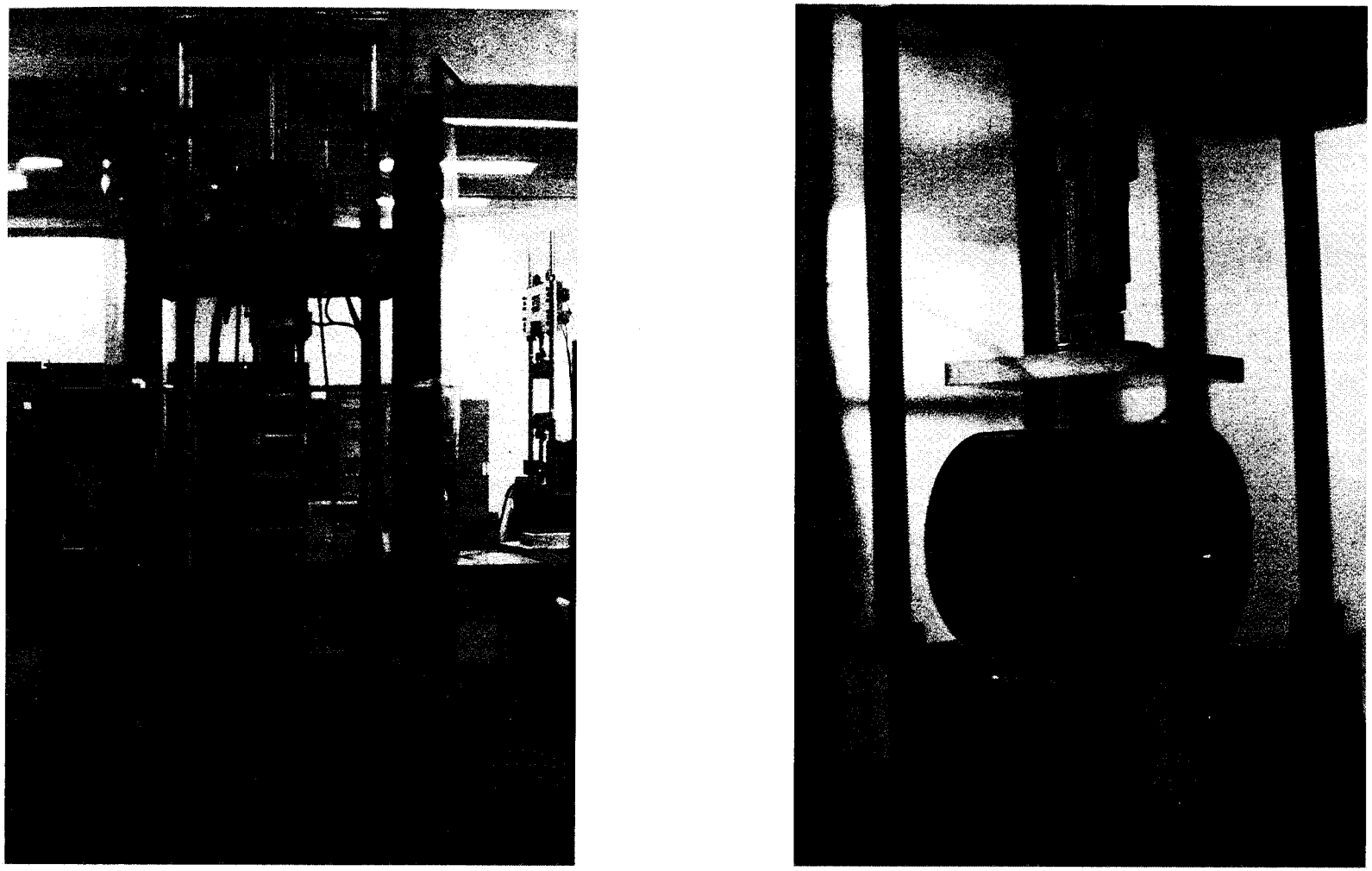

FIGURE 12 SCALE MODEL DYNAMIC TEST FIXTURE

Table 4. Total Energy Absorbed by Model Rubber Cylinders (75 ft/sec Impact Speed)

Sample No.	Wall Thickness (in.)	Hardness (Durometer)	Measure Energy Absorption (in.-lb) Static	Dynamic 38 ft/sec	Dynamic 75 ft/sec
1	0.30	50	35		836
2	0.30	60	58		930
3	0.30	70	95		830
4	0.30	80	152	525	990
5	0.45	50	85		865
6	0.45	60	140		972
7	0.45	70	223		1184
8	0.45	80	330	1140	1240
9	0.60	50	158		1730
10	0.60	60	271		1440
11	0.60	70	466		1760
12	0.60	80	616	1380	1830
13	0.60	--	413		2183
14	1.20	50	453	1335	3141
15	1.20	60	743	3797	3930
16	1.20	85	1461	4870	5560
17	1.20	90	1536		2930
18	1.20	--	1026		3273
19	0.31	80	126		787
20	0.44	80	322		1340
21	0.61	80	537		2200

E_T = total energy absorbed during dynamic test (in-lb), and

E_E = energy attributable to elastic stiffness (in-lb).

As shown in Table 5, energy absorbed by internal damping was found to be approximately the same for the 30 and 75 ft/sec tests. Therefore, it can be concluded that damping within the tested rubber materials is of a hysteretic nature and that energy absorbed by the rubber cylinders, with the exception of momentum transfer, is largely independent of the impact velocity.

To estimate the energy absorbed by a full-scale cylinder, it was assumed that the ratio of elastic energy absorbed to damping energy absorbed was constant for each rubber compound and was unrelated to cylinder size or wall thickness. Table 6 shows estimated ratios between the static and damping energy levels for each rubber compound. Static force-deflection characteristics of large scale rubber cylinders can be estimated directly from tests of scale model specimens as mentioned above. Thus, elastic and damping energy absorption for a 28-inch diameter rubber cylinder can be estimated as shown below.

$$E_{Ef} = E_{Es} (b_f/b_s)^2$$

where:

E_{Ef}= energy absorbed by a full size cylinder attributable to elastic stiffness,

E_{Es} = energy absorbed by a scale model cylinder attributable to elastic stiffness, and

b_f = bore diameter of full size cylinder.

b_s = Bore diameter of scale model cylinder.

Energy absorption characteristics of various sized cylinders were estimated in this manner for each of the materials tested. Figure 13 shows a plot of the estimated energy absorption capacity of a 28-inch diameter rubber cylinder constructed from compound A with an 80 durometer hardness (see Appendix I).

C. Design of Prototype Crash Cushion

Rubber has a relatively high density. As a result even thin-walled rubber cylinders have a relatively high mass. If components near the front of a crash cushion are too heavy, high momentum transfer from an impacting vehicle to the crash cushion will decelerate the vehicle too quickly. Therefore, thin-walled cylinders must be used at the front of the cushion. Further, since the strain energy associated with the collapse of a thin-walled cylinder is relatively small, as shown in Figure 13, the front of the cushion will behave essentially as an inertial system. Thick wall cylinders can be used in the rear of the cushion. Energy remaining in the impacting vehicle after collapse of the thinner cylinders can be dissipated via strain energy in and momentum transfer to the thicker cylinders.

In view of the aforementioned properties, a relatively hard rubber (80 durometer) was selected for further study. This material had higher strain-

Table 5. Energy Attributable to Internal Damping

Sample No.	Wall Thickness (in.)	Hardness (Durometer)	Energy Dissipated by Internal Damping (in.-lb) 38 ft/sec	75 ft/sec
1	0.30	50		305
2	0.30	60		377
3	0.30	70		235
4	0.30	80	308	343
5	0.45	50		75
6	0.45	60		125
7	0.45	70		257
8	0.45	80	565	205
9	0.60	50		659
10	0.60	60		259
11	0.60	70		384
12	0.60	80	464	304
13	0.60	--		857
14	1.20	50	553	1177
15	1.20	60	2472	2157
16	1.20	85	2699	2395
17	1.20	90		--
18	1.20	--		734
19	0.31	80		184
20	0.44	80		333
21	0.63	80		863

Table 6. Ratio Between Damping and Static Energy Dissipation

Material	Durometer	Energy Dissipation Ratio Damping/Static
Natural Rubber A	50	2.5
Natural Rubber A	60	1.0
Natural Rubber A	70	1.5
Natural Rubber A	80	0.6
Natural Rubber B	80	2.4
Synthetic	60	2.9
Synthetic	85	1.5
Synthetic	90	1.5
Neoprene	--	2.4

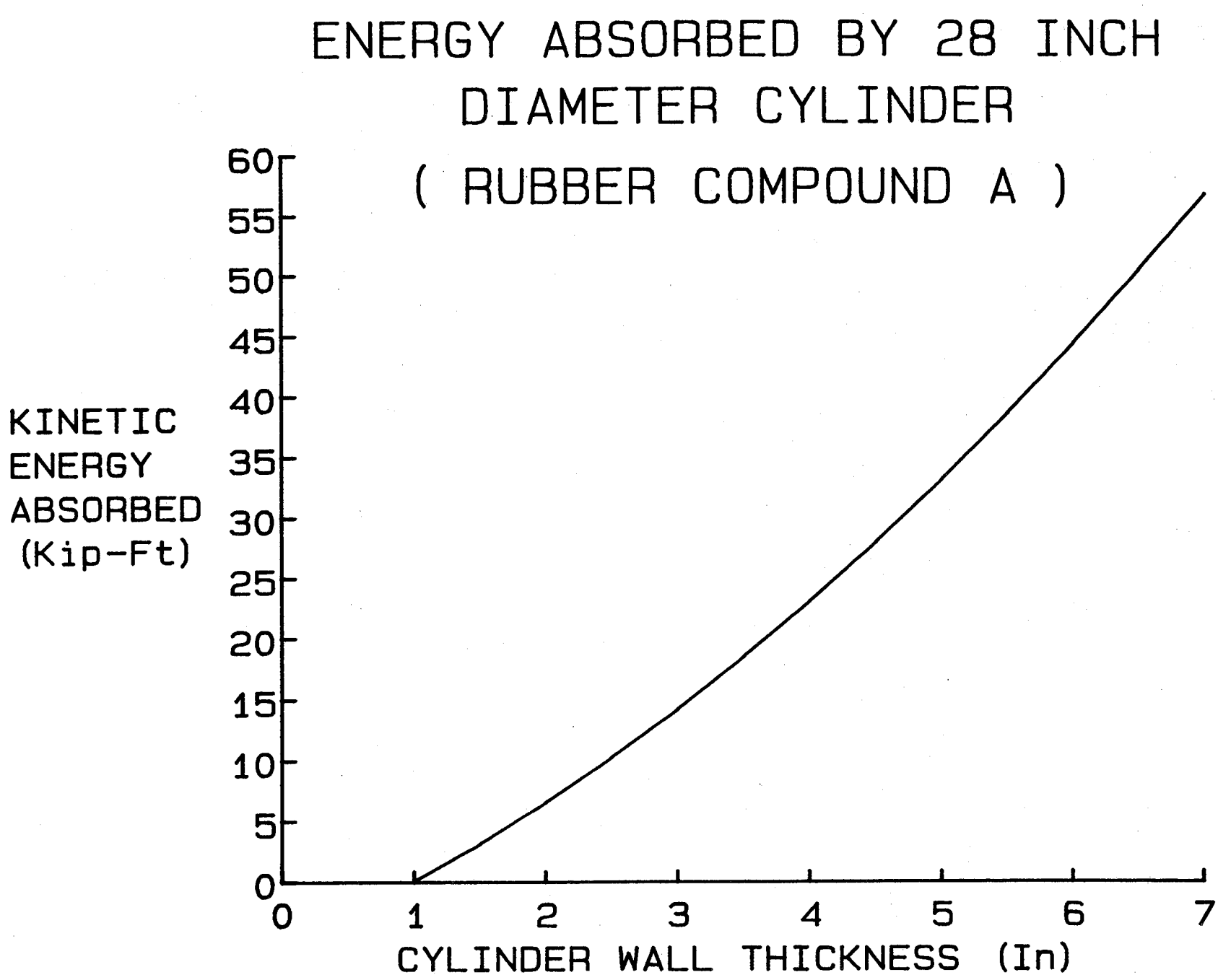

FIGURE 13 IMPACT ENERGY ABSORBED BY FULL SCALE RUBBER CYLINDER

energy absorption capacity than any of the other materials considered. Table 7 shows properties of the selected compound.

A prototype end treatment was then designed consisting of a single row of rubber cylinders. The cylinders were supported by steel diaphragms, and thrie-beam fender panels were used to provide redirection capablities. The center of the cylinders are approximately 21 inches above the ground, coinciding with the approximate center of mass of a typical automobile. To meet the 21-inch height requirement the outside diameter of the cylinders could be no greater than 28 inches. Larger cylinders would drag the ground when fully collapsed, causing excessive frictional forces and creating a potential ramp to launch an impacting vehicle.

The end treatment was modeled for head-on impacts as a series of lumped masses and springs. The principles of conservation of energy and momentum were employed to determine the impact severity of various sizes of vehicles when impacting different rubber cylinder configurations as discussed in reference 11. This analysis procedure is based on the assumption that the cylinders will collapse sequentially such that one cylinder is almost completely collapsed before the next cylinder begins to collapse. Preliminary analysis revealed that an end treatment could be designed to meet safety criteria using 1.75-inch thick cylinders in the front of the treatment and 4.5-inch thick cylinders at the rear, with all cylinders having an outside diameter of 28 inches. Rubber compound A with a durometer of 80 (see Appendix I) was selected. Variations in energy absorbed by this material were less than 35% for temperatures between -20°F and 120°F. Further, temperature effects on the thin-walled cylinders in the front of the treatment are of little consequence since they act primarily as an inertial cushion. It was therefore possible to design the end treatment to perform acceptable at all anticipated temperatures.

Two cylinders having an outside diameter of 28 inches and wall thicknesses of 1.75 inches and 4.5 inches, respectively, were fabricated from 80 durometer, rubber coupound A (see Appendix I). They were then tested statically and dynamically to verify preliminary designs. Dynamic tests involved impacting the cylinders at relatively low speeds with an instrumented cart as shown in Figure 14. The cart weighed approximately 5000 lb. The 1.75-inch thick cylinder test results were inconclusive since the cart decelerated very little as the cylinder collapsed. The cart impacted at about 5 mph. Table 8 shows the estimated and measured energy absorption characteristics of the 28-inch cylinders. As shown in the table, predicted values based on results of the previously discussed scale model tests compared well with the full-scale tests.

Using data gathered from previously described tests, the end treatment design was then finalized. Details are shown in Figures 15 and 16. It contains six thin-walled (1.75 in.) cylinders at the front and seven thick-walled (4.5 in.) cylinders at the rear. The cylinders are separated and supported by steel diaphragms. A rubber cylinder is placed vertically in front of the end treatment to capture an impacting vehicle, thus minimizing the potential for vehicular override or underride. The remaining cylinders are placed to allow unrestrained collapse of the cylinders. Thrie beam fender panels attached to the diaphragms and four 5/8-inch longitudinal cables provide redirectional capabilities. Fender panels are attached to the diaphragms with hinges to allow the panels to open outward during impact.

Table 7. Material Specifications for Natural Rubber A

PROPERTY	VALUE			
Durometer (Shore A)	50	60	70	80
Tensile Strength (psi)	3600	4145	3700	3715
Elongation %	623	670	530	596
Modulus at (psi)				
100% Elongation	175	245	345	615
200% Elongation	393	560	830	1678
300% Elongation	787	1100	1670	2668
Compression Set (%)		25	25	25

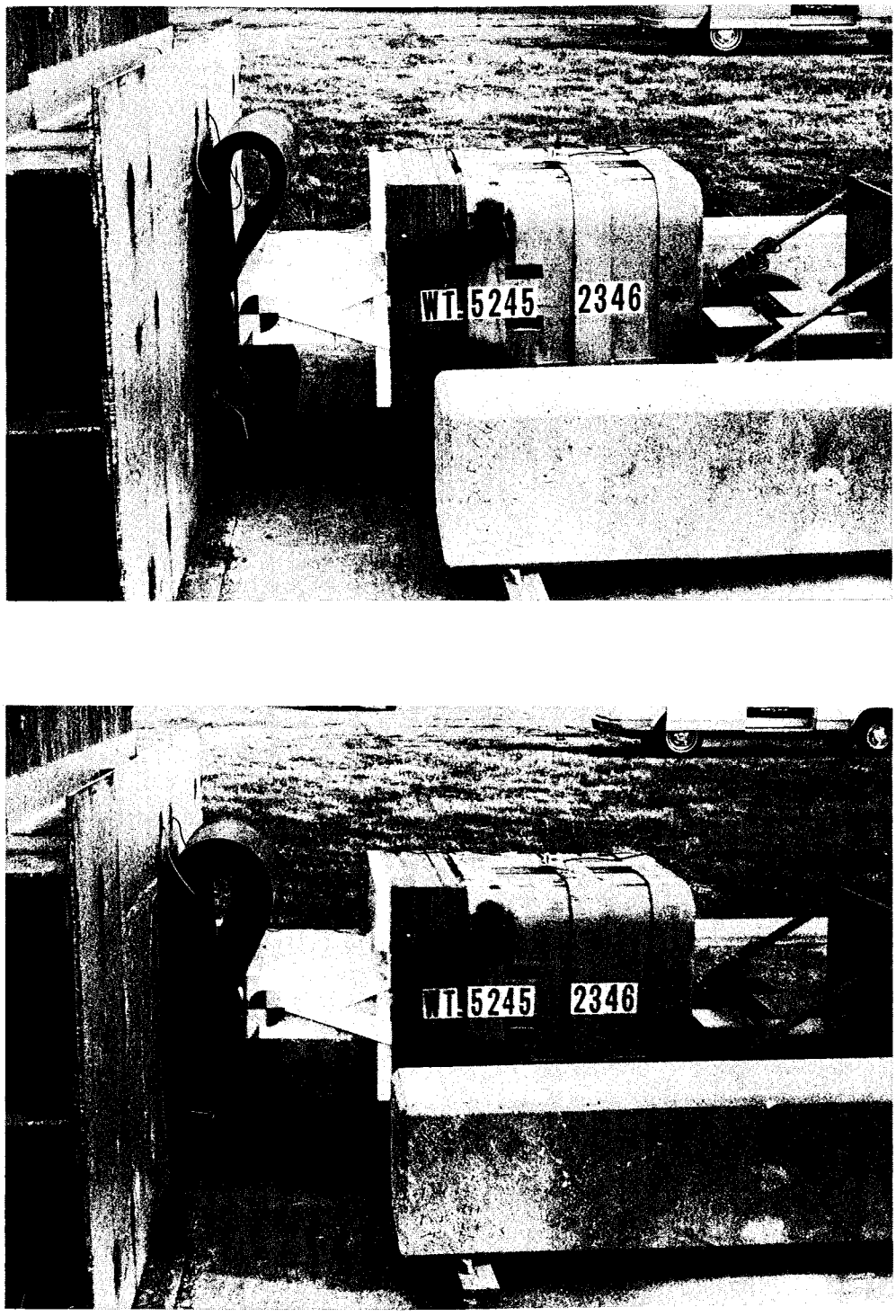

FIGURE 14 DYNAMIC TESTS OF FULL-SCALE RUBBER CYLINDERS

Table 8. Energy Absorption Properties of Full-Scale Rubber Cylinders

Sample			Total Energy Absorbed			
			Static Test		Dynamic Test	
Wall Thickness (in.)	Outside Diameter (in.)	Length (in.)	Measured (ft-lb)	Predicted (ft-lb)	Measured (ft-lb)	Predicted (ft-lb)
1.75	28	24	1995	1876	*	3000
4.50	28	24	15030	15400	20100	24600

*Test Data Recorder Error

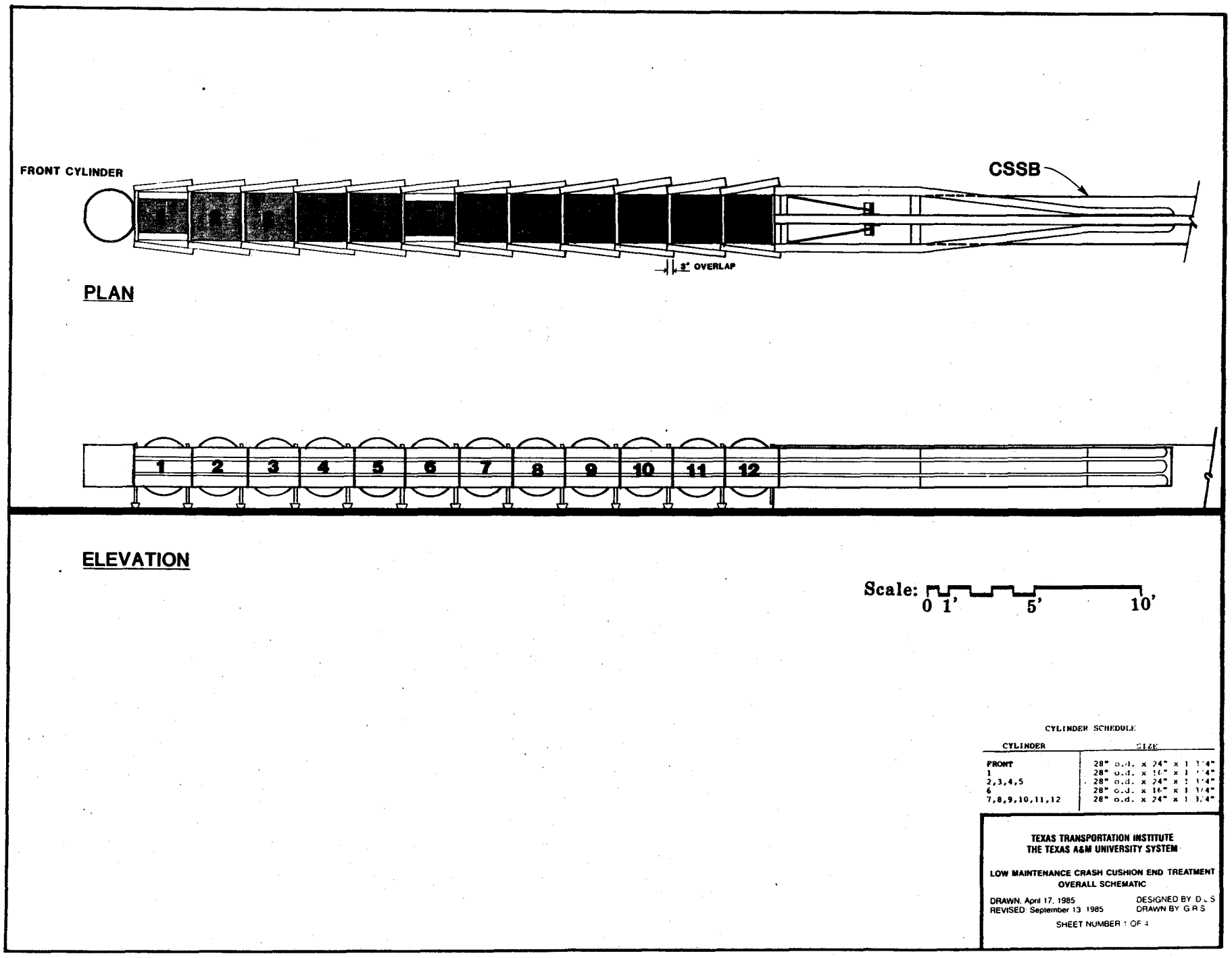

FIGURE 15 CONSTRUCTION DRAWINGS OF FINAL END TREATMENT DESIGN

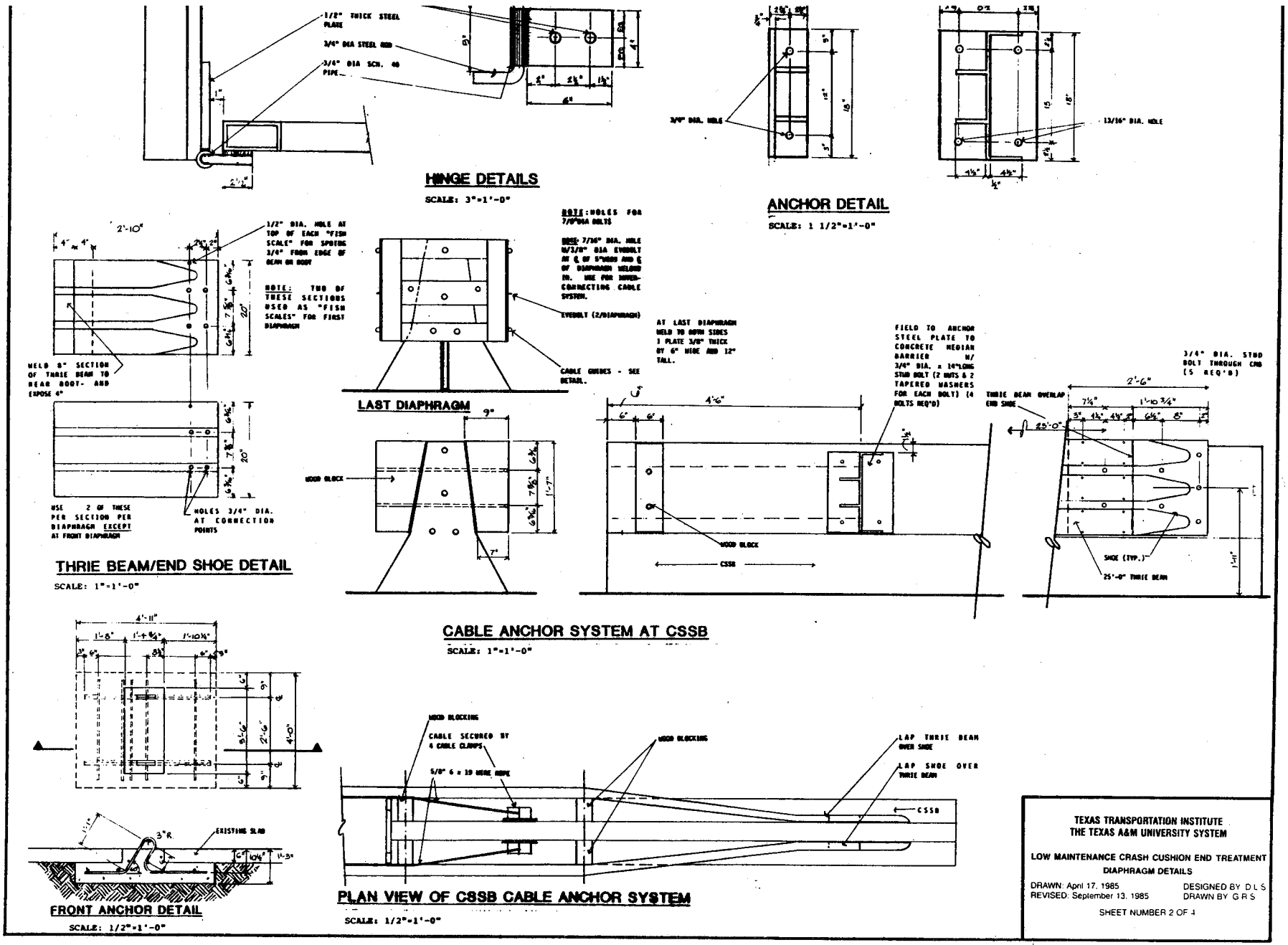

FIGURE 15 CONSTRUCTION DRAWINGS OF FINAL END TREATMENT DESIGN (CONT.)

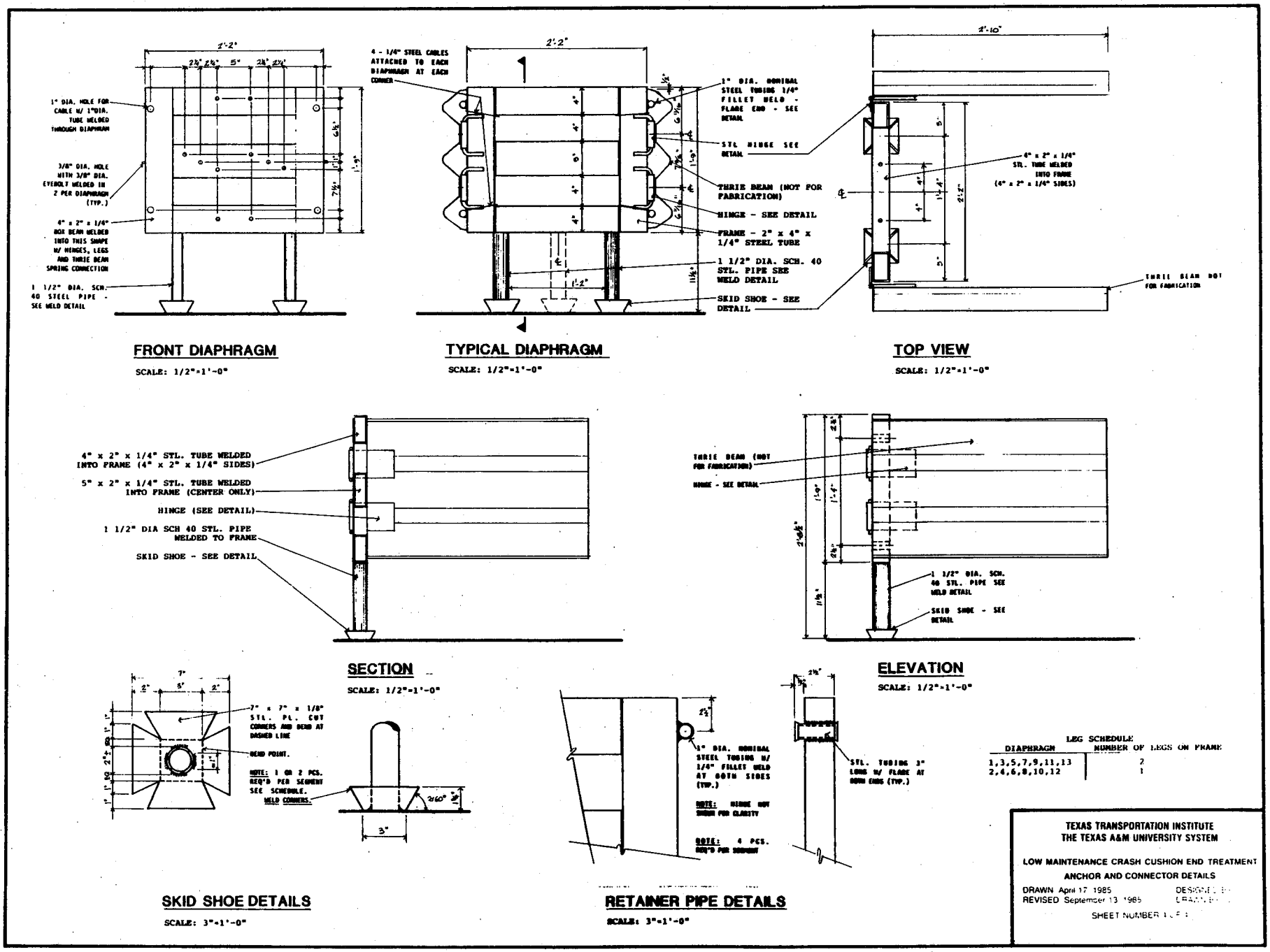

FIGURE 15 CONSTRUCTION DRAWINGS OF FINAL END TREATMENT DESIGN (CONT.)

NOTE: VERIFY CYLINDER THICKNESS AND SIZE IN FIELD BEFORE ASSEMBLY.

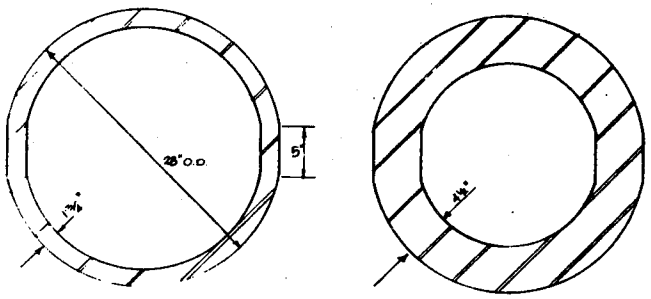

CYLINDER TOP VIEW

SCALE: 1 1/2"=1'-0"

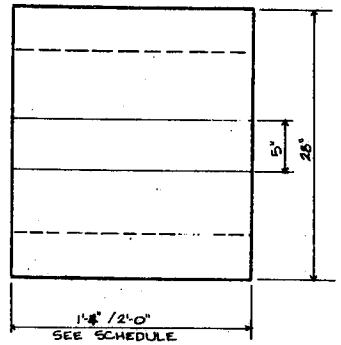

CYLINDER SIDE VIEW

SCALE: 1 1/2"=1'-0"

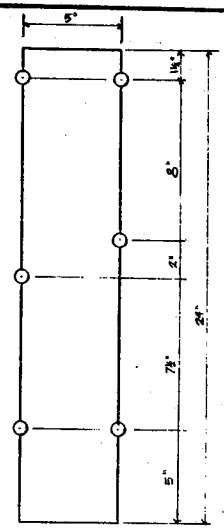

FRONT CYLINDER FLAT SPOT

SCALE: 3"=1'-0"

NOTE: CHECK DIMENSIONS FOR LENGTH IN FIELD. VERIFY ALL DIMENSIONS

NOTE: ALL FIGURES ARE SHOWN WITH TOP SIDE ABOVE AND BOTTOM SIDE OF FLAT SPOT BELOW.

NOTE: ON TYPICAL CYLINDER ALTERNATE BOLT PATTERN FRONT TO BACK SO THAT NO BOLTS GO HEAD TO HEAD WHEN COMPACTED.

NOTE: VERIFY CYLINDER THICKNESS & SIZE IN FIELD BEFORE ASSEMBLY

NOTE: REFER TO SHEET 1 AND SCHEDULE FOR CLARIFICATION OF LOCATION OF RUBBER CYLINDERS.

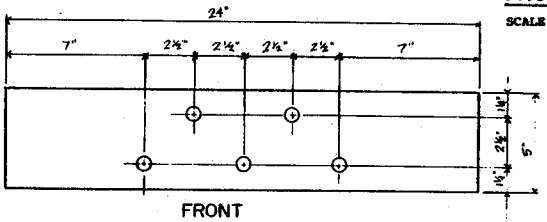

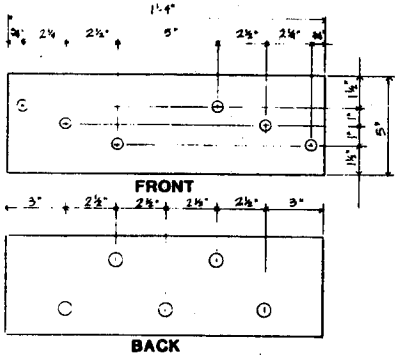

CYLINDER #1 FLAT SPOT

SCALE: 3"=1'-0"

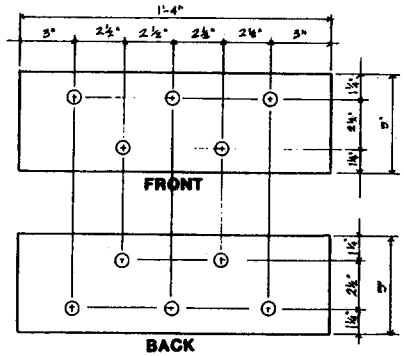

TYPICAL CYLINDER FLAT SPOT

SCALE: 3"=1'-0"

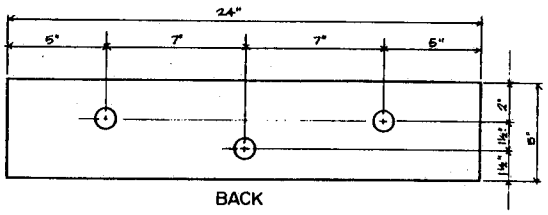

REAR CYLINDER FLAT SPOT

SCALE: 3"=1'-0"

CYLINDER SCHEDULE

CYLINDER	SIZE
FRONT	28" o.d. x 24" x 1 3/4"
1	28" o.d. x 16" x 1 3/4"
2,3,4,5	28" o.d. x 24" x 1 3/4"
6	28" o.d. x 16" x 1 3/4"
7,8,9,10,11,12	28" o.d. x 24" x 1 3/4"

TEXAS TRANSPORTATION INSTITUTE
THE TEXAS A&M UNIVERSITY SYSTEM

LOW MAINTENANCE CRASH CUSHION END TREATMENT
RUBBER DETAILS

DRAWN: April 17, 1985 DESIGNED BY D L S
REVISED: September 13 1985 DRAWN BY G R S

SHEET NUMBER 3 OF 4

FIGURE 15 CONSTRUCTION DRAWINGS OF FINAL END TREATMENT DESIGN (CONT.)

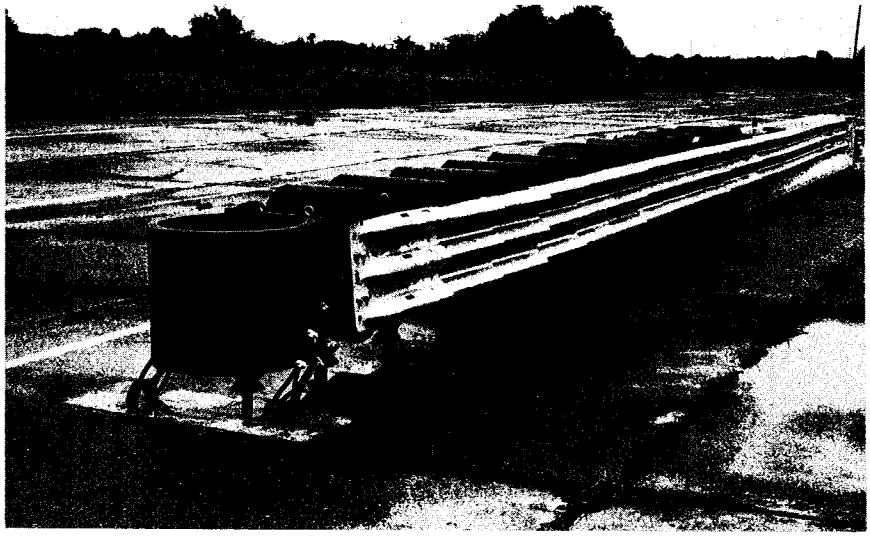

FIGURE 16 PHOTOGRAPHS OF PROTOTYPE LOW MAINTENANCE END TREATMENT

Steel springs are used to prevent the fender panels from opening under wind loadings. Head-on impact severity measures for the design, predicted by a conservation of energy and momentum analysis, are shown in Table 9.

The rubber cartridges do not have sufficient elastic stiffness to completely restore the system after it has been impacted. Four lightweight cables are attached between each diaphragm to allow the cushion to be pulled back into place after an impact. The end treatment is designed to sustain most impacts without replacement of any parts and to be restored to its original configuration in less than an hour.

The prototype end treatment, shown in Figure 16, was constructed at a cost of approximately $20,000. However, several design changes during construction significantly increased prototype construction costs. Futher, the $10,000 paid for the rubber cylinders used in the prototype cushion included the cost of molds necessary for manufacture of the cylinders. Therefore it is estimated that rubber cylinder costs can be reduced to $5,500 per unit, and total construction costs for the low maintenance end treatment can be reduced to approximately $13,000.

TABLE 9. PREDICTED OCCUPANT IMPACT VELOCITIES FOR 60 MPH HEAD-ON IMPACTS

VEHICLE WEIGHT (lb)	LONGITUDINAL OCCUPANT IMPACT VELOCITY (ft/sec)
1800	32
2250	31
3000	30
4500	28

IV. FULL-SCALE CRASH TESTS

Full-scale crash testing was conducted in two phases, (1) a preliminary phase to evaluate performance and restorability of the design at low to moderate impact speeds, and (2) a compliance phase to verify the design meets current safety standards. Accelerometer traces from compliance tests are shown in Appendix II and sequential photos of tests 3 through 6 are given in Appendix III

A. Preliminary Testing

Three preliminary full-scale crash tests were conducted. All three tests involved a 4390 lb, 1975 Ford Torino impacting the cushion head-on.

Tests 1 and 2

The first test was conducted at 30 mph with an uninstrumented vehicle. The cushion performed well and stopped the vehicle in approximately 15 ft. The test vehicle exhibited no tendency to vault over or underride the cushion. The vehicle rebounded off the cushion at approximately 5 mph. As shown in Figure 17 the test vehicle was only lightly damaged and cushion damage, shown in Figure 18, was limited to minor bending of some of the skid shoes under the steel diaphragms.

The end treatment was pulled back into place in less than an hour, and a second test was conducted at 40 mph the same day. The end treatment smoothly decelerated the test vehicle over a distance of 17.5 ft and vehicle damage was light. The vehicle again rebounded off the cushion at approximately 5 mph. Some of the hinges supporting the thrie-beam fender panels were damaged and the legs under the leading diaphragm were bent when they contacted the legs under the second diaphragm. Figure 19 shows the end treatment and test vehicle after the second test.

Test 3

The hinges on the front of the cushion were strengthened and the method of attaching the hinges to the diaphragms was improved to reduce the possibility of damage. The legs on the first diaphragm were removed and replaced with a single leg in the center such that it would not contact the legs on the second diaphragm during impact. The test vehicle was then instrumented and a third test was conducted at 51 mph. The test vehicle was smoothly decelerated and was pushed back out of the cushion at approximately 7 mph. The vehicle was only moderately damaged, as shown in Figure 20. All occupant risk values, shown in Table 10, were well below recommended limits (4). The end treatment, shown in Figure 21, was pulled back into place in less than an hour and, with the exception of some of the strengthened hinges, was undamaged. Test 3 is summarized in Figure 22.

a) Test Vehicle before Test-1

b) Test Vehicle after Test-1

FIGURE 17. TEST VEHICLE DAMAGE FROM TEST-1, 30 MPH IMPACT

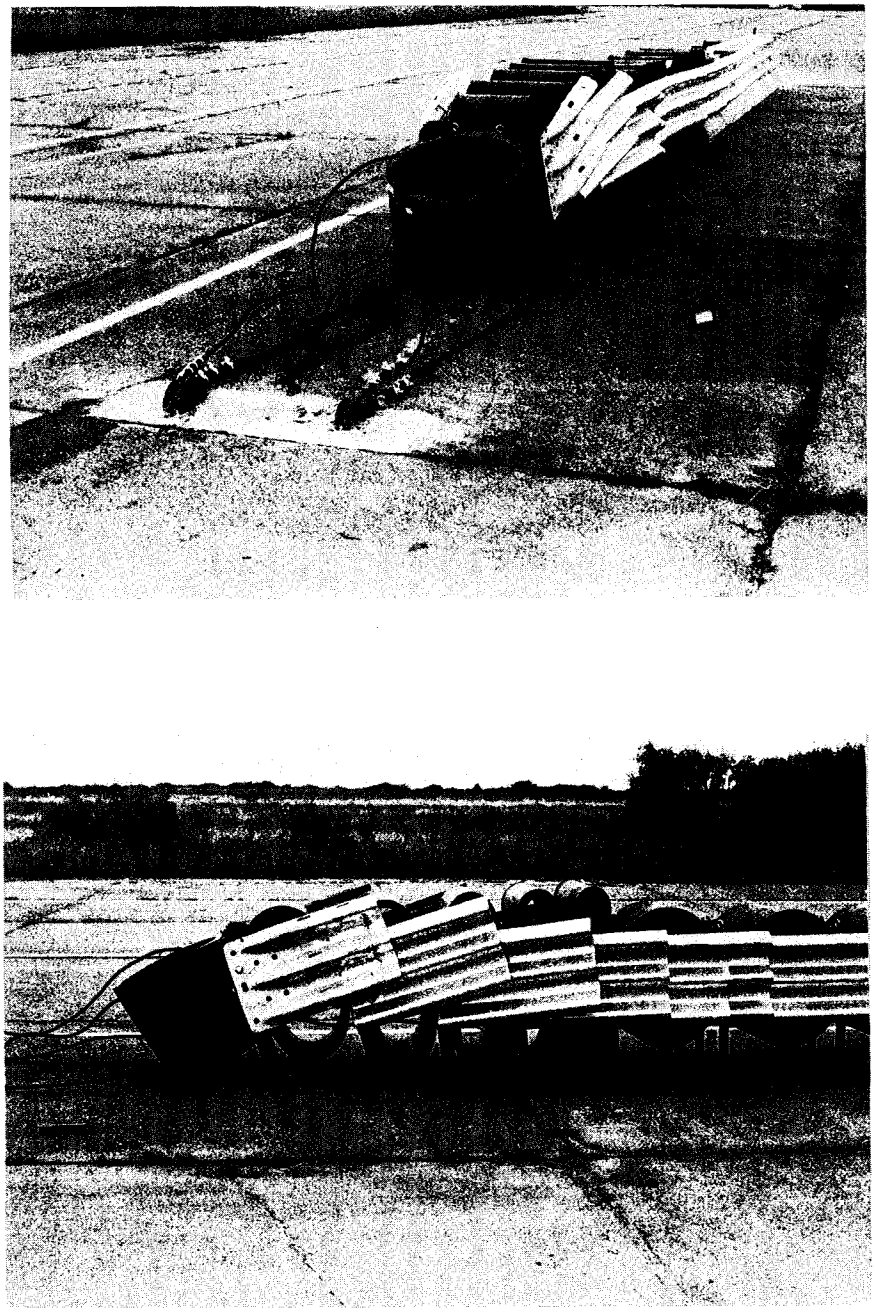

FIGURE 18. END TREATMENT AFTER TEST-1

a) Test Vehicle after Test 2

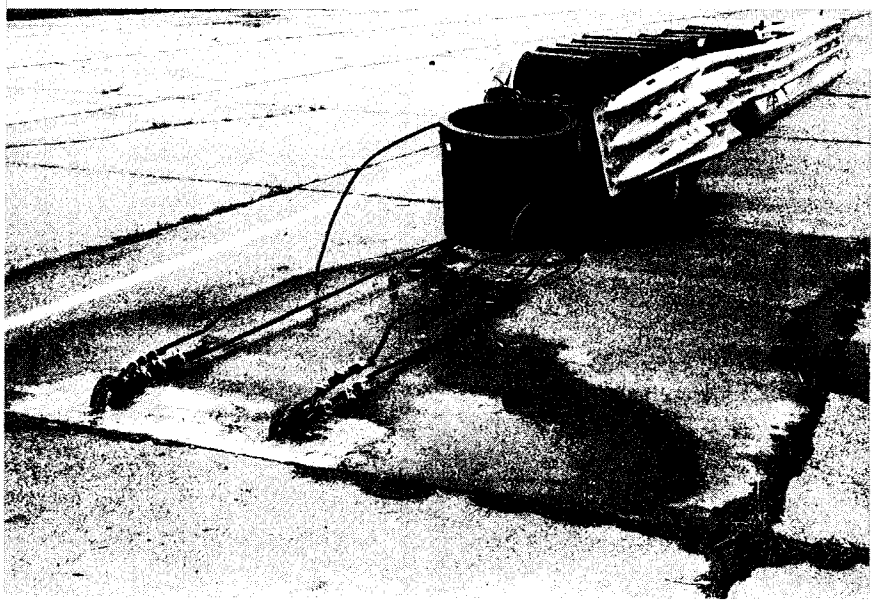

b) End Treatment after Test 2

FIGURE 19 END TREATMENT AND TEST VEHICLE AFTER TEST 2, 40 MPH IMPACT

a) Vehicle before Test 3

b) Vehicle after Test 3

FIGURE 20 VEHICLE DAMAGE AFTER TEST 3

TABLE 10. SUMMARY OF CRASH TEST RESULTS

TEST NO.	VEHICLE WEIGHT (lb)	IMPACT SPEED (mph)	ANGLE OF IMPACT (deg)	POINT OF IMPACT	VEHICLE STOPPING DISTANCE (ft)	OCCUPANT IMPACT VELOCITY (ft/sec)		OCCUPANT RIDEDOWN ACCELERATIONS (10 ms Avg. g's)	
						Long.	Lat.	Long.	Lat.
1	4390	30	0	Nose	15	*	*	*	*
2	4390	40	0	Nose	17.5	*	*	*	*
3	4390	51	0	Nose	22.5	22.0	*	7.7	*
4	1810	58	0	Nose	17.5	35.5	4.2	9.0	1.5
5	4500	57	0	Nose	23.5	26.4	N/A	14.1	N/A
6	4420	61	25	8th Fender Panel	N/A	32.7	18.9	20.9	32.5

*Not Measured
N/A - Occupant did not strike side of vehicle.

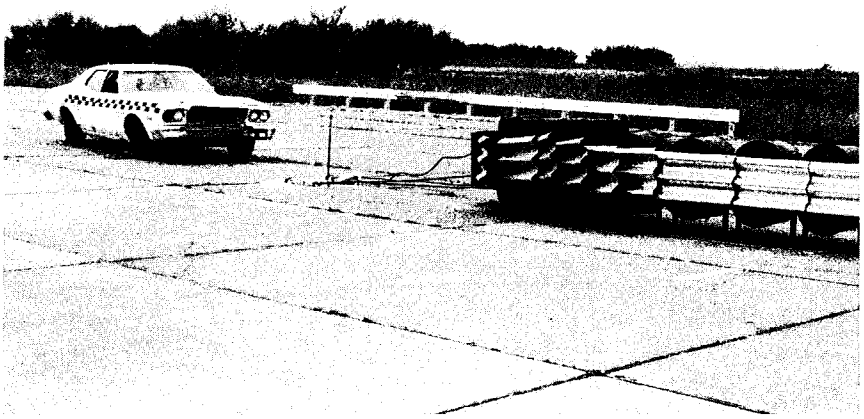

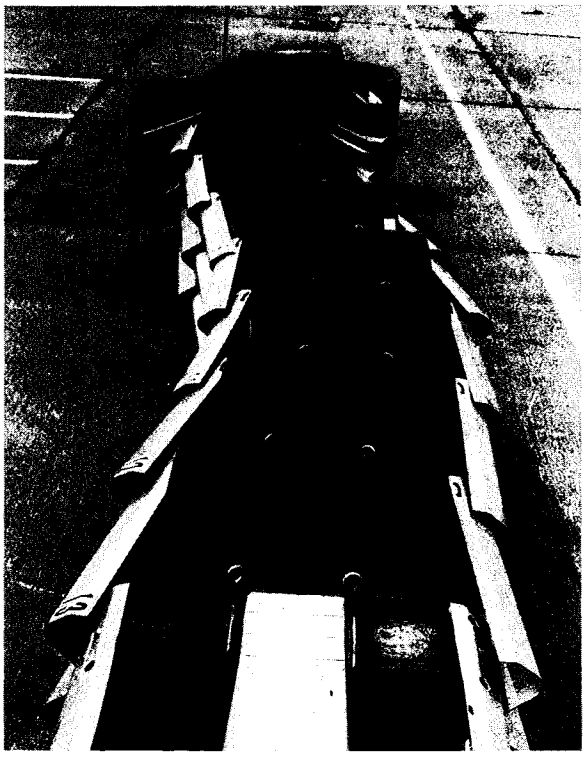

FIGURE 21 LOW MAINTENANCE END TREATMENT AFTER TEST 3

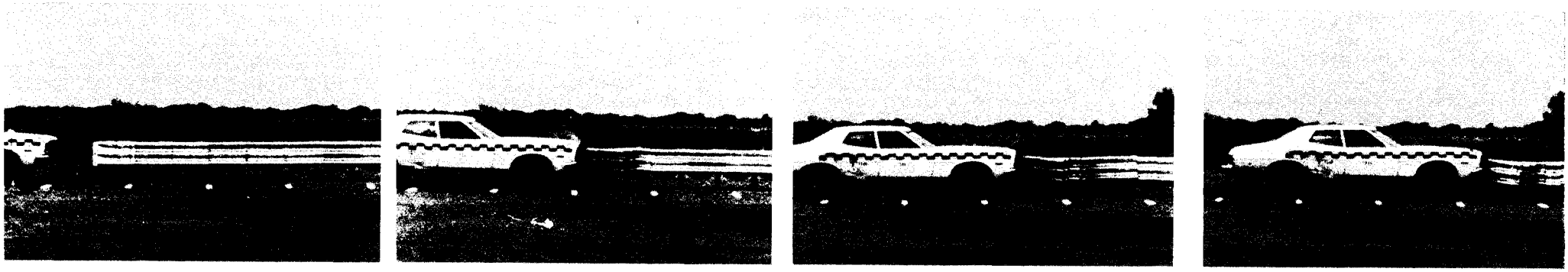

0.0 sec .172 sec .343 sec .515 sec

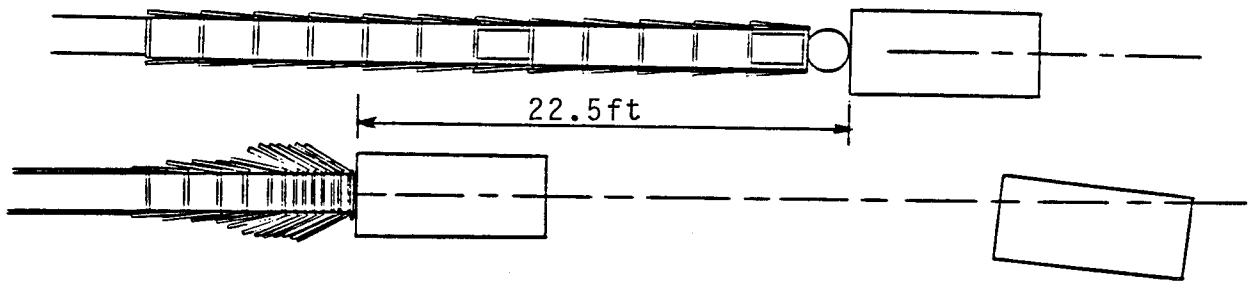

Test No.	2346-3
Date	7-19-85
Installation	
Drawing No.	LMET 1-5 (Figure 13)
Maximum crush ft(m)	22.5(6.86)
Vehicle	
Model	1975 Ford Grand Torino
Mass lb(Kg)	4390(1991)
Speed mph(Kph)	
Impact	51(82.1)
Exit	-7(-11.3)
Angle deg	
Impact	0
Occupant Impact velocity fps(m/s)	
Forward	22(6.71)
Lateral	*
Occupant ridedown accelerations g's	
Forward	7.7
Lateral	*
Vehicle damage	
TAD	12-FD-1
VDI	12FCMW1

Figure 22. Summary of Test 3

B. NCHRP 230 Compliance Testing

NCHRP Report 230 (4) recommends that four full-scale crash tests be conducted to evaluate an end treatment. In one of these tests an 1800 lb car is to impact the middle of the end treatment at 60 mph and 15 deg. Standard thrie-beam barriers and cable supported narrow end treatments utilizing thrie-beam fender panels have performed well under these test conditions (11,12). It was therefore concluded that this test was unnecessary, and it was eliminated from the matrix.

Test 4

Analysis of Test 3 showed that the hinges were being subjected to relatively high inertia forces as the fender panels were accelerated at approximately 200 G's. The hinges were again redesigned. The new hinges were fabricated from 3/4-inch steel pipe, 3/4-inch steel rod, and 1/8-inch steel plate. Compliance testing was then begun with a 1979 Honda weighing 1810 lb. impacting the end treatment at 58 mph and zero degrees. The center of the test vehicle was offset 16 inches from the center of the end treatment. The test vehicle was smoothly decelerated to a stop over a distance of approximately 17 ft. As the front of the car came to a stop, the rear began to spin around. As shown in Figure 23, the vehicle was yawed approximately 90 degrees from its original direction of travel when it stopped. Figure 24 summarizes results from Test 4.

Analysis of the test showed the redesigned hinges contacted adjacent fender panels and prevented the front five cylinders from collapsing completely. As a result, the longitudinal occupant impact velocity was 35.7 ft/sec, while the recommended value is 30 ft/sec and the maximum allowable value is 40 ft/sec. If the hinges had not prevented the front cylinders from collapsing completely, the test vehicle would have traveled approximately 2.5 in. further between impacts with each diaphragm and the occupant impact velocity would have been lower. There would have been very little additional speed reduction between diaphragms since, as discussed previously, the front of the end treatment behaves as an inertial cushion. The longitudinal occupant impact velocity can be estimated for this condition by integrating the vehicle's deceleration and adding 2.5 inches of free travel (no acceleration) after collapsing each cylinder. The predicted occupant impact velocity from this type of analysis is approximately 31 ft/sec.

As shown in Table 10, all other severity measures were within recommended limits (4). No components on the crash cushion were damaged, and it was restored to its original condition with less than four man-hours of labor. After the fourth test the hinges were notched to allow full compression of each cylinder.

Test 5

The fifth test involved a 1978 Mercury Grand Marquis, weighing 4500 lb, impacting the treatment head-on at 57 mph. The end treatment performed well and brought the vehicle to rest over a distance of approximately 23 ft. All measures of occupant risk were below recommended limits as shown in Table 10. The vehicle rebound velocity of 10.5 mph is not substantially higher than exit velocities measured from tests of the GREAT (13,14). Figure 25 summarizes the results of Test 5.

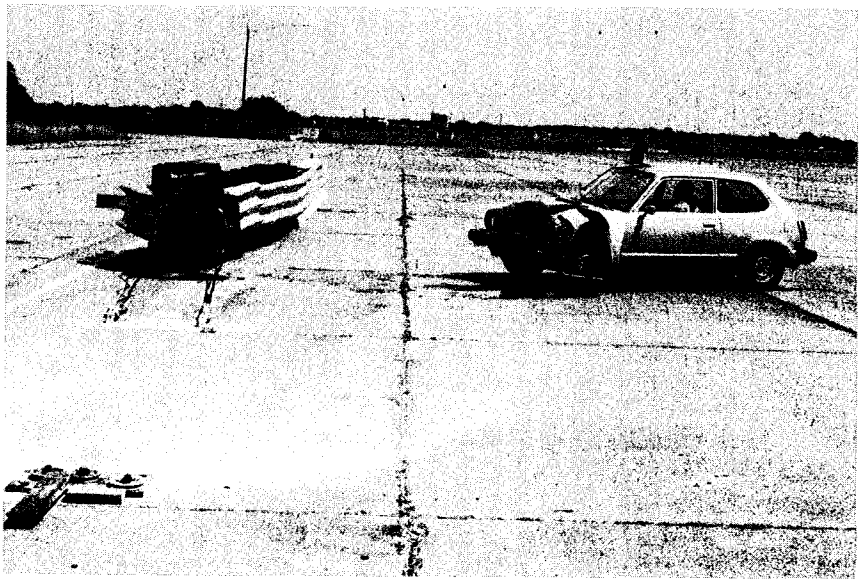

a) Test vehicle and End Treatment after Test 4

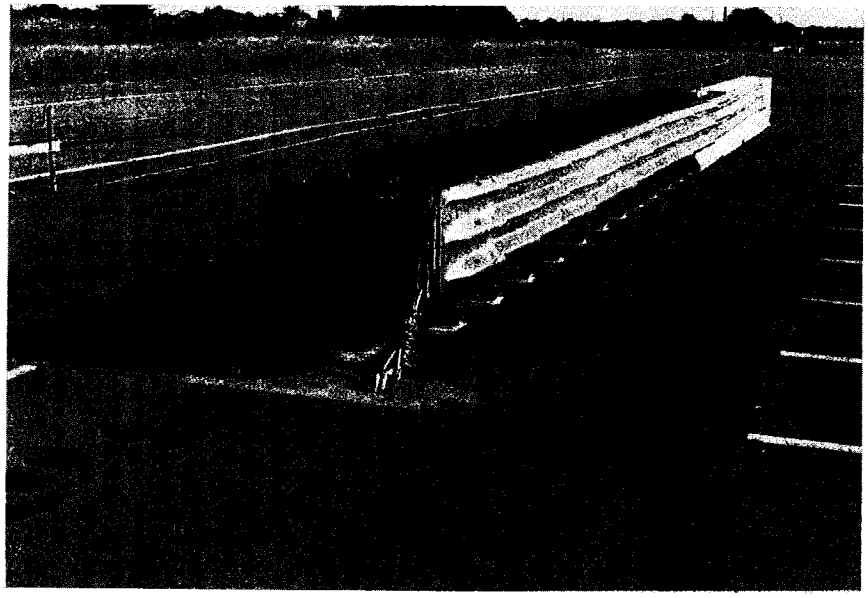

b) End Treatment after Restoration

FIGURE 23 VEHICLE AND END TREATMENT DAMAGE AFTER TEST 4

.691 sec

.391 sec

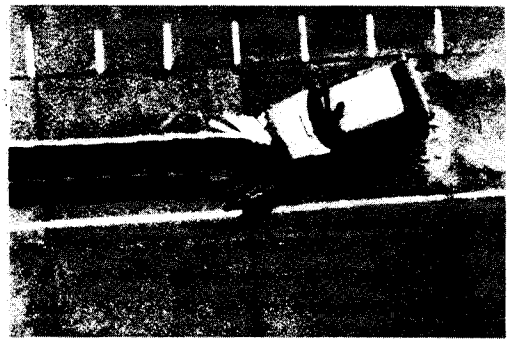

.196 sec

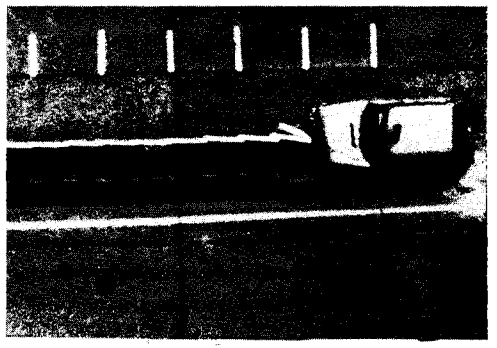

.065 sec

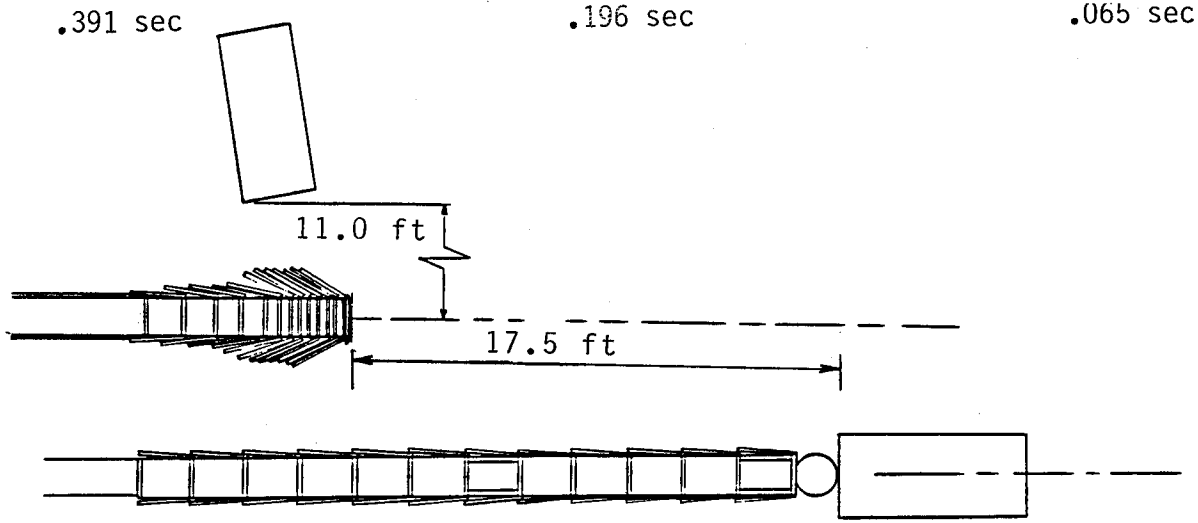

Test No..... 2346-4
Date..... 7-26-85
Installation
    Drawing No..... LMET 1-5
    (Figure 13)
Maximum crush ft(m)..... 17.5(5.33)
Vehicle
    Model..... 1979 Honda Civic
    Mass lb(Kg)..... 1810(821)
Speed mph(Kph
    Impact..... 58(93.3)

Angle deg
    Impact..... 0
Occupant impact velocity fps(m/s)
    Forward..... 35.5(10.82)
    Lateral..... 4.2(1.28)
Occupant ridedown accelerations g's
    Forward..... 9.0
    Lateral..... 1.5
Vehicle damage
    TAD..... 11-FL-4
    VDI..... 11FLMW3

Figure 24 Summary of Test 4

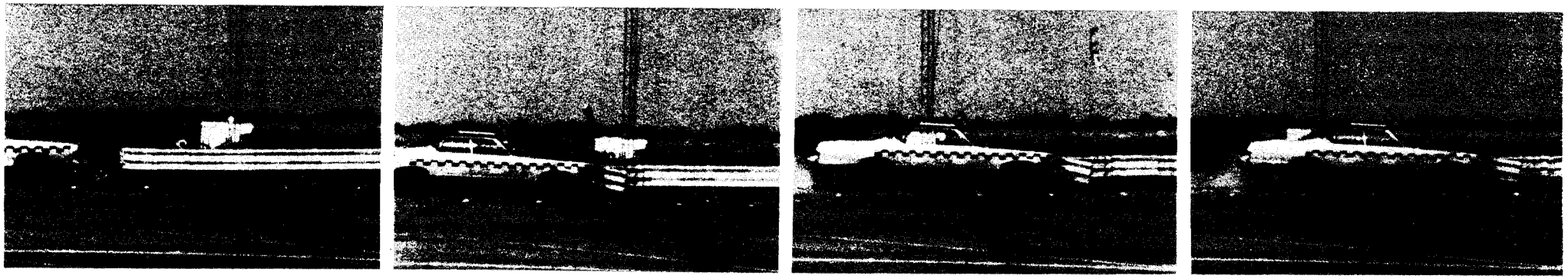

0.0 sec .126 sec .405 sec .712 sec

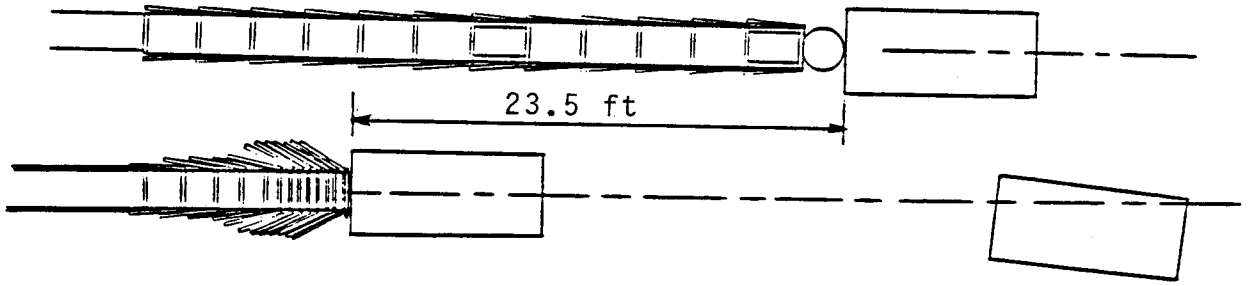

Test No..... 2346-5
Date..... 7-30-85
Installation
Drawing No..... LMET-(1-5)
(Figure 13)
Maximum crush ft(m)..... 23.5(7.16)
Vehicle
Model..... 1978 Mercury
Grand Marquis
Mass lb(Kg)..... 4500(2041)
Speed mph(Kph)
Impact..... 57(91.7)
Exit..... -10.5(-16.9)

Angle deg
Impact..... 0
Occupant impact velocity fps(m/s)
Forward..... 26.4(8.05)
Lateral..... N/A
Occupant ridedown accelerations g's
Forward..... 14.1
Lateral..... N/A
Vehicle damage
TAD..... 12-FD-4
VDI..... 12FCMW1

Figure 25 Summary of Test 5

The end treatment and test vehicle were damaged moderately as shown in Figure 26. One of the redirectional cables snagged on a diaphragm and was broken and one of the lightweight restoration cables was cut. As a result, the cushion could not be pulled back into position as in previous tests. In addition, there was minor damage to several of the hinges and the legs under the diaphragms. There was still minor contact between the 3/4-inch rods on the hinges and the fender panels. It was concluded that the hinges should be replaced with a flat plate design as shown in the construction drawings on Figure 15. This design will have strength slightly greater than the hinges used in the compliance testing and should eliminate all contact between adjacent diaphragms.

Repair of the end treatment was accomplished by replacing two 5/8-inch diameter lateral restraint cables and two 1/4-inch diameter restoration cables. It should be noted that the damaged lateral restraint cables were old and may have been frayed or damaged during previous tests. However, it is recommended that all lateral restraint cables be visually inspected after severe accidents.

Analysis of test films indicates that all of the test vehicle's rebound energy originated from the large diameter cylinders at the rear of the treatment. If the 10.5 mph exit velocity is a significant concern, vehicle rebound can be virtually eliminated by placing displacement limiting devices on the redirectional cables at the sixth diaphragm. These devices would allow the diaphragms to be freely pushed backward during impact, but would limit any rebound motion of the diaphragm after the vehicle stopped.

Test 6

The final test involved a 4420 lb Ford Ltd impacting the end treatment at 61 mph and an encroachment angle of 25 deg. The center of the test vehicle was directed at the center of the concrete barrier end. This is believed to be a critical set of side impact conditions and is intended to determine if the vehicle will snag on the end of the concrete barrier. Figure 27 gives a summary of Test 6.

Upon impact the end treatment deflected laterally approximately 2 ft. As the vehicle was being redirected the anchor bolts supporting the concrete barrier fractured, allowing the concrete barrier to slide laterally approximately 5 inches. As the concrete barrier deflected, it also tilted away from the impacting vehicle exposing the lower surface of the barrier. As a result both of the left side wheels on the test vehicle contacted the lower surface of the concrete barrier. This generated relatively high impact forces on the car and the 33 ft/sec change in vehicle velocity was higher than the recommended limit of 22 ft/sec. Although barrier anchorage for field installations would likely be more substantial and eliminate the aforementioned problem, it is recommended that the barrier end be transitioned to a vertical wall. The vertical face of the barrier should be set back at least 6 inches from the face of the end treatment to further reduce the likelihood of such an occurrence.

The end treatment was not damaged heavily for a test of this severity as shown in Figure 28. Repair would have been limited to the replacement of the last diaphragm, two thrie-beam fender panels, one wood block-out on the face

a) Test Vehicle Damage

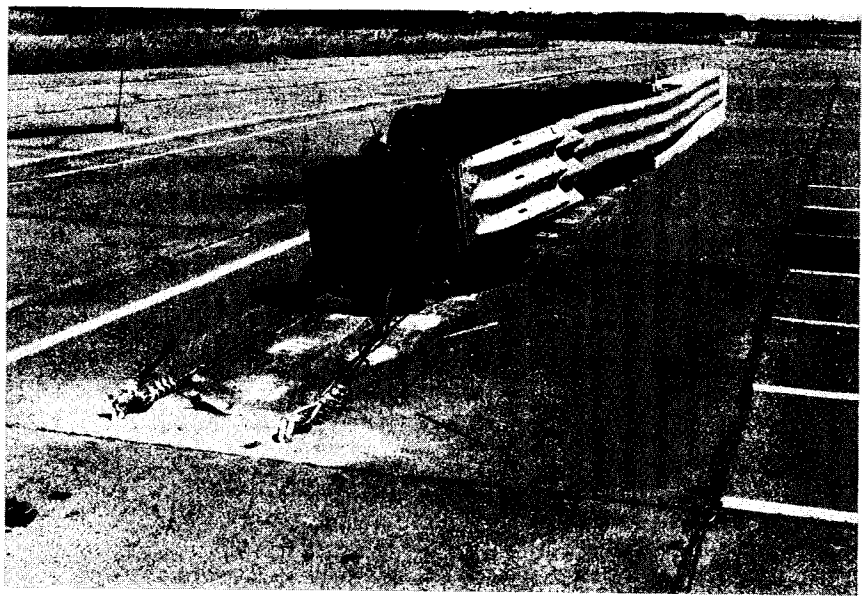

b) End Treatment Damage

FIGURE 26 TEST VEHICLE AND END TREATMENT AFTER TEST 5

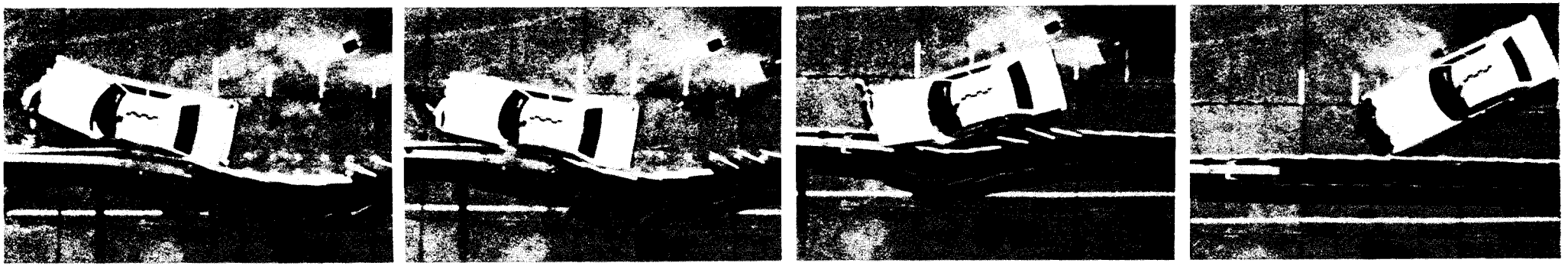

.334 sec .267 sec .134 sec o.o sec

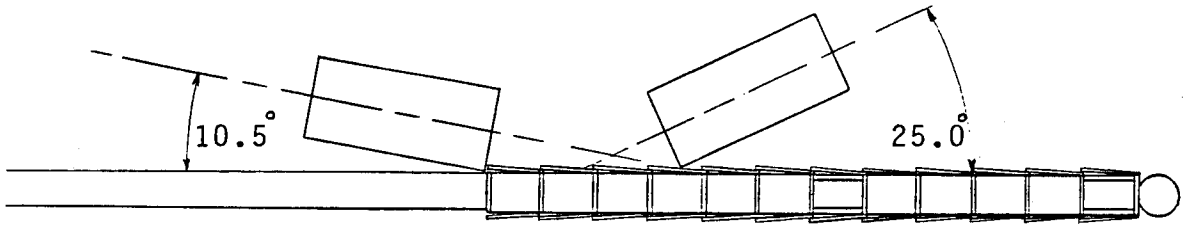

Test No..... 2346-6
Date..... 8-6-85
Installation
Drawing No..... LMET-(1-5) (Figure 13)
Maximum crush ft(m)..... *
Vehicle
Model..... 1978 Ford Ltd
Mass lb(Kg)..... 4420(2005)
Speed mph(Kph)
Impact..... 61(98.2)
Exit..... 36(57.9)

Angle deg
Impact..... 25.0
Exit..... 10.5
Occupant impact velocity fps(m/s)
Forward..... 32.7(9.97)
Lateral..... 18.9(5.76)
Occupant ridedown accelerations g's
Forward..... 20.9
Lateral..... 32.5
Vehicle damage
TAD..... 11-LD-7
VDI..... 11LYES2

Figure 27 Summary of Test 6

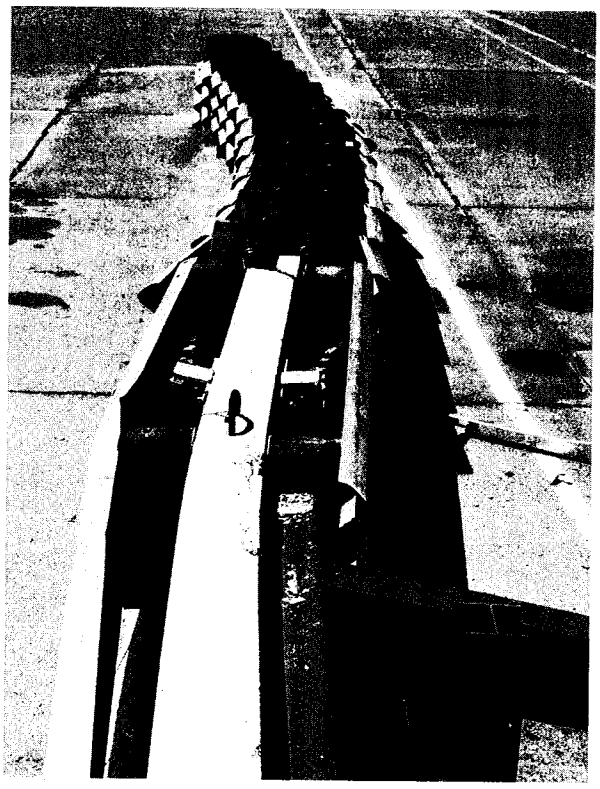

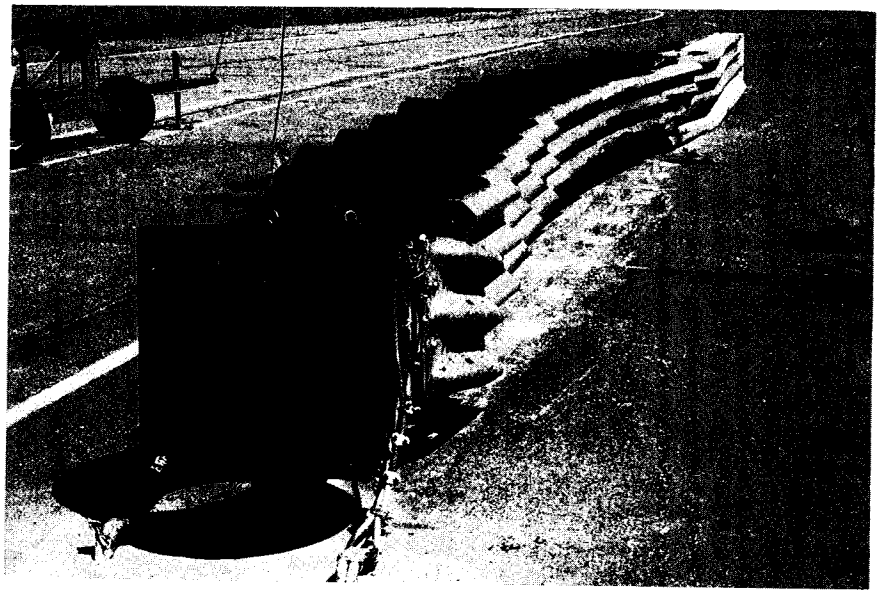

FIGURE 28 LOW MAINTENANCE END TREATMENT AFTER TEST 6

of the concrete barrier, and one redirectional cable. No rubber cylinders showed any sign of damage. As in most impacts of this severity, the test vehicle, shown in Figure 29, sustained considerable damage.

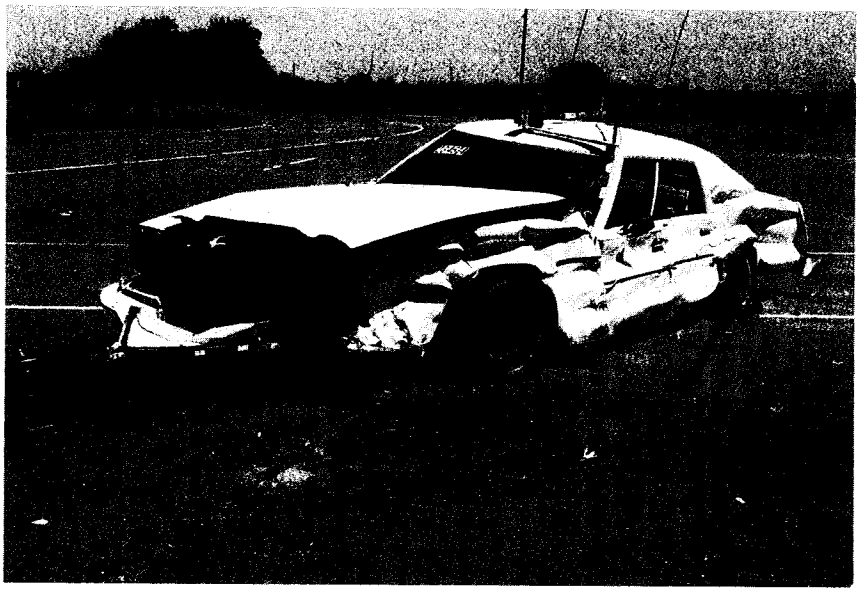

FIGURE 29 TEST VEHICLE DAMAGE AFTER TEST 6

V. CONCLUSIONS AND RECOMMENDATIONS

Three major problems associated with the use of concrete safety shaped barriers on the roadside have been addressed, including (1) guidelines for the use of concrete barrier on the roadside, (2) analysis of concrete barrier footing requirements, and (3) development of a low maintenance crash cushion end treatment for roadside concrete barriers.

A benefit/cost analysis procedure was used to compare the benefits and costs associated with the use of W-beam guardrail and the concrete safety shaped barrier on the roadside. Figure 6 shows the resulting guidelines.

To support the concrete barrier on the roadside, it is recommended that a paved shoulder be used. It should be of sufficient width to provide the necessary shoulder width and support the barrier. This will minimize problems with roadway drainage and vegetation control. Recommendations are also presented regarding barrier anchorage to prevent lateral movement during vehicular impacts.

A low maintenance end treatment for concrete barriers has been successfully designed and crash tested. The cushion (1) has no sacrificial energy absorbing elements, (2) has sufficient strength to withstand most impacts without damage to any components, (3) is not significantly wider than the standard concrete safety shaped barrier, and (4) has been shown to meet nationally recognized safety standards (4). Rubber cylinder energy absorbing elements used in the design have withstood six relatively severe crash tests with little damage.

The end treatment described herein represents a significant step toward reducing maintenance costs associated with such devices. It is not damaged during impacts with small cars traveling at speeds up to 60 mph and large cars traveling at speeds up to 50 mph. For these accidents the end treatment can be repaired in less than an hour and the total repair costs are usually below $100. These impact conditions include over 95% of expected head-on accidents (15). Further, even relatively severe side impacts do not cause major damage to the system. Finally, the design concepts proven in this study can probably be adapted to conventional crash cushions with a similar reduction in maintenance costs.

Finally, it is recommended that the end treatment developed in this study be installed on an experimental basis at several locations to examine its in-service performance. Minor design improvements discussed previously and shown in Figure 15 should be incorporated into field designs. Subject to its acceptable field performance, the end treatment can then be installed as an operational system.

REFERENCES

1. Calcote L. R.,"Development of a Cost-Effectiveness Model for Guardrail Selection", FHWA Report No. FHWA-RD-78-74, January, 1980

2. Sicking, Dean L., and Ross, Hayes E. Jr., "Benefit/Cost Analysis of Roadside Safety Alternatives", Transportation Research Record Transportation Research Board, Washington D. C., (in publication)

3. Ross, Hayes E. Jr., and Sicking, Dean L., "Guidelines for Use of Temporary Barriers in Work Zones", Final Report on Contract DOT-FH-9688, Texas Transportation Institute, Texas A&M University System, College Station, Texas, July 1983.

4. Michie, Jarvis, D., "Recommended Procedures for the Safety Performance Evaluation of Highway Appurtenances," National Cooperative Highway Research Program Report 230, March 1981.

5. Norsorex, Registered Trade Mark of Cdf Chimie S. A., Paris, France.

6. Sorbothane, Hamilton Kent, Division of BTR Inc., Kent, Ohio.

7. "Marine Dock Fenders", Goodyear Industrial Products Division, Akron, Ohio.

8. "Marine Fendering Systems", Uniroyal Inc., Marine Fender Systems, Mishawaka, Ind.

9. P. K. Freakley and A. R. Payne, Theory and Practice of Engineering with Rubber, Applied Science Publishers LTD, London, 1978.

10. Regal International, Inc., P. O. Box 1237, Corsicana, Texas

11. Sicking, D. L., and Ross, Hayes E. Jr., "An End Treatment for Narrow Objects," Transportation Research Record 942, Transportation Research Board, Washington D. C., 1983.

12. Ivey, D. L., Robertson, R. G., and Buth, C. E., "Test and Evaluation of W-Beam and Thrie-Beam Guardrails," Texas A&M Research Foundation, Texas A&M University System, March 1982.

13. "Impact Attenuators, A Current Engineering Evaluation", Test Report for Test No. 1625-C-01-84, FHWA Contract No. DTFH61-83-C-00140, Ensco Inc., Springfield, VA, Sept., 1984.

14. "Impact Attenuators, A Current Engineering Evaluation", Test Report for Test No. 1625-C-02-84, FHWA Contract No. DTFH61-83-C-00140, Ensco Inc., Springfield, VA, Sept., 1984.

15. Mak, King K., Sicking, D. L., and Ross, H. E. Jr., "Real World Impact Conditions", Transportation Research Record, Transportaion Research Board, Washington D. C., (in publication)

16. Buffington, J. Damon, "Selection of a Self-Restoring Energy Absorbing Medium for a Highway Safety Crash Cushion", Texas A&M University Dept. of Civil Engineering, College Station, Texas, November, 1983.

17. Mak, King K., Mason, Robert L., "Accident Analysis - Breakaway and Nonbreakaway Poles Including Sign and Light Standards Along Highways", Final Report, FHWA Contract DOT-HS-5-01266, Southwest Research Institute, San Antonio, Tx., August 1980.

18. Energy Absorption Systems Inc., One IBM Plaza, Chicago, Ill.

19. "Guide for Selecting, Locating, and Designing Traffic Barriers", American Association of State Highway and Transportation Officials, 1977.

APPENDIX I. TESTING OF RUBBER CYLINDERS

Mr. William Gaugler, research assistant under the supervision of the authors, conducted an in-depth laboratory study of rubber cylinders. Appendix I is a copy of Mr. Gaugler's research report, prepared in partial fulfillment of his M.E. degree requirements in Civil Engineering at Texas A&M University.

INTRODUCTION

The concrete safety shaped barrier has begun to be used as a permanent roadside barrier. Although it has proven to be a low maintenance barrier, the exposed end poses a serious hazard to the motorist. Several end treatments have been developed for this barrier. The end treatments primarily consist of inertial or energy absorbing crash cushions which have costly sacrificial components that are destroyed during impacts. A study was undertaken to develop a crash cushion/end treatment for concrete barriers that does not have sacrificial components. It was decided to evaluate the potential of using rubber as an energy absorbing median in a proposed end treatment shown in Figure 1. The chosen shape would have to satisfy energy absorption criteria for impact loading, ease of design and construction for future use, as well as economy in manufacturing. A cylinder was chosen as the shape that best met these criteria.

The objective of this phase of the study was to determine the static and dynamic response of hollow, circular cylinders loaded in radial compression. Also, included in this report are attempts to model the behavior of the rubber cylinders. Two viscoelastic behavior models were used for this part of the project.

THE MATERIAL

Rubber was chosen as the test material because of its energy absorbing characteristics. Natural rubber has good mechanical properties, high elasticity, and low hysteresis and is one of the most versatile of the general purpose elastomers (1). Mechanical

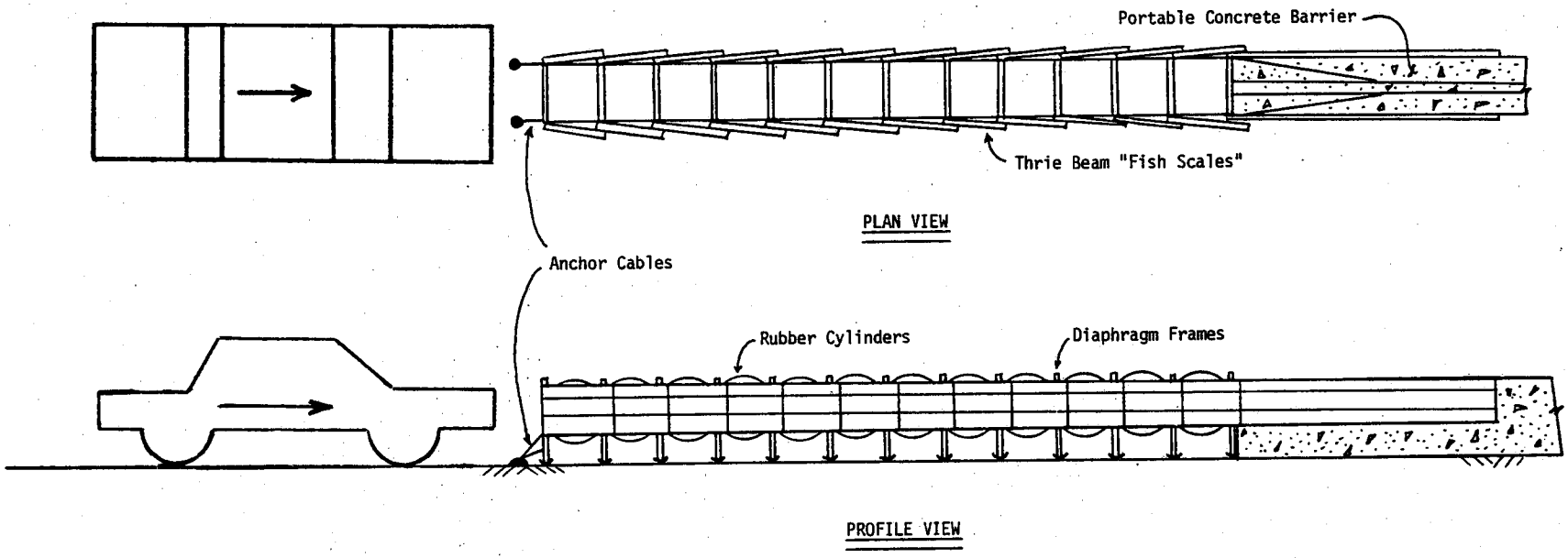

Figure I-1. - Conceptual Illustration of Proposed Crash Cushion

properties such as elongation, modulus of elasticity,hardness, and tear and abrasion resistance are important for this particular use of rubber and can easily be modified by changing the particular compound of rubber being used. Elasticity affects the rebound characteristics and energy absorbing capabilities of the crash cushion. Natural rubber's resitance to oxidation and ozone attack is poor, although this may be overcome by additives for most applications. Ozone attack is a surface condition that effects the appearance, but not the performance, of rubber over time.

The samples tested were one fifth scale models of the cylinders used in a preliminary design. All samples had an outside diameter of 4.8 in. and a length of 4.8 in. The cylinders had wall thicknesses ranging from .3 in. to 1.2 in. and durometer readings from 50 to 90. The four wall thicknesses are illustrated in Figure 2. Four compounds of rubber were tested, two natural rubbers, a synthetic rubber, and a neoprene. Table 1 is a sample matrix showing the wall thickness, hardness and material type for each cylinder. Table 2 gives the material specifications for several hardness ratings of natural rubber A.

TESTING

Selecting and determining the best test procedures were critical in meeting the objectives of the project. Generally, testing was divided into three phases. The first phase consisted of static, closed loop, and high rate dynamic testing. The second phase consisted of high and low rate tests, frozen sample tests, and accelerometer tests. The third phase consisted of the static

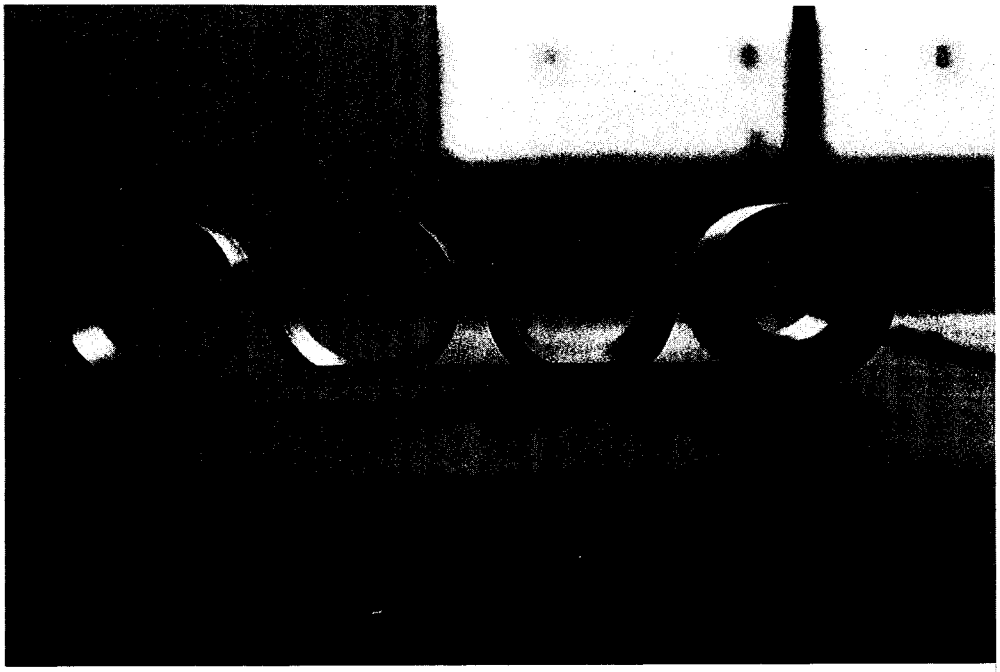

Figure I-2. - Illustration of Various Wall Thicknesses

TABLE I-1 Sample Matrix

Sample No.	Wall Thickness (in)	Hardness Durometer	Material Type
1	.30	50	N.R.-A
2	.30	60	N.R.-A
3	.30	70	N.R.-A
4	.30	80	N.R.-A
5	.45	50	N.R.-A
6	.45	60	N.R.-A
7	.45	70	N.R.-A
8	.45	80	N.R.-A
9	.60	50	N.R.-A
10	.60	60	N.R.-A
11	.60	70	N.R.-A
12	.60	80	N.R.-A
13	.30	85	Synthetic
14	.30	90	Synthetic
15	.45	85	Synthetic
16	.45	90	Synthetic
17	.60	85	Synthetic
18	.60	90	Synthetic
19	1.20	50	N.R.-A
20	1.20	60	Synthetic
21	1.20	85	Synthetic
22	1.20	90	Synthetic
23	.60	--	Neoprene
24	1.20	--	Neoprene
25	.31	80	N.R.-B
26	.44	80	N.R.-B
27	.63	80	N.R.-B
28	1.20	80	N.R.-B

and dynamic testing of full scale cylinders.

The static tests of scale model cylinders were run on an Instron testing machine. The samples were compressed to 90% of the inside diameter, and load deflection data were recorded. The samples were loaded at a rate of one inch per minute. The energy absorbed by the cylinder during static testing was calculated as the area under the force-deflection curve.

The closed loop test was conducted on the Material Testing System (MTS) hydraulic high rate test machine , as were all of the dynamic tests. The system included an MTS load frame, a digital function generator, a counter and display panel, a high rate control panel, and a transducer conditioner. The data was plotted using a HP 9845 computer and HP 9872 plotter. The MTS is capable of a maximum load of 20000 pounds in tension or compression. The system is capable of being operated in stroke control, strain control, or high rate modes. The velocity of the ram in the high rate mode is controlled by varying the flow rate of the hydraulic fluid through the system. The movement of the ram is controlled by the high rate control panel when the system is being operated in the strain control or stroke control modes.

In the closed loop test, a stroke control test, the impact plate is initially in contact with the sample, and the sample is loaded at a rate of about 17.5 in/sec. In this test the ram compresses a specified length and returns at a constant velocity. The load deflection data is recorded on the down and up strokes. The inertia effects of the system were found to be repeatable and were subtracted from the test data automatically by the

TABLE I-2 - Material Specifications for Natural Rubber A

PROPERTY	VALUE			
Durometer (Shore A)	50	60	70	80
Tensile Strength (psi)	3600	4145	3700	3715
Elongation (%)	623	670	530	596
Modulus at (psi)				
100% Elongation	175	245	345	615
200% Elongation	393	560	830	1678
300% Elongation	787	1100	1670	2668
Compression Set (%)		25	25	25

transducer conditioner. The test data were used in the viscoelastic behavior models (see page 22). The closed loop test configuration is shown in Figure 3.

High rate impact loading was also performed during Phase I of the testing. As shown in Figure 4 the load cell was placed below the support frame for the Phase I tests, and the sample was compressed until the support pegs were sheared off. The support pegs were used to provide a failure mechanism that would allow the ram to compress the cylinder with a constant velocity without fear of damaging the load cell. The pegs were designed to fail at a load that would fully compress all of the test samples. The samples were loaded at approximately 950 in/sec and force deflection data was gathered. However, the location of the load cell proved to be a problem during the high rate loading. Acceleration of the support frame was detected by the load cell. The support frame accelerations were caused by an upward movement of the entire MTS frame during the downward stroke of the ram. Further, because of the 45 lb weight of the support frame the inertia effects of the system overrode the test data. The inertia curves were not repeatable because the accelerations of the ram and frame were found to be inconsistent. Reducing the impact speed to 450 in/sec did not solve this problem. These difficulties led to the second phase of the testing.

Phase II testing consisted of high and low rate testing of the natural rubber and neoprene samples, as well as testing of frozen samples. In Phase II the load cell was placed above the impact plate to avoid the problems associated with Phase I testing, and the inertia data gathered in Phase II were

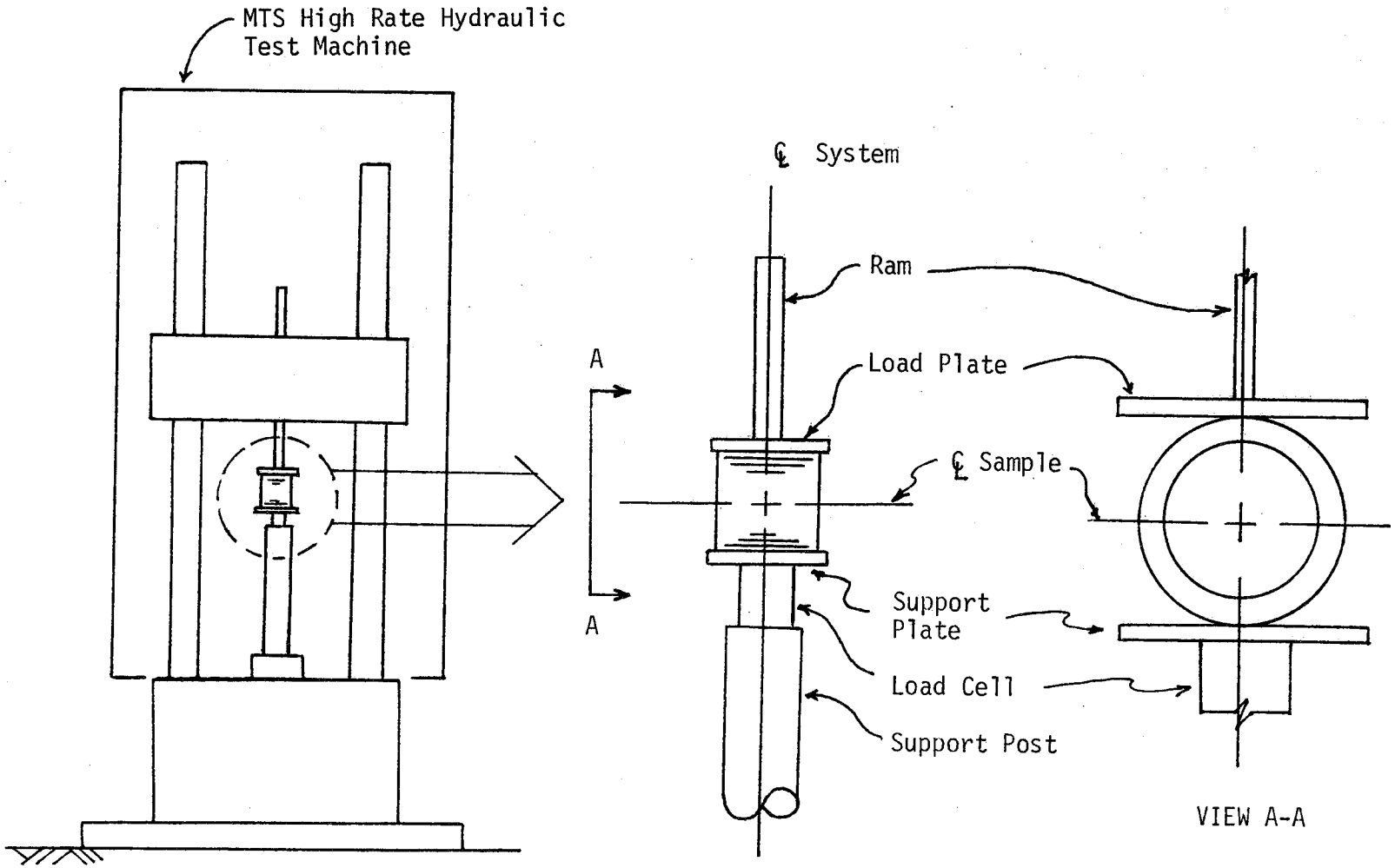

Figure I-3. - Closed Loop Test Configuration

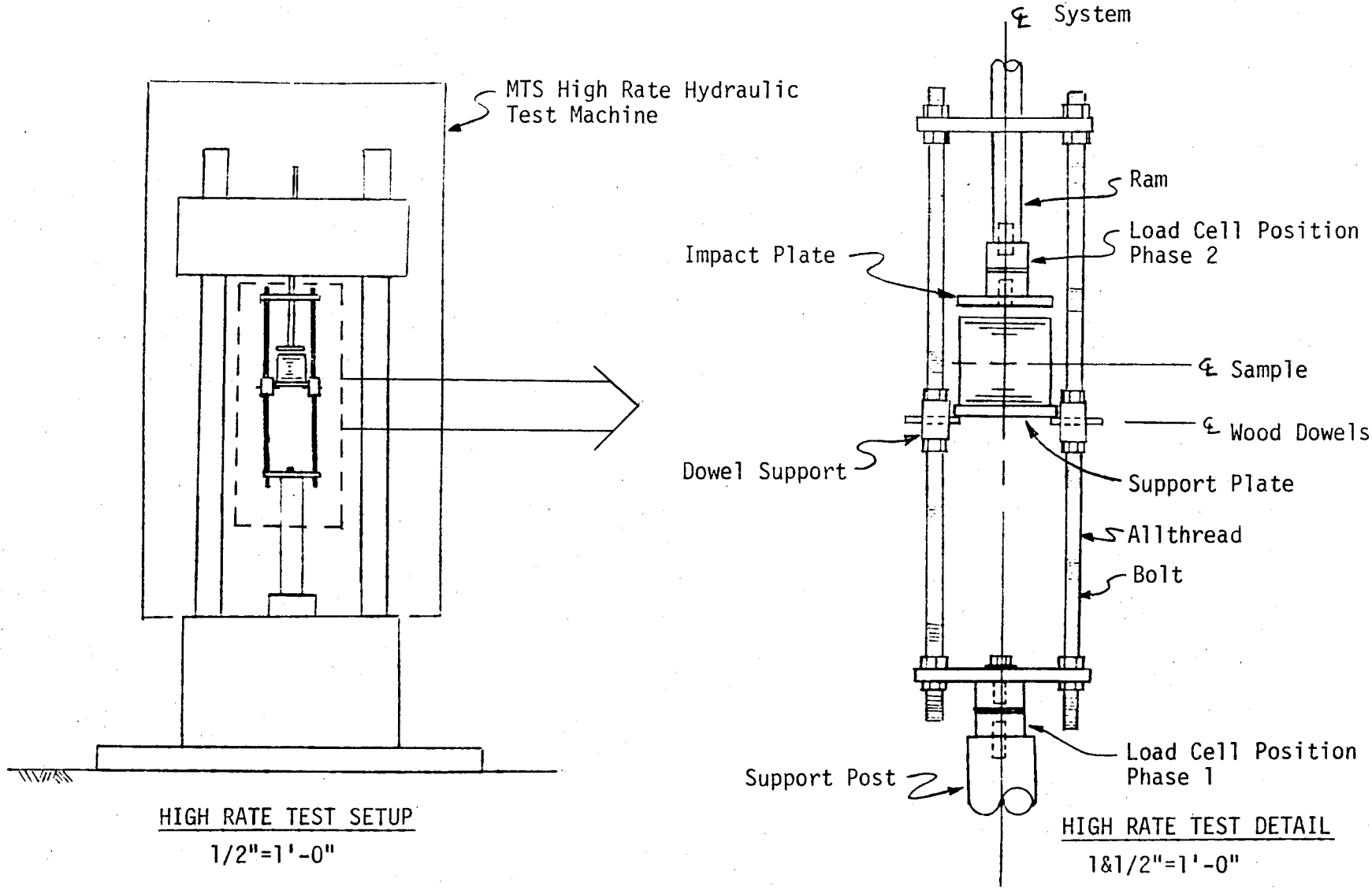

Figure I-4. - High Rate Test Configuration

reasonably consistent. Natural rubber and neoprene samples were impacted at 450 in/sec and 950 in/sec during this phase.

In addition to the high and low rate testing of Phase II an accelerometer was attached to the load cell to measure the acceleration of the impact plate. These tests were run in an effort to measure the inertia effects of the system, and they consisted of running a high rate test without a sample or support plate in position. By measuring the force and acceleration at each time step the mass below the load cell may be calculated from the relationship force equals mass times acceleration. If the mass below the load cell can be calculated, then the inertia effects of the system can be subtracted from the test results. The accelerometer was also used to gather acceleration data on the samples. However, the accelerometer was operating in its upper limits of acceptable accelerations and was damaged during this testing. The data gathered was not used to determine the energy absorbing characteristics of the cylinders.

Data from the accelerometer tests indicated that the acceleration of the ram was consistent when the high rate test machine was the only hydraulic test system in operation, and an inertia test was conducted after every third or fourth sample was tested. This was done to verify the consistency of the inertial effects.

Static testing of the full scale cylinders was conducted using a hydraulic jack in conjunction with an electronic load cell. As the cylinder was compressed the deflections were measured manually and the load was recorded. An illustration of

the test configuration is shown in Figure 5.

ENERGY CALCULATIONS AND SCALE MODELING

Data gathered from the dynamic testing is the total amount of energy imparted on the sample by the MTS. The purpose of the dynamic testing is to determine the amount of energy that a cylinder will absorb during dynamic loading. This may be calculated using the following equation.

$$DE = EI - E_t - E_{is} \qquad \text{Eq-1}$$

where,

DE = the amount of energy absorbed by the sample from dynamic loading

EI = the apparent energy imparted to the sample by the MTS as determined from the load cell output.

E_t = inertial energy of the MTS

E_{is} = energy associated with the inertia of the sample

Energy due to the inertia of the MTS system may be obtained by firing the load cell without a sample or support plate in place. When this is done the load cell measures a force that is approximately equal to the mass of the impact plate times its acceleration. The energy due to the inertia of the system is subtracted from the apparent energy imparted on the sample.

When the ram initially contacts the sample the inertia of the system may be accurately represented by the data obtained from a

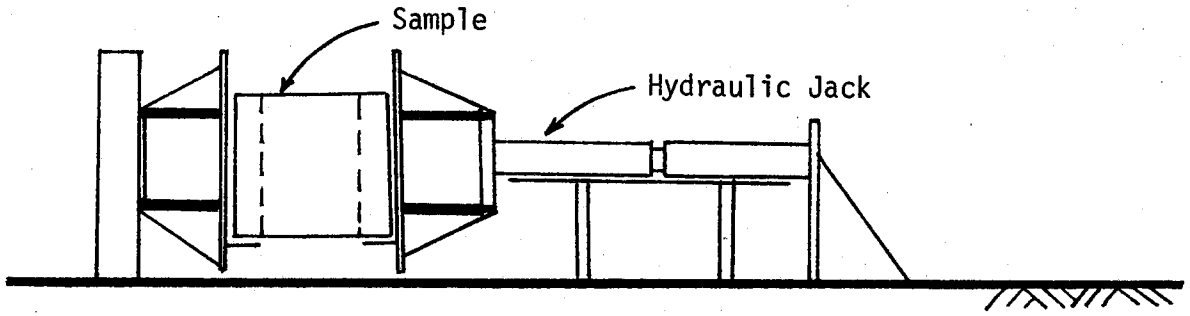

Figure I-5. - Full Scale Static Test Configuration

dry firing of the ram because the only mass that is moving is the impact plate. The mass that is being accelerated once the plate contacts the cylinder is continuously increasing with time. At the instant the support pegs fail the entire sample is moving at the velocity of the ram, and the kinetic energy of the system now includes the mass of the rubber cylinder as well as the mass of the impact plate. The kinetic energy associated with movement of the sample's mass is called the inertial energy of the sample (E_{is}). To calculate the kinetic energy of the sample at any given time the amount of mass in contact with the ram and the velocity of that mass must be known. Since the deformation behavior could not be determined within the scope of the study a constant value of one half the mass of the sample was assumed to be traveling at the velocity of the ram at the instant the pegs began to shear.

To relate test results from the small cylinders to the results from the full scale cylinders a scale modeling procedure was used. The procedure involved measuring the energy absorbed by the small cylinders in static and dynamic tests. The ratio of the dynamic energy absorbed to the static energy absorbed was defined as the dynamic magnification factor (DMF), and it was assumed to remain constant for a given diameter to wall thickness ratio. According to theory and published experimental results the slope of the static force-deflection curve is constant for a given diameter to wall thickness ratio (1,4). An example of the procedure is shown below.

EXAMPLE: SCALE MODELING PROCEDURE

Req'd: Compute the amount of energy absorbed by a cylinder that has a 28 in. outside diameter, 1.75 in. wall thickness, and is 24 in. long.

Sol'n: 1) Calculate the shape factor as

$$\frac{D}{T} = \frac{28}{1.75} = 16$$

2) Measure the static and dynamic response of a cylinder with the same shape factor (D=4.8 in, T=.30 in)

The static energy absorbed, SE = 152 in-lb

The dynamic energy absorbed, DE = 495 in-lb

3) Calculate the dynamic magnification factor (DMF) and the static stiffness from the test results.

$$DMF = \frac{DE}{SE} = \frac{495}{152} = 3.3$$

The static stiffness can be measured from the force-deflection curve as k=15 lb/in.

4) Calculate the deflection of the large cylinder as

$$x = D - 2T$$

$$= 28 - 2(1.75) = 24.5 \text{ in}$$

5) Calculate the predicted static energy absorbed by the large cylinder as

$$SE = \frac{1}{2} k x^2 \left(\frac{LL}{LS}\right)$$

where LL = length of large cylinder and

LS = length of small cylinder

$$SE = \frac{1}{2}(15)(24.5)^2 \left(\frac{24}{4.8}\right) = 22510 \text{ in-lb}$$

6) Calculate the predicted dynamic energy absorbed as

$$DE = SE * DMF$$

$$= 22510(3.3) = 74280 \text{ in-lb}$$

RESULTS

The closed loop test results were studied with the purpose of trying to obtain a better overall understanding of the behavior of the cylinders. This was primarily done using the viscoelastic behavior models that were developed. These models were used in an attempt to estimate the dynamic response of the cylinders. These models will be discussed in greater detail later, but generally they were unsuccesfull because the behavior was found to depend on several factors.

Other Phase I testing included static testing on an Instron. The data were used to determine the static stiffness and static energy absorbed. The static energy absorbed by the sample may be directly calculated from the Instron test results as the area under the force-deflection curve. Table 3 summarizes the static test results, and the force-deflection curves are plotted in Appendix A. The high rate test data gathered in Phase I was somewhat erratic because of the problems associated with the test configuration. The data was not used because of this problem.

With the load cell placed on top of the impact plate and the support frame secured to the MTS the data collected during Phase

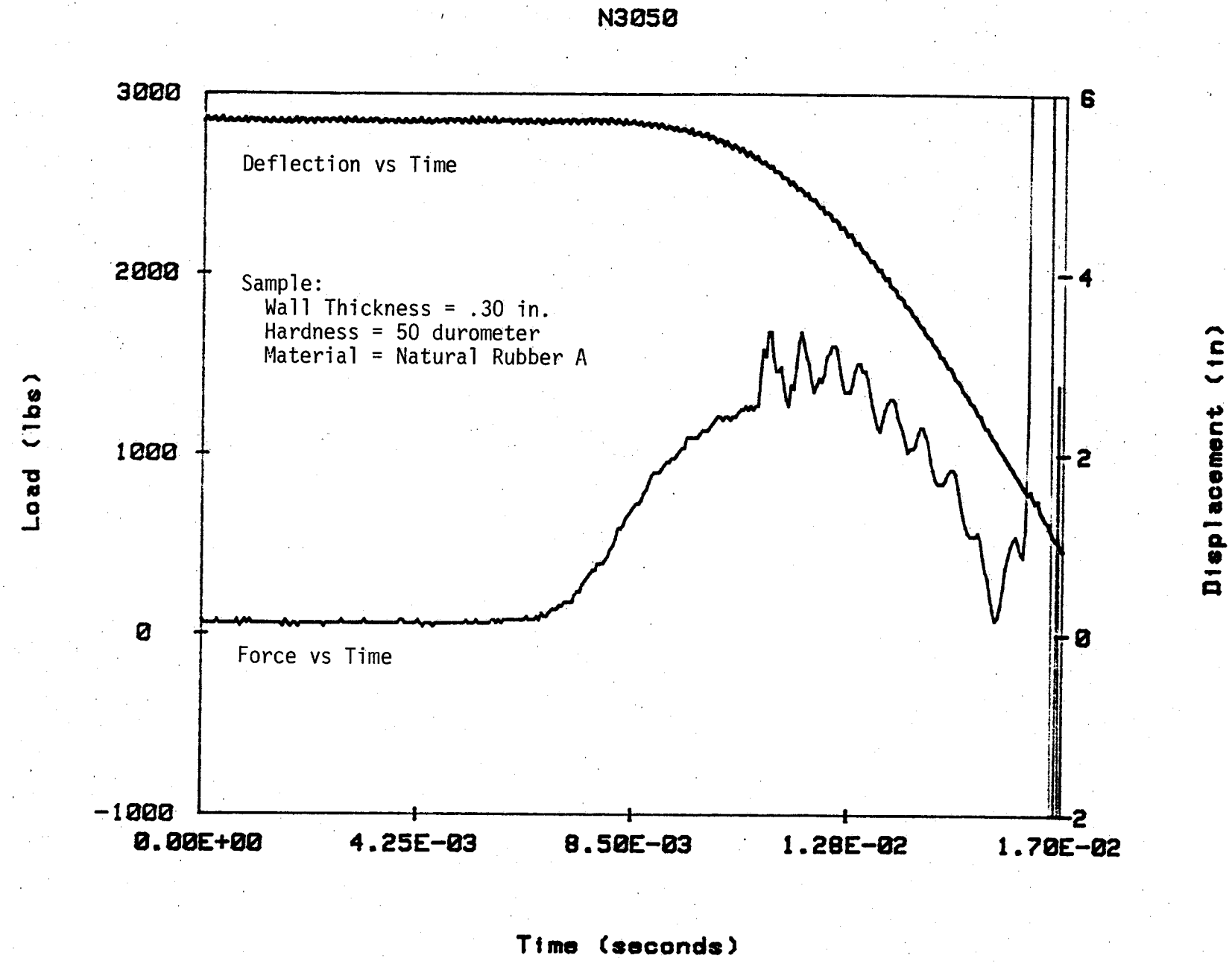

Figure I-6. - Sample Output From Phase II High Rate Testing

TABLE I-3 - Static Test Results

Sample Wall Thickness (in)	Hardness (durometer)	Static Energy Absorbed (in-lb) Unfrozen	Frozen
.30	50	35	
.30	60	58	
.30	70	95	
.30	80	152	182
.30	85	206	
.30	90	717	
.45	50	85	
.45	60	140	
.45	70	223	
.45	80	330	443
.45	85	344	
.45	90	1308	
.60	50	158	467
.60	60	271	
.60	70	466	562
.60	80	616	837
.60	85	619	
.60	90	1963	
.60	N	413	
1.20	50	453	
1.20	60	743	
1.20	85	1631	
1.20	80	1536	1953
1.20	90	2494	
1.20	N	1026	
.31	80	126	155
.44	80	322	378
.63	80	537	691

II testing produced a repeatable inertia curve. The accelerometer was used to measure acceleration data of the samples, however the accelerometer broke shortly after this testing began and the data was not used.

The force-deflection curves that were plotted from MTS data clearly indicate the point of contact and point when the support pins began to shear. Figure 6 shows a sample of output from the high rate testing performed in Phase II. The load deflection curves were integrated to calculate the amount of energy absorbed by the sample. The integration procedure calculated the energy absorbed by the sample as the area under the force-deflection curve while subtracting the inertia effects as shown in Equation-1. Plots of energy absorbed and deflection were made for the samples. Table 4 gives a summary of the dynamic testing performed at room temperature, and the results are plotted in Appendix C.

For these cylinders to perform under the desired service conditions they must be able to withstand extremes in temperature. For this application high temperatures are less critical than low ones. When the temperature goes below the brittleness temperature, or glass temperature, of the compound the sample can shatter on impact. Also, prior to reaching the brittleness temperature a sample of natural or synthetic rubber will exhibit a marked increase in stiffness. This increase in stiffness means that a greater percentage of the energy dissipated in a collision will be absorbed by the impacting vehicle.

TABLE I-4 - Summary of Dynamic Tests

Sample Wall Thickness (in)	Hardness (durometer)	Dynamic Energy (in-lb)	Static Energy (in-lb)	D:F
.30	50	340	35	9.7
.30	60	435	58	7.5
.30	70	330	95	3.5
.30	80	495	152	3.3
.45	50	160	85	1.9
.45	60	265	140	1.9
.45	70	480	223	2.2
.45	80	535	330	1.6
.60	50	817	158	5.2
.60	60	530	271	2.0
.60	70	850	466	1.8
.60	80	920	616	1.5
.60	N	1270	413	3.1
1.20	50	1630	453	3.6
1.20	60	2900	743	3.9
1.20	80	1310	1536	0.9
1.20	85	4026	1631	2.5
1.20	N	1760	1026	1.7
.31	80	310	126	2.5
.44	80	655	322	2.0
.63	80	1400	537	2.6

Static and dynamic testing was performed on seven cylinders that were stored for three days at zero degrees Farenheit. The seven cylinders were made of two natural rubber compounds. Compound B is supposed to be less sensitive to cold temperatures than compound A. This is supported in Table 5 which summarizes the static testing of the frozen samples. However, the dynamic test results, shown in Table 6, indicate a mixed performance of the two samples.

Several samples were impacted at about 30 mph during Phase II of the testing. The results of these tests are tabulated in Table 7. The table also shows the results of the high rate loading for comparison.

The results of the static testing of the full size cylinders are shown in Table 8. The average energy absorbed by the thin wall cylinder was 23910 in-lb, while the thick wall cylinder absorbed 180360 in-lbs. on average. The thick wall cylinder absorbed 231600 in-lbs. of energy in a full scale dynamic test. The cylinder was impacted with a 5200 lbs cart traveling at about 10 mph. The force-deflection curves for the full scale static tests are plotted in Appendix B.

MODELING

For a material to realize its full potential of use in engineering the designer must have some way of being able to predict the behavior of that material. A secondary odjective of this project was to develop a mathmatical model that would sufficiently predict the behavior of the test cylinders. With this goal in mind two viscoelastic behavior models were

TABLE I-5 - Summary of Frozen, Static Testing

Sample Wall Thickness (in)	Hardness (durometer)	Energy Absorbed Unfrozen (in-lb)	Energy Absorbed Frozen (in-lb)	% Change
.30	80	152	182	19.7
.45	80	330	443	34.2
.60	80	616	837	35.9
.31	80	126	155	23.0
.44	80	322	378	17.4
.63	80	537	691	28.7
1.20	80	1536	1953	27.2

TABLE I-6 - Summary of Frozen, Dynamic Testing

Sample Wall Thickness (in)	Hardness (durometer)	Energy Absorbed Unfrozen (in-lb)	Energy Absorbed Frozen (in-lb)	% Change
.30	80	575	475	(17.4)
.45	80	755	1425	88.7
.60	80	1140	1750	53.5
.31	80	310	405	30.6
.44	80	655	545	(16.8)
.63	80	1400	2310	65.0
1.20	80	1310	2530	93.1

TABLE I-7 - Comparison of results for high and low rate dynamic testing.

Sample Wall Thickness (in)	Hardness (durometer)	Velocity (in/sec)	Deflection (in)	Dynamic Energy (in-lb)
.30	80	450	3.75	460
		950	3.75	495
.45	80	450	3.50	895
		950	3.50	535
.60	80	450	3.25	1080
		950	3.25	920
1.20	50	450	2.00	1006
		950	2.00	1630
1.20	60	450	2.00	3215
		950	2.00	2900
1.20	85	450	2.00	4330
		950	2.00	4026

TABLE I-8 - Full Scale Static Test Results and Scale Modeling Predictions

Sample Wall Thickness (in)	Outside Diameter (in)	Length (in)	Static Energy Measured (in-lb)	Static Energy Predicted (in-lb)	Dynamic Energy Measured (in-lb)	Dynamic Energy Predicted (in-lb)
1.75	28	24	23940	22510	----	74280
1.75	28	24	23880	22510	----	74280
4.50	28	24	180360	134640	231600	215400

developed.

When the brittleness temperature is below service conditions elastomers can have both elastic strain and viscous flow (2). this condition is generally refered to as viscoelasticity. In the simplest situation, known as the Maxwell model, the behavior of rubber may be represented by a mass supported by a spring and dashpot in parallel. The governing equation of motion for this model is

$$F = kx + cv + ma \qquad \text{Eq-2}$$

where, F = the applied force

k = the spring constant

c = the damping coefficient

m = the mass of the sample

x = displacement of the impact plate

v = velocity of the impact plate

a = acceleration of the impact plate.

Integration of the force over the length of the compression stroke will produce the work done while compressing the sample. The derivation of Eq-2 is given in Appendix D. Examination of Eq-2 indicates that the behavior of the sample depends on several properties.

By rearranging Eq-2, the damping coefficient was computed at each time step using the data from the dynamic tests. An average value for the damping coefficient was calculated for the samples,and relationships between damping coefficient and

velocity or displacement were computed.With a known relationship for the damping coefficient the deflection data were used to calculate an applied force. This predicted force was integrated over the length of the stroke to compute an estimated value for the energy imparted on the sample. Predicting the amount of energy absorbed by a sample using the Maxwell model produced results that were not reasonable when compared to test results.

Because of the poor results obtained using the Maxwell model a more sophisticated mass-spring-dashpot model was developed. In this model the cylinder was represented by four lumped masses connected by weightless rods. A complete derivation of this model is given in Appendix D. Although the governing equation is somewhat more complicated than the one for the Maxwell model, the basic form is the same. Also, similar results were obtained when trying to predict the amount of energy that the cylinders would absorb. It was concluded that the behavior of the cylinders was more complicated than that which could be predicted using simple, viscoelastic models.

CONCLUSIONS

A method of testing and measuring the response of the rubber cylinders to static and dynamic loading was developed during the project. Using the MTS data in conjunction with the static load-deflection data the amount of energy absorbed by the sample due to dynamic loading only may calculated after accounting for the inertial effects involved.

Tests on numerous samples were conducted at high and low rates. The findings from these tests, in general, indicate for a

given durometer reading the thicker wall samples will absorb more energy than the thin wall samples, and for a given wall thickness the higher durometer samples require more energy to compress than the samples with a lower hardness. Also, several samples were frozen and tested to measure the effects that subfreezing temperatures would have on the stiffness and energy absorbing capabilities of the cylinders. The frozen sample testing indicated that a natural rubber compound would perform best under cold temperatures. A scale modeling procedure was developed to predict the amount of energy a full size cylinder would absorb.

In addition, two attempts were made to mathematically model the behavior of the cylinders. Two simple viscoelastic models consisting of mass, spring, and dashpot combinations were derived. The results of this portion of the study indicated that the behavior of the cylinders could not be accurately predicted using simple viscoelastic models.

APPENDIX A

FIGURE-A1

STATIC TEST RESULTS
(SAMPLES: .30"-50 , .30"-60 & .30"-70)

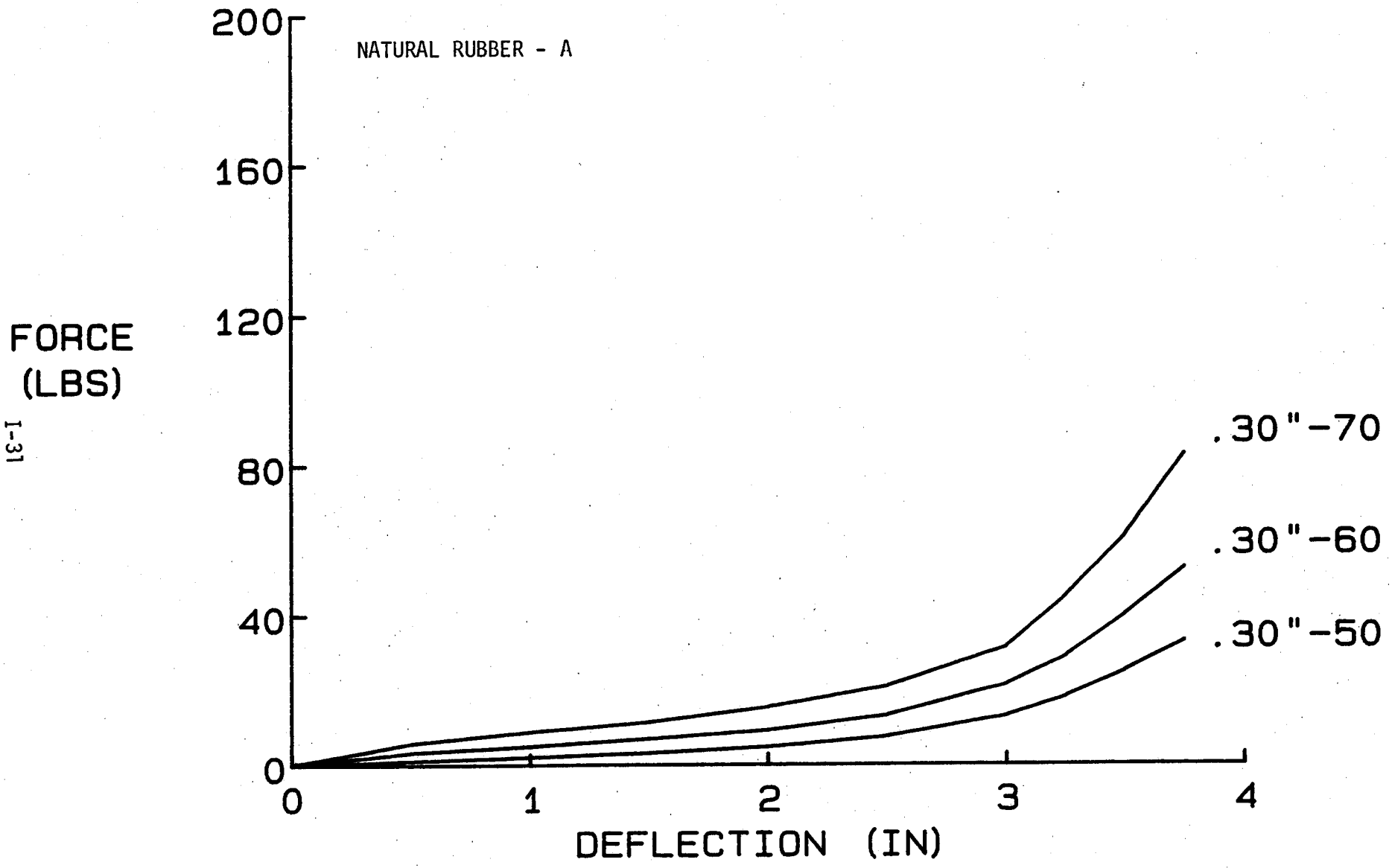

FIGURE - A2

STATIC TEST RESULTS
(SAMPLE .30"-80: FROZEN AND UNFROZEN)

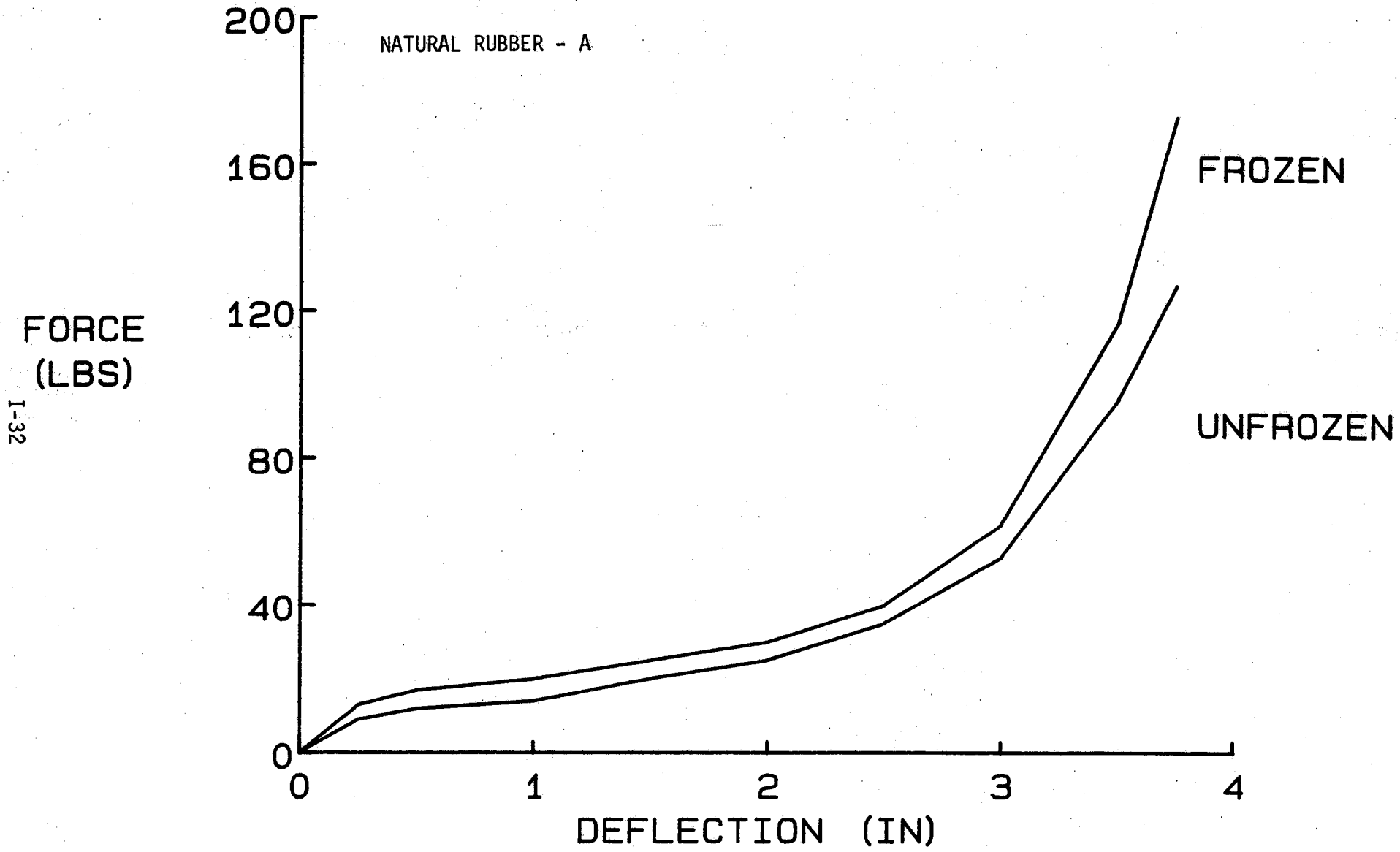

FIGURE - A3

STATIC TEST RESULTS
(SAMPLE .45"-80: FROZEN AND UNFROZEN)

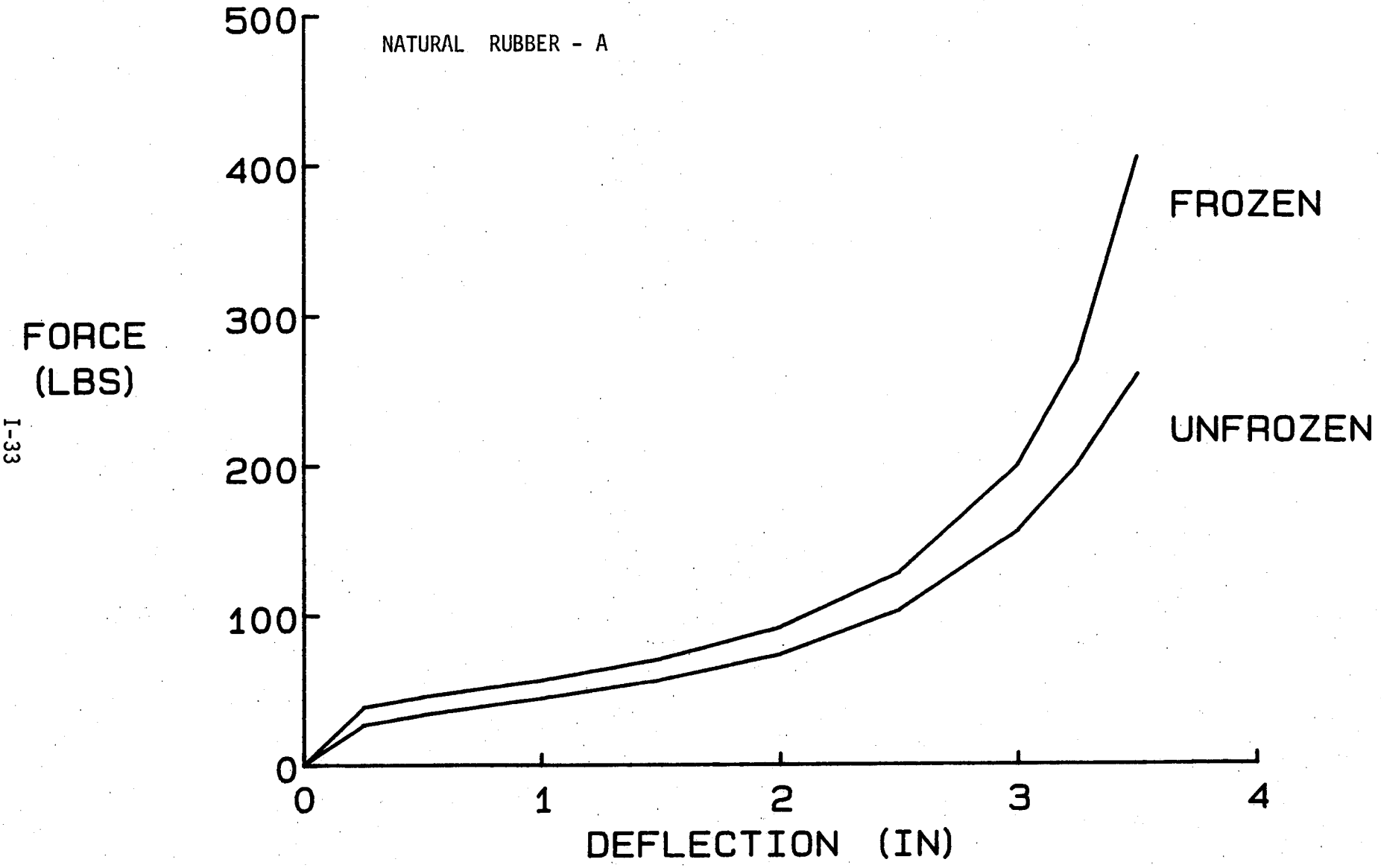

FIGURE - A4

STATIC TEST RESULTS

(SAMPLES: .45"-50, .45"-60 & .45"-70)

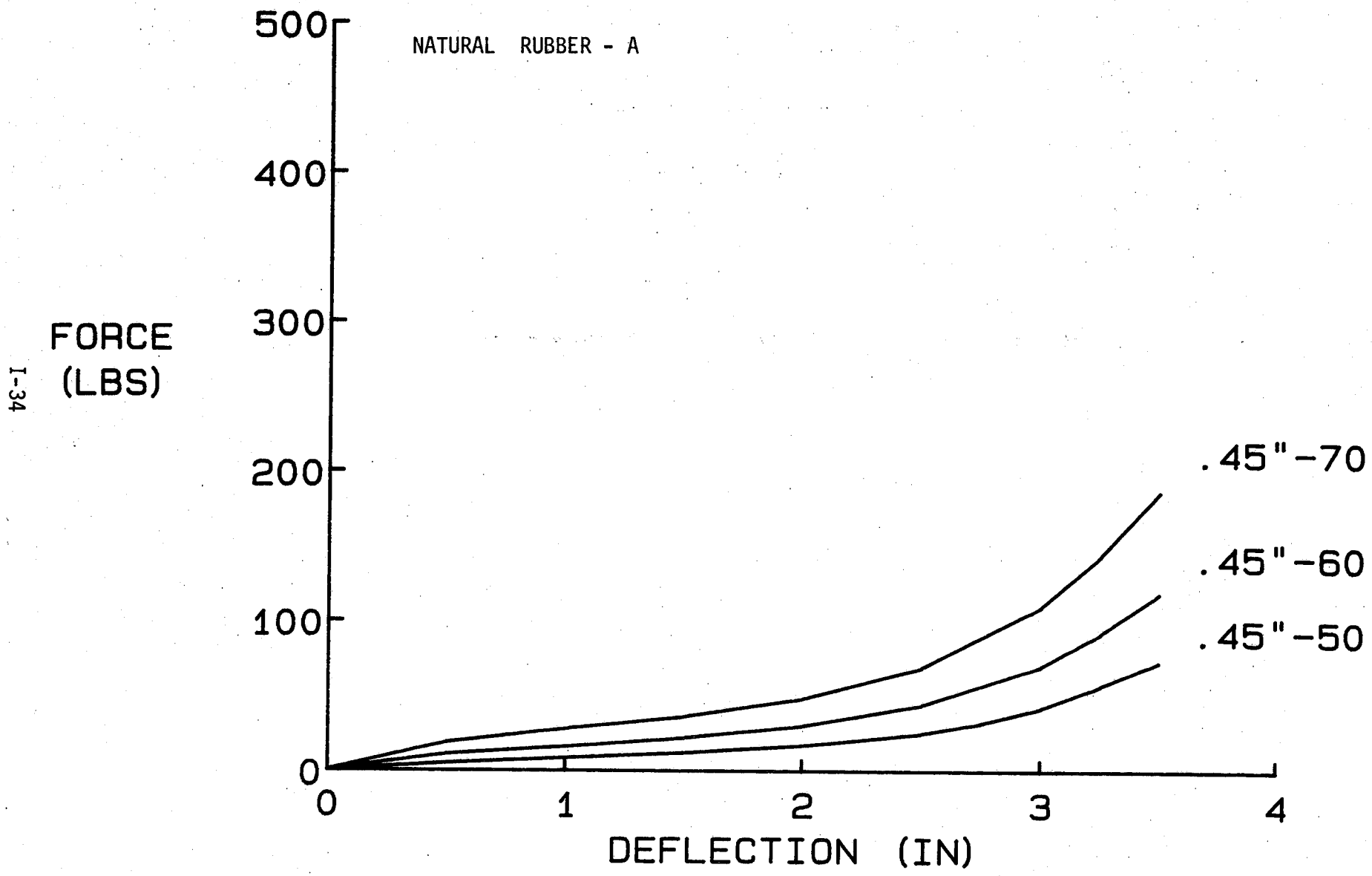

FIGURE - A5

STATIC TEST RESULTS
(SAMPLE .60"-80: FROZEN AND UNFROZEN)

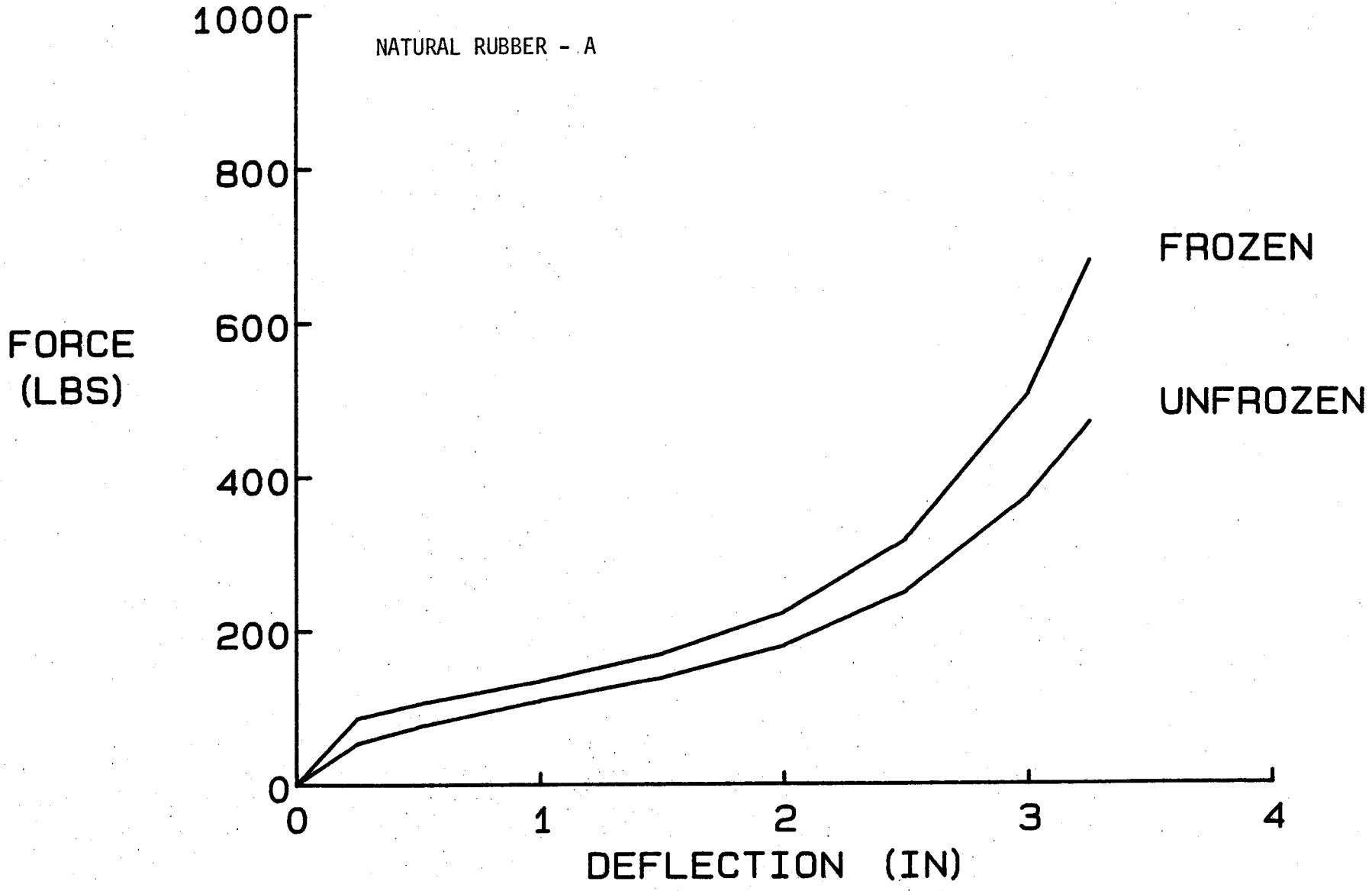

FIGURE - A6

STATIC TEST RESULTS
(SAMPLE .60"-50: FROZEN AND UNFROZEN)

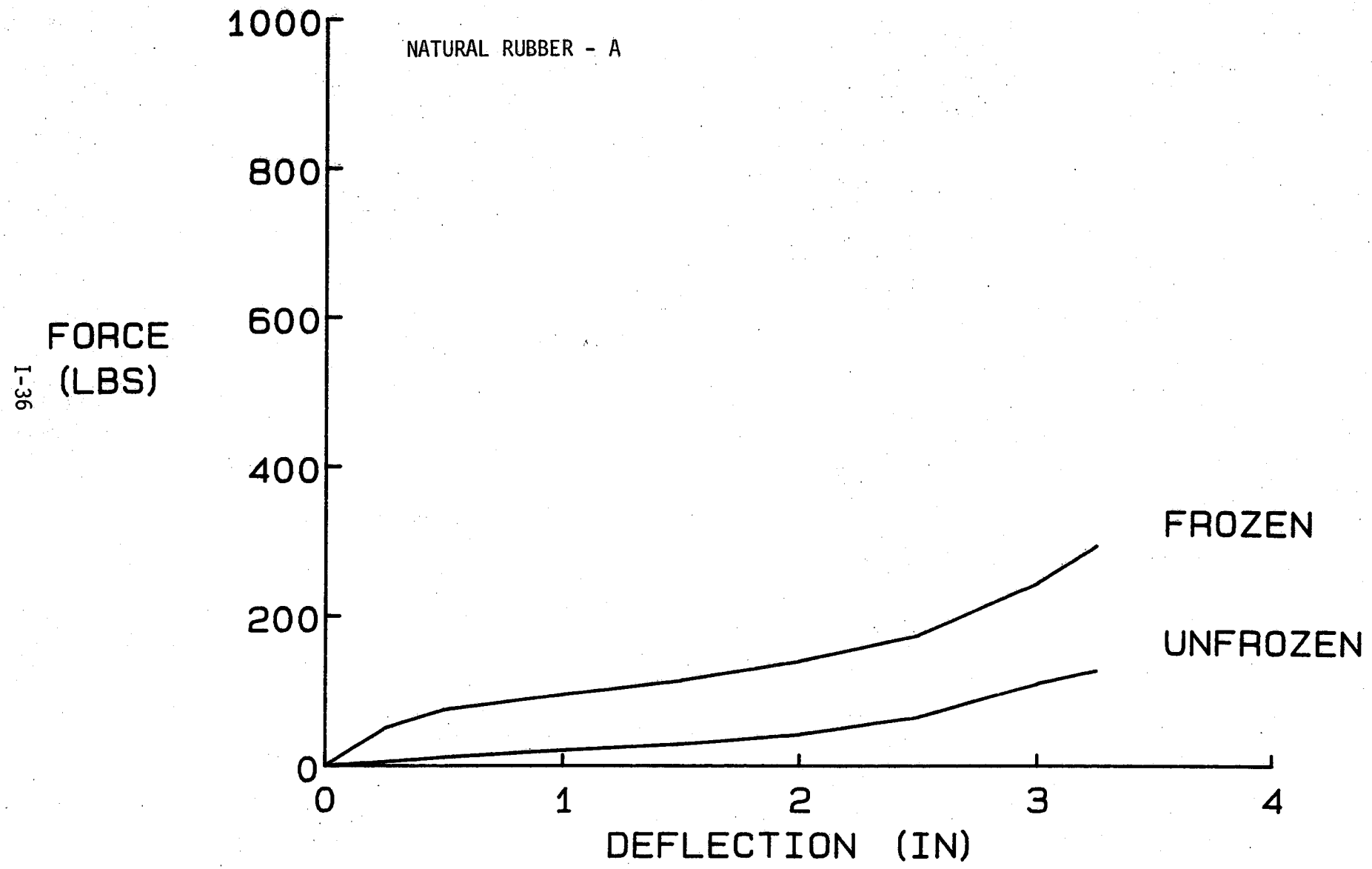

FIGURE - A7

STATIC TEST RESULTS
(SAMPLE .60"-70: FROZEN AND UNFROZEN)

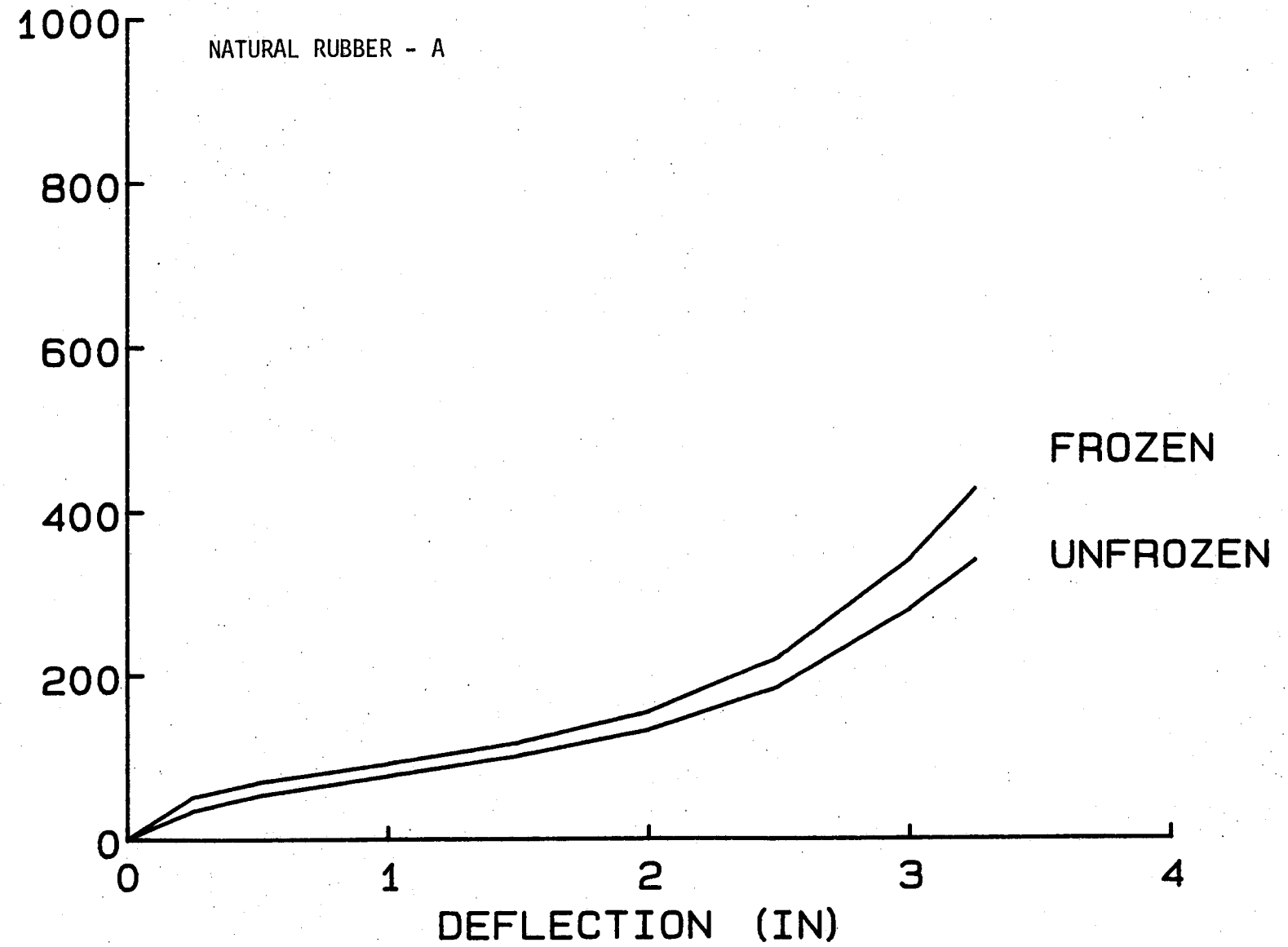

FIGURE - A8

STATIC TEST RESULTS

(SAMPLES: .60"-60 & .60"-NEOPRENE)

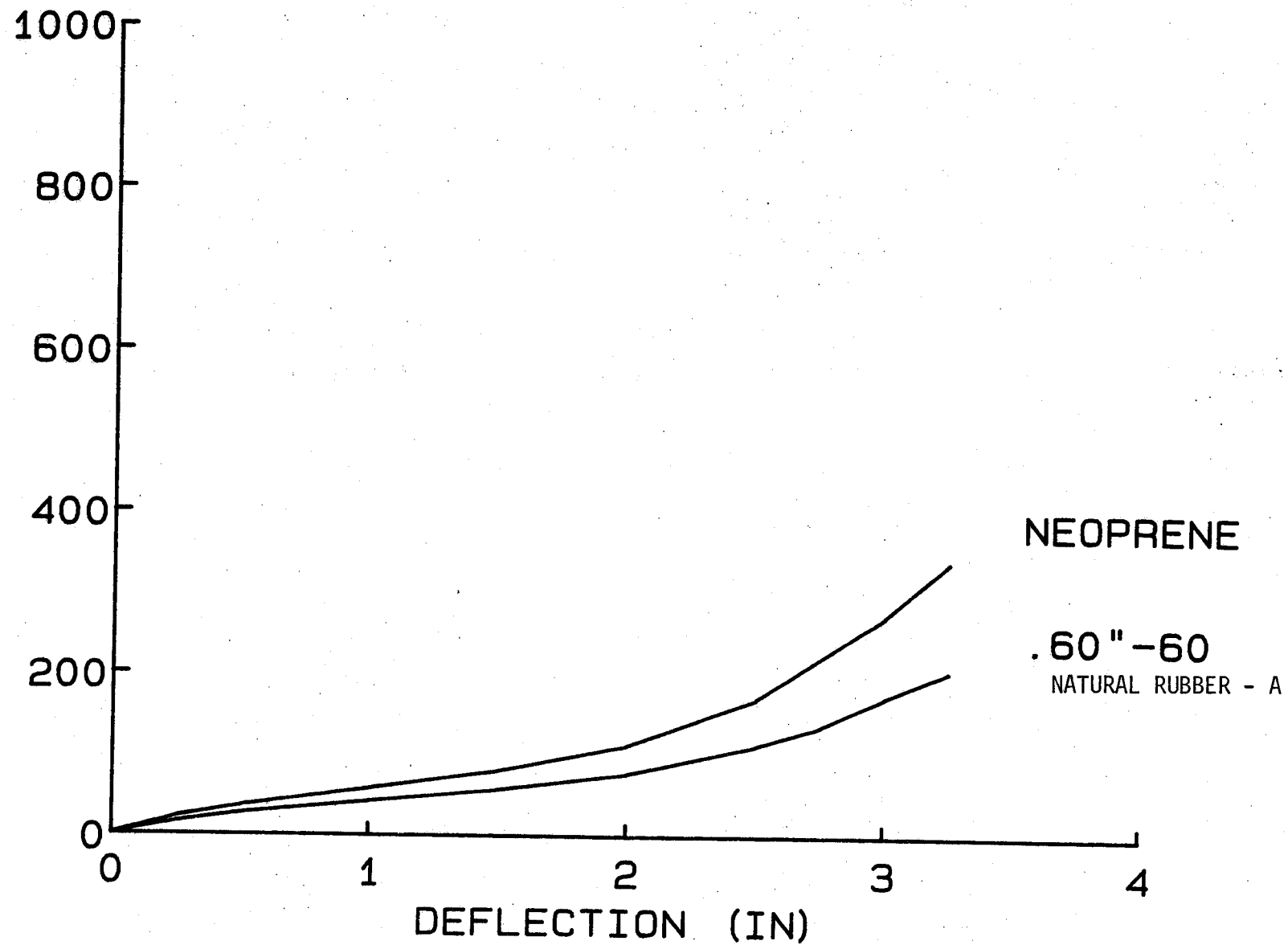

FIGURE - A9

STATIC TEST RESULTS
(SAMPLES: .30"-85 & .30"-90)

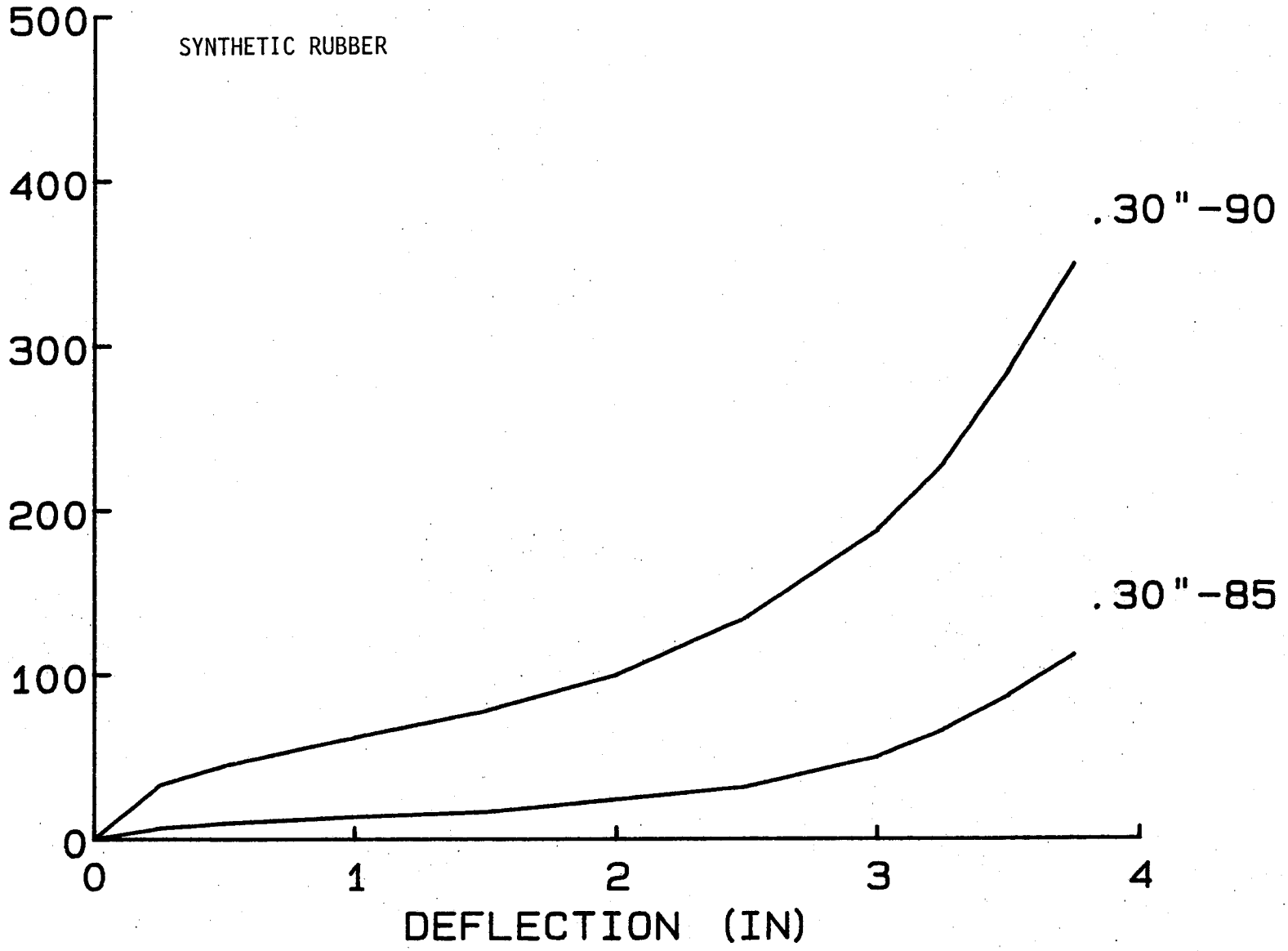

FIGURE - A10

STATIC TEST RESULTS

(SAMPLES: .45"-85 & .45"-90)

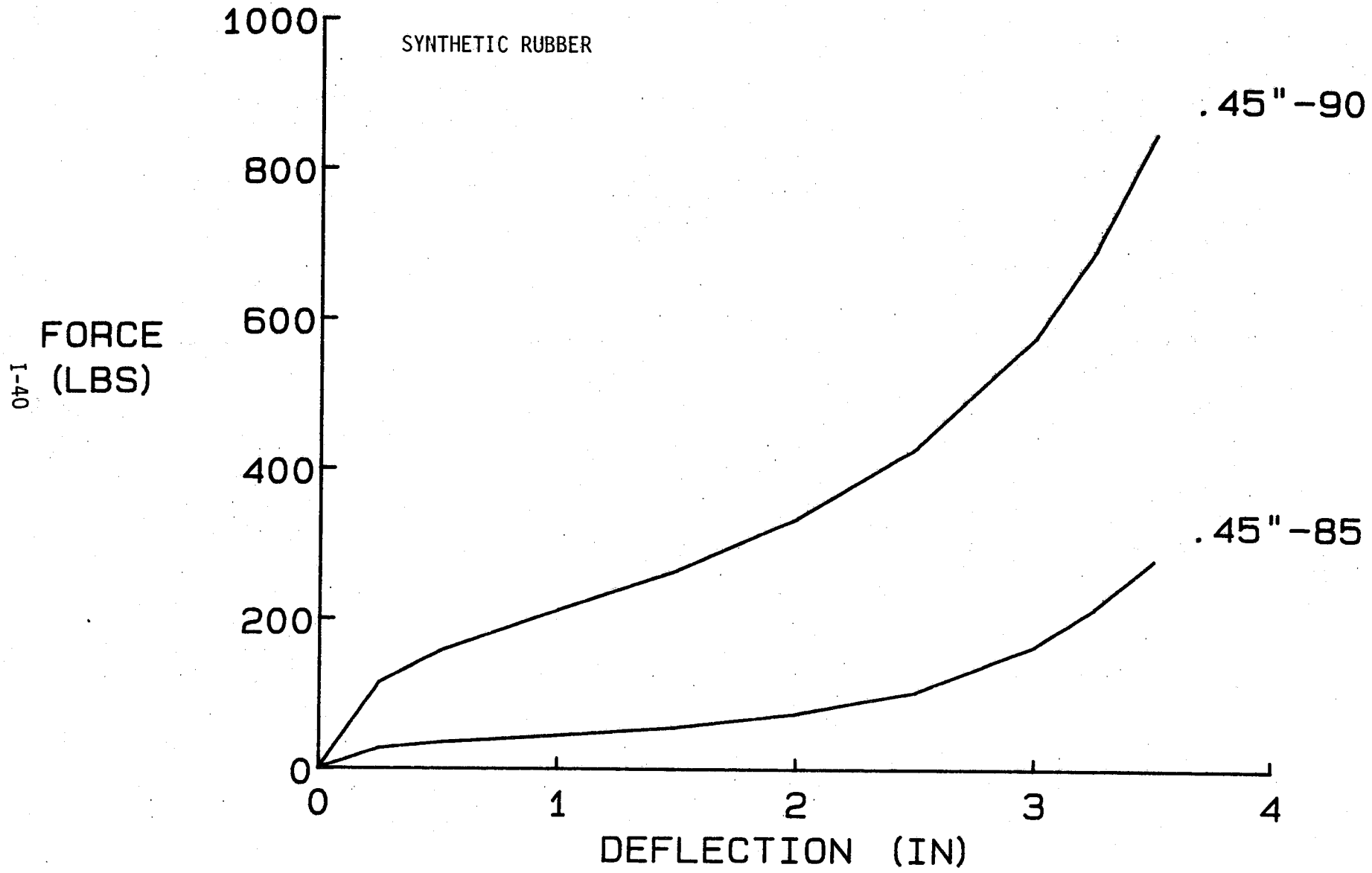

FIGURE - A11

STATIC TEST RESULTS
(SAMPLES: .60"-85 & .60"-90)

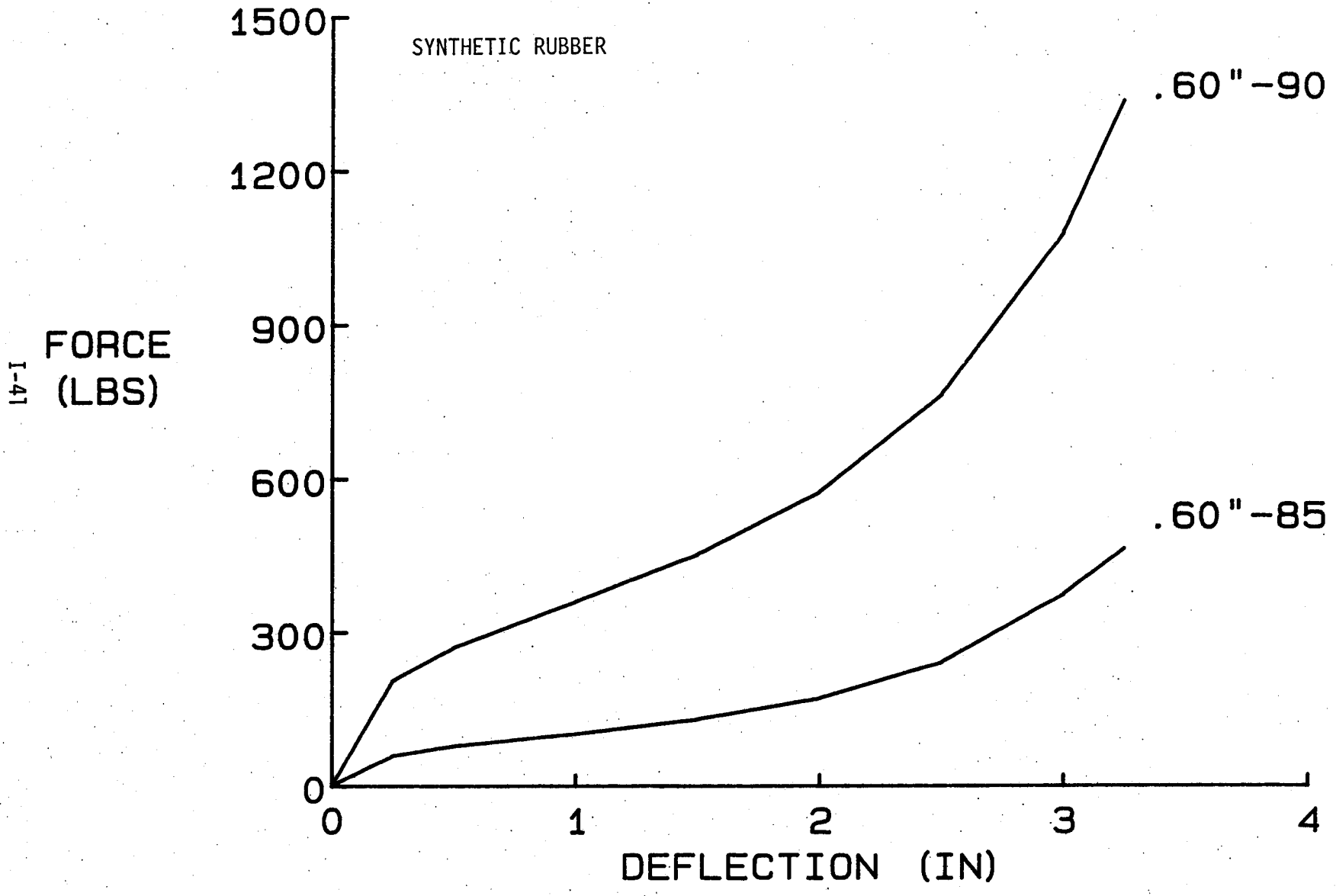

FIGURE - A12

STATIC TEST RESULTS

(SAMPLE 1.20"-80: FROZEN AND UNFROZEN)

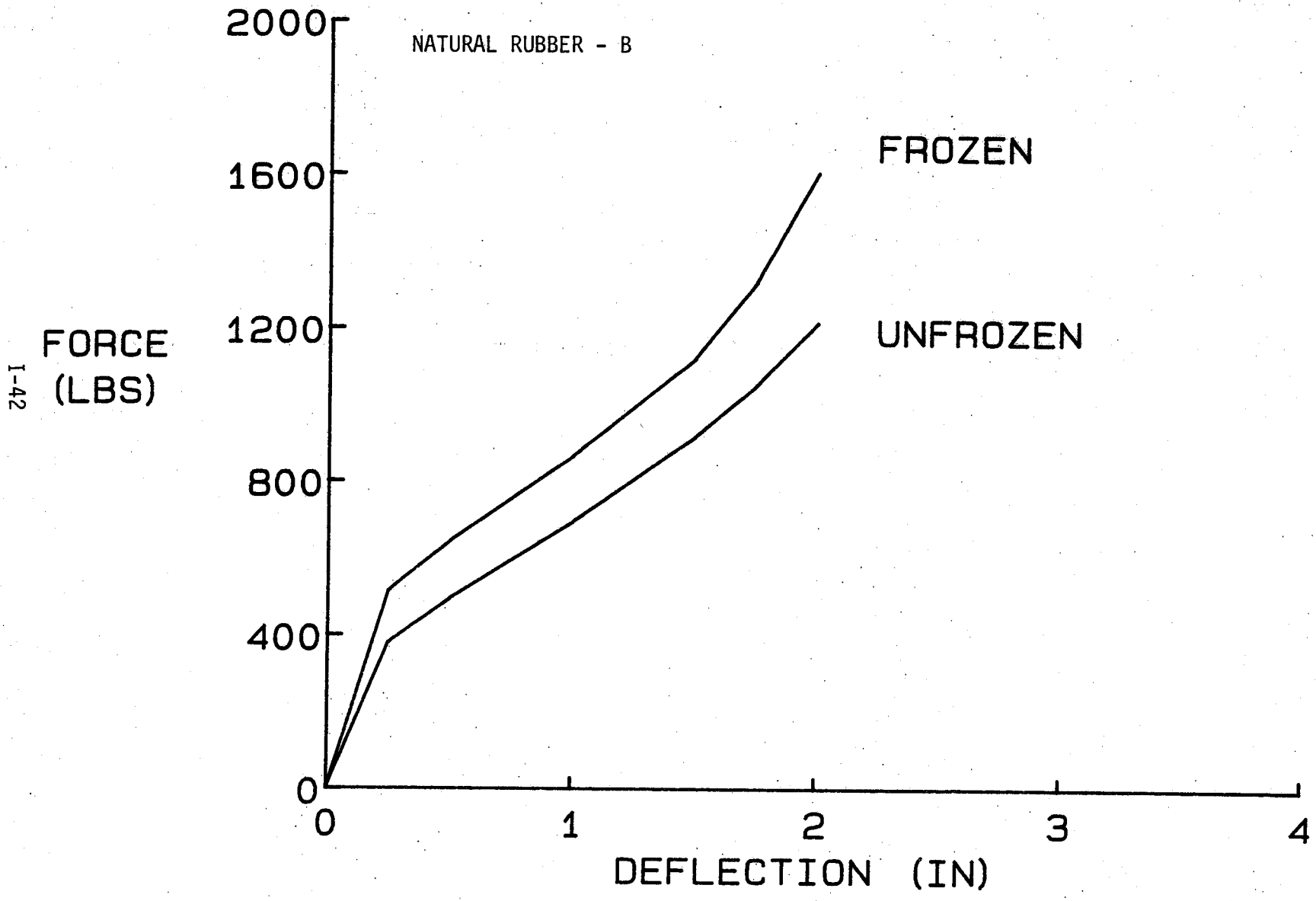

FIGURE - A13

STATIC TEST RESULTS

(SAMPLES: 1.20"-50 , 1.20"-60 & 1.20"-NEOPRENE)

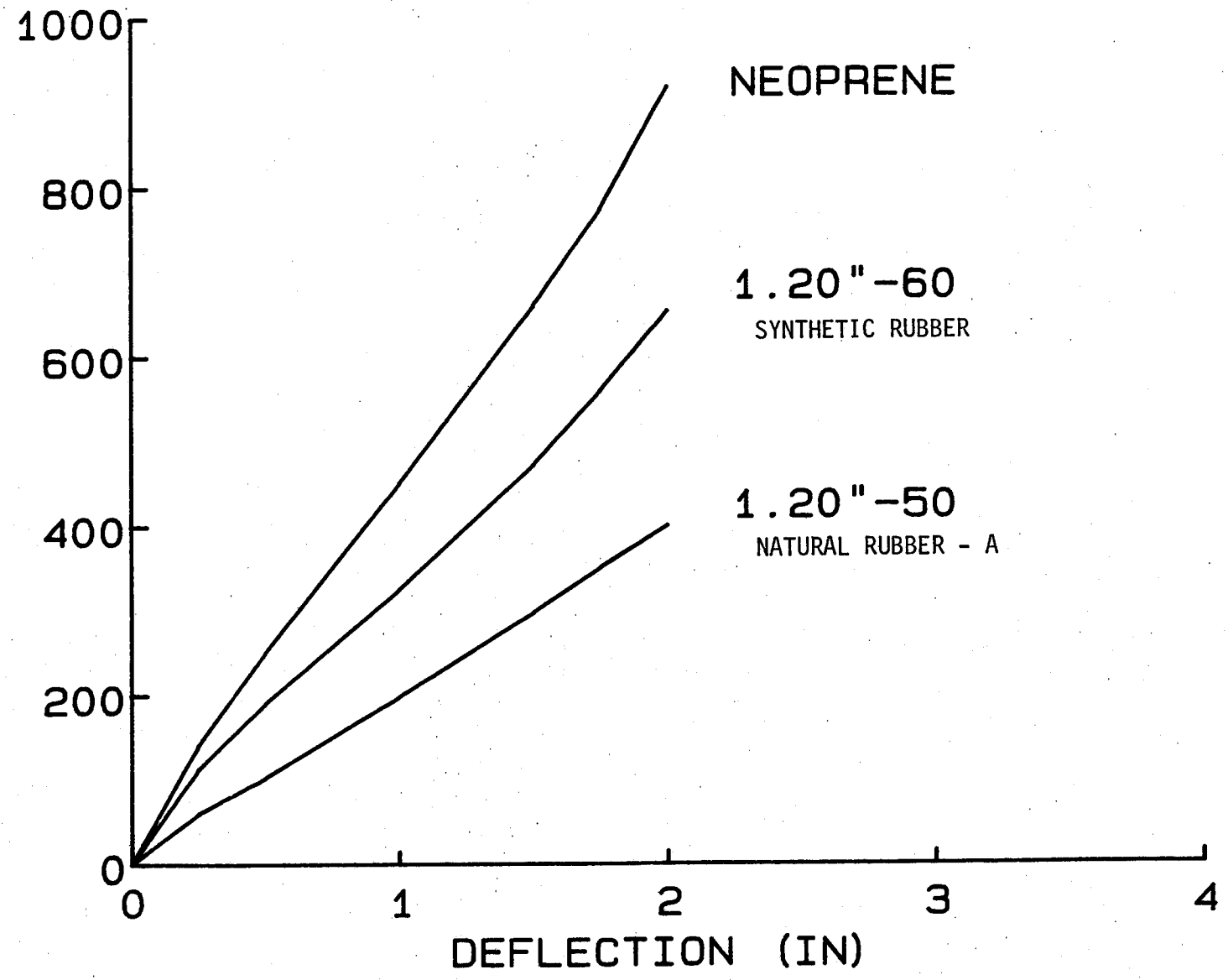

FIGURE - A14

STATIC TEST RESULTS

(SAMPLES: 1.20"-85 & 1.20"-90)

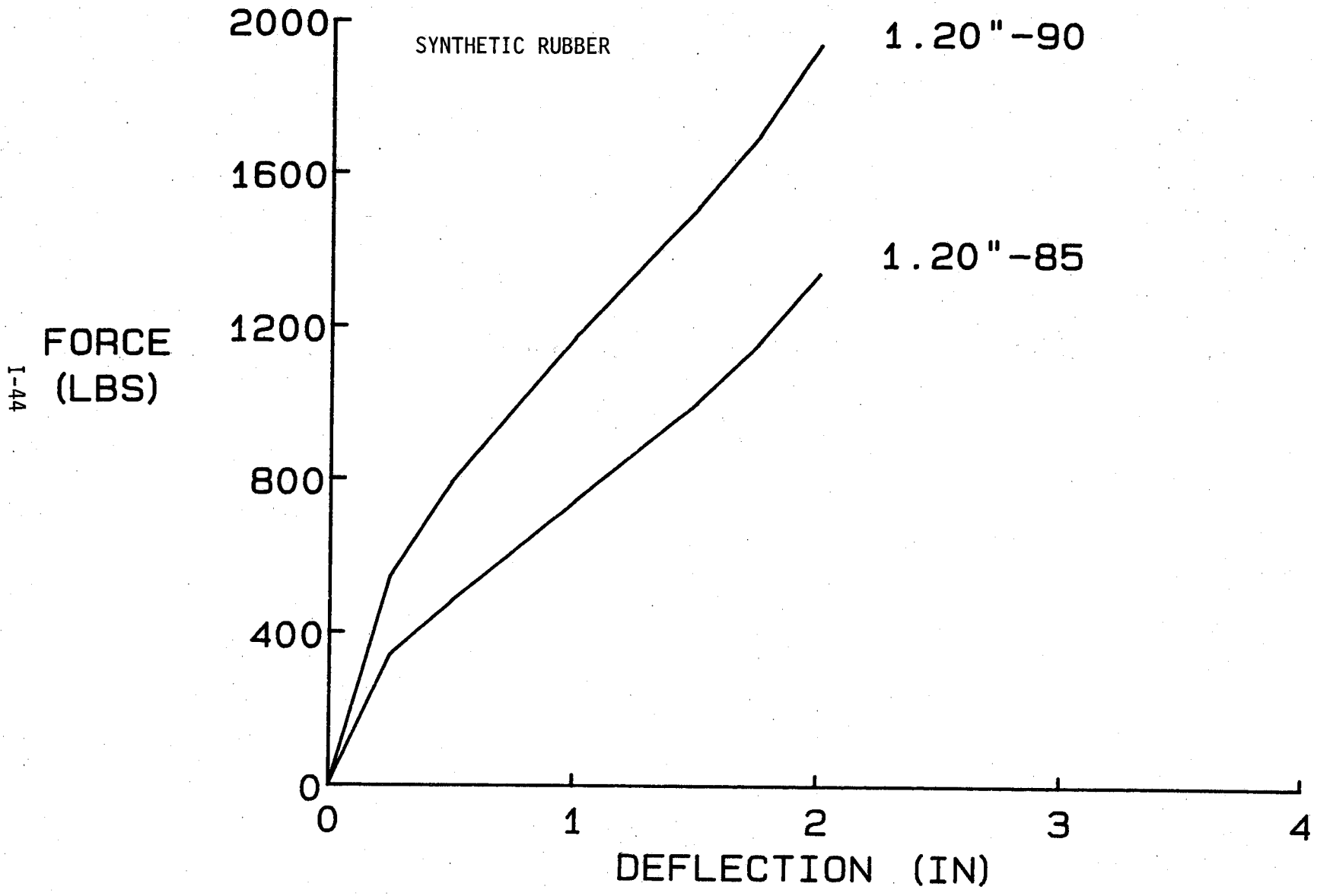

FIGURE - A15

STATIC TEST RESULTS

(SAMPLE .312"-80: FROZEN AND UNFROZEN)

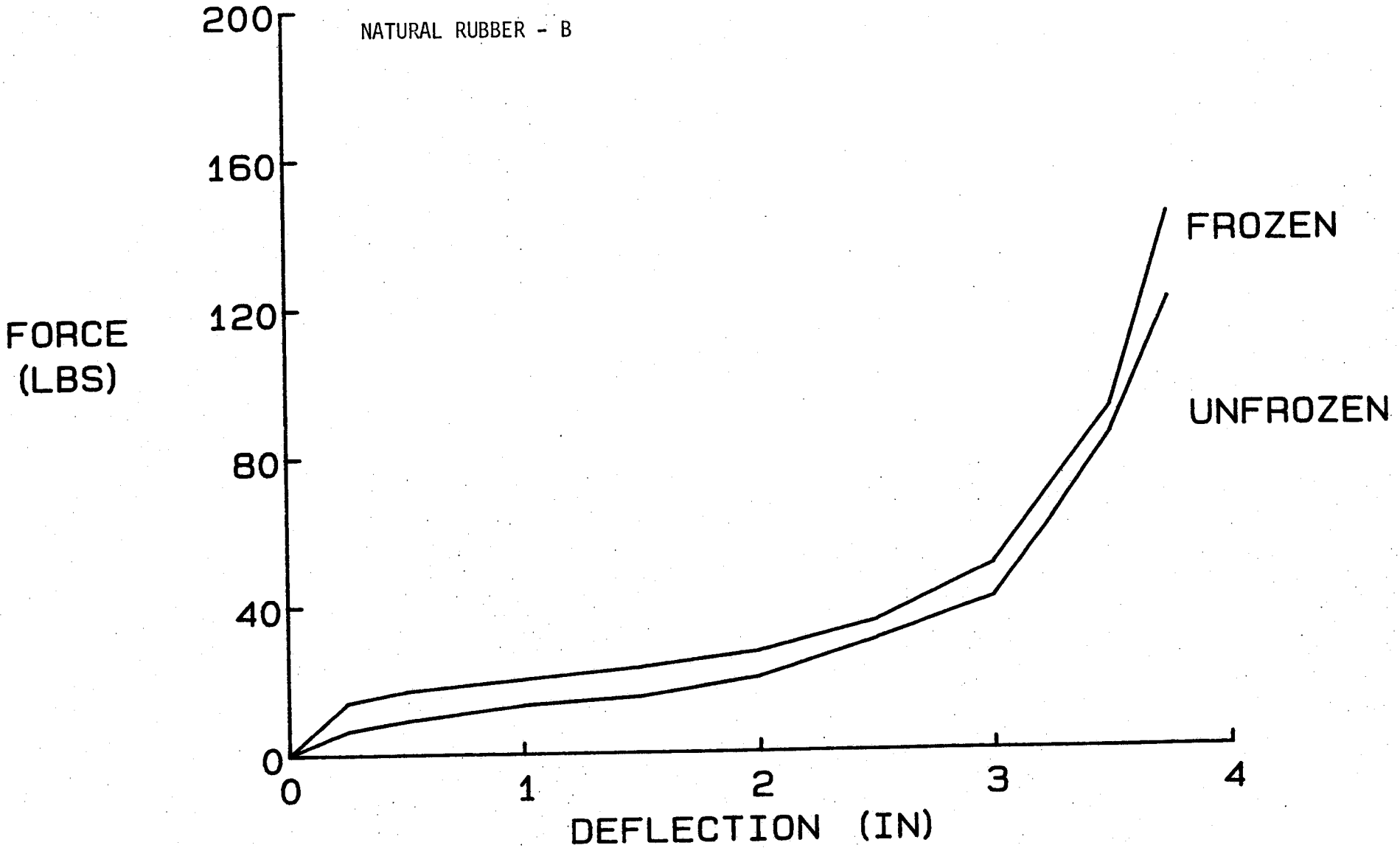

FIGURE - A16

STATIC TEST RESULTS
(SAMPLE .437"-80: FROZEN AND UNFROZEN)

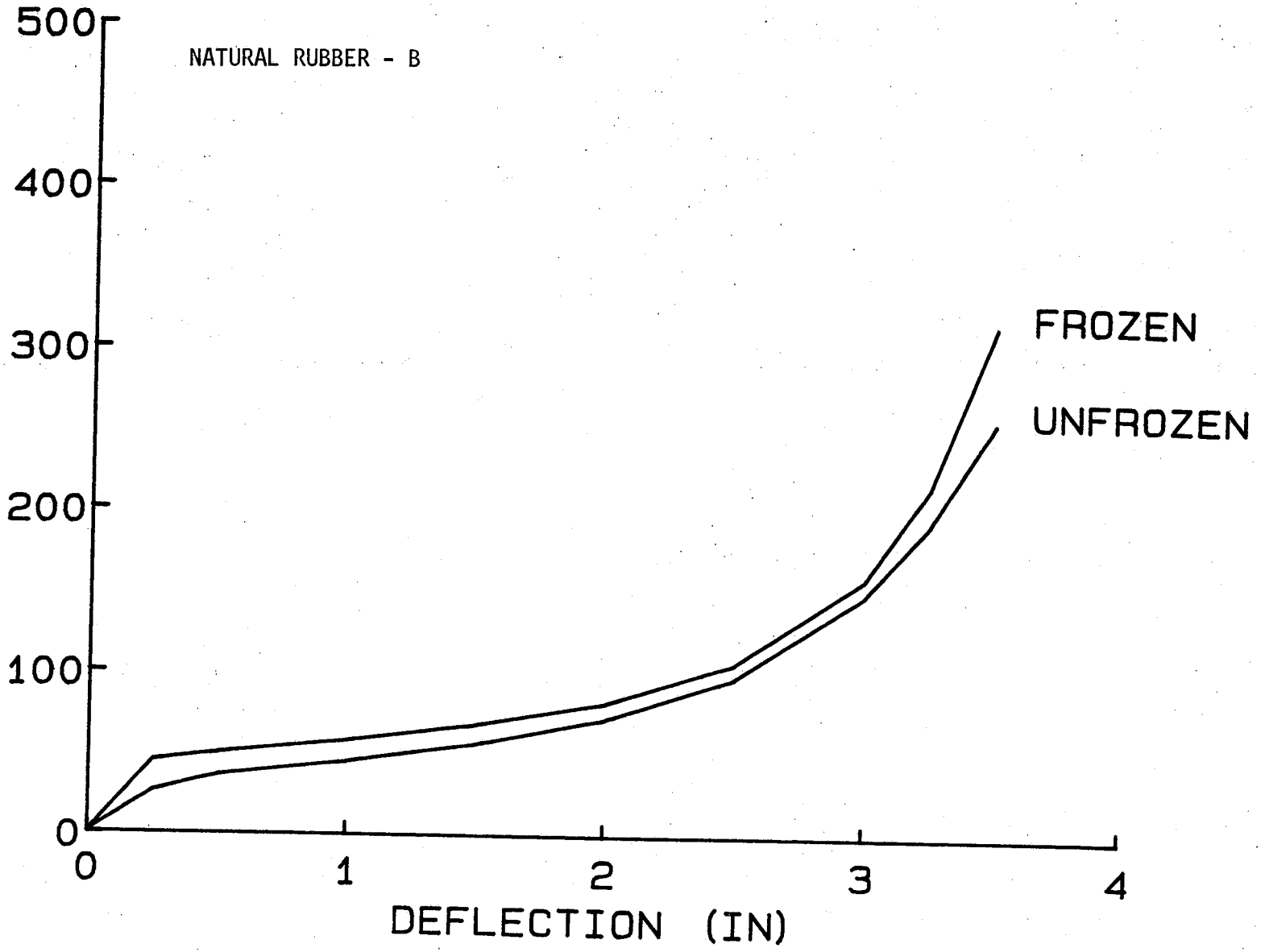

FIGURE - A17

STATIC TEST RESULTS

(SAMPLE .625"-80: FROZEN AND UNFROZEN)

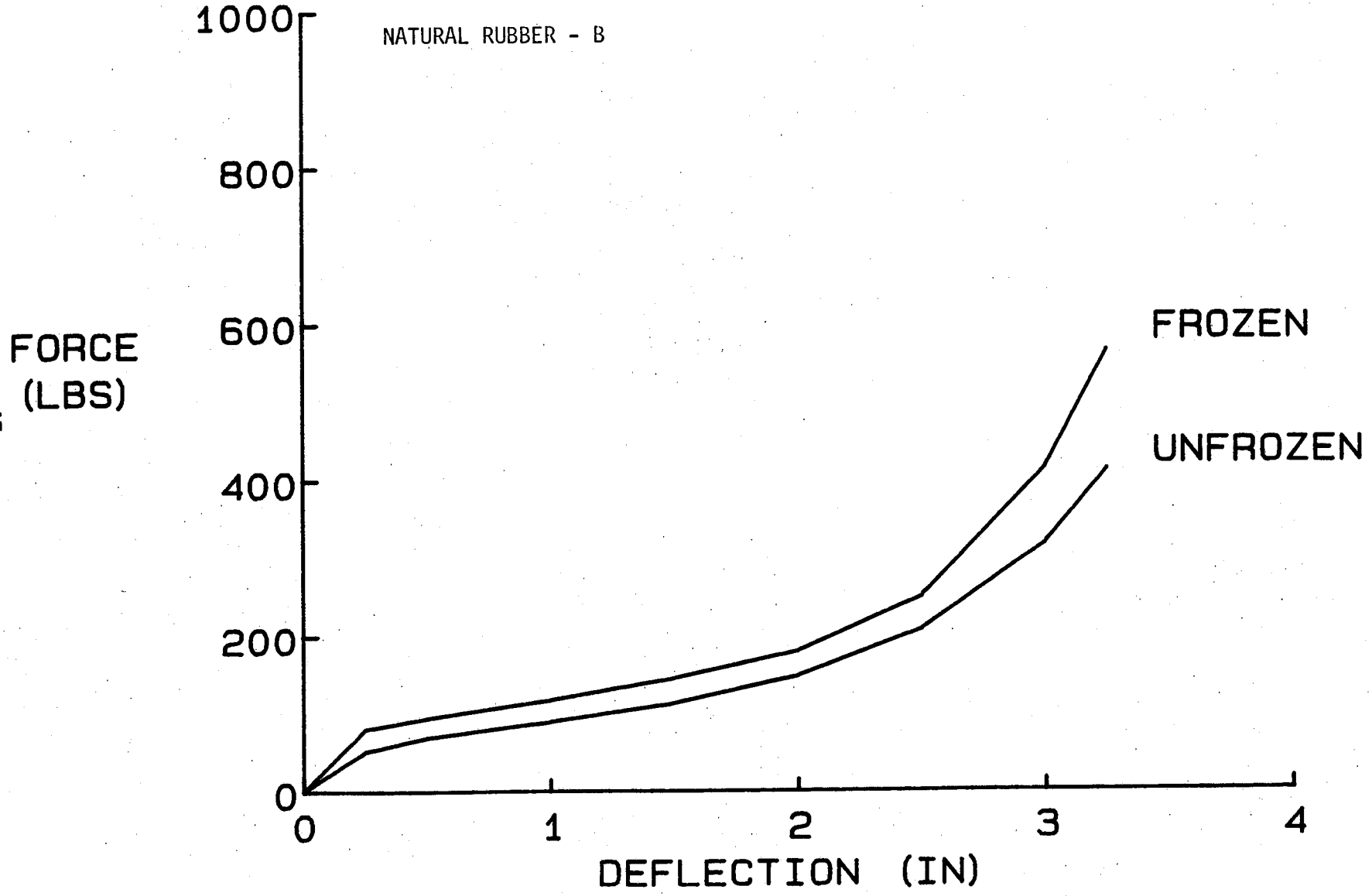

APPENDIX B

FIGURE - B1

STATIC TEST RESULTS
(SAMPLE: 1.75" X 28.5" X 24")

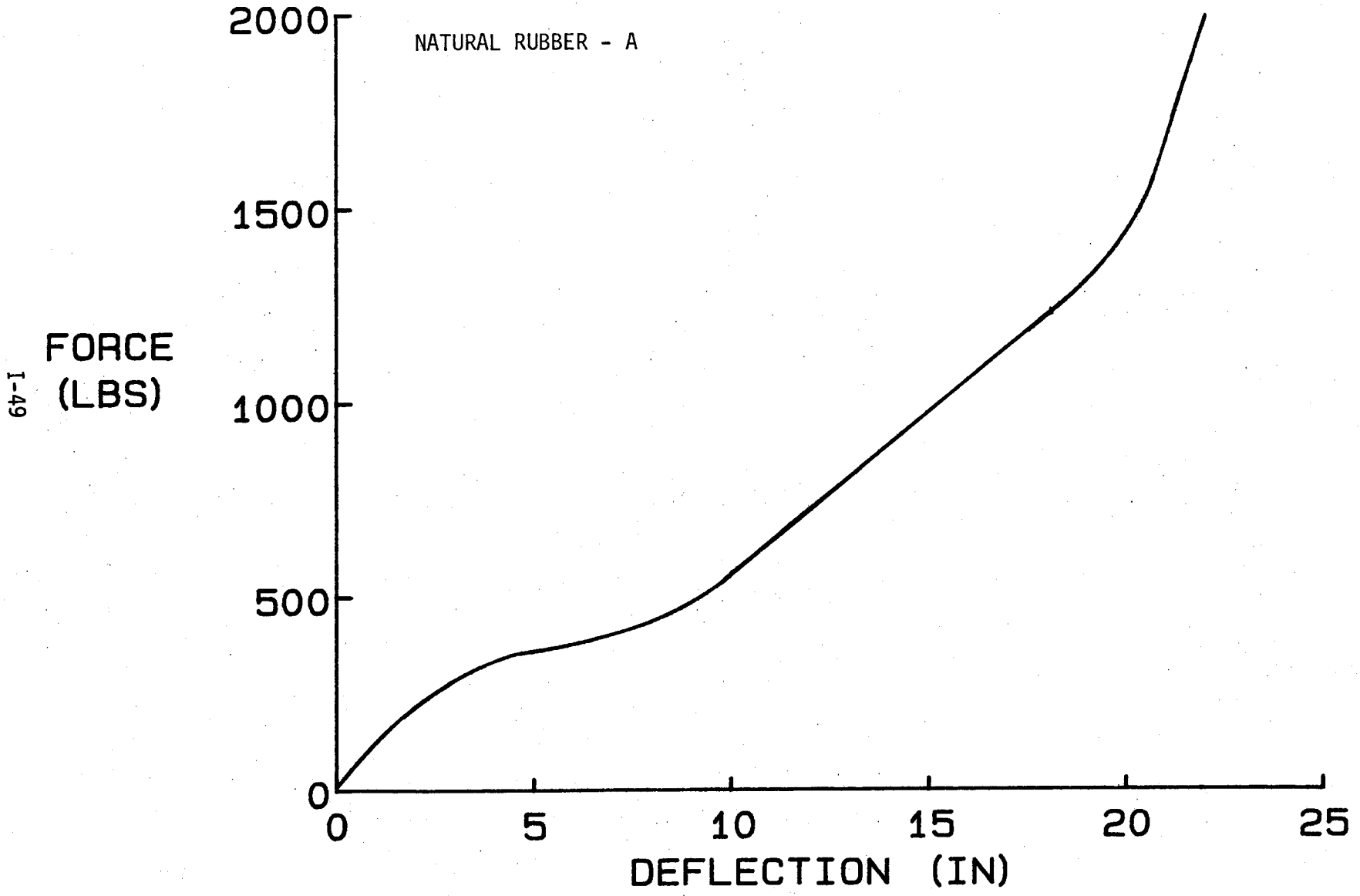

FIGURE - B2

STATIC TEST RESULTS
(SAMPLE: 1.75" X 28.5" X 24")

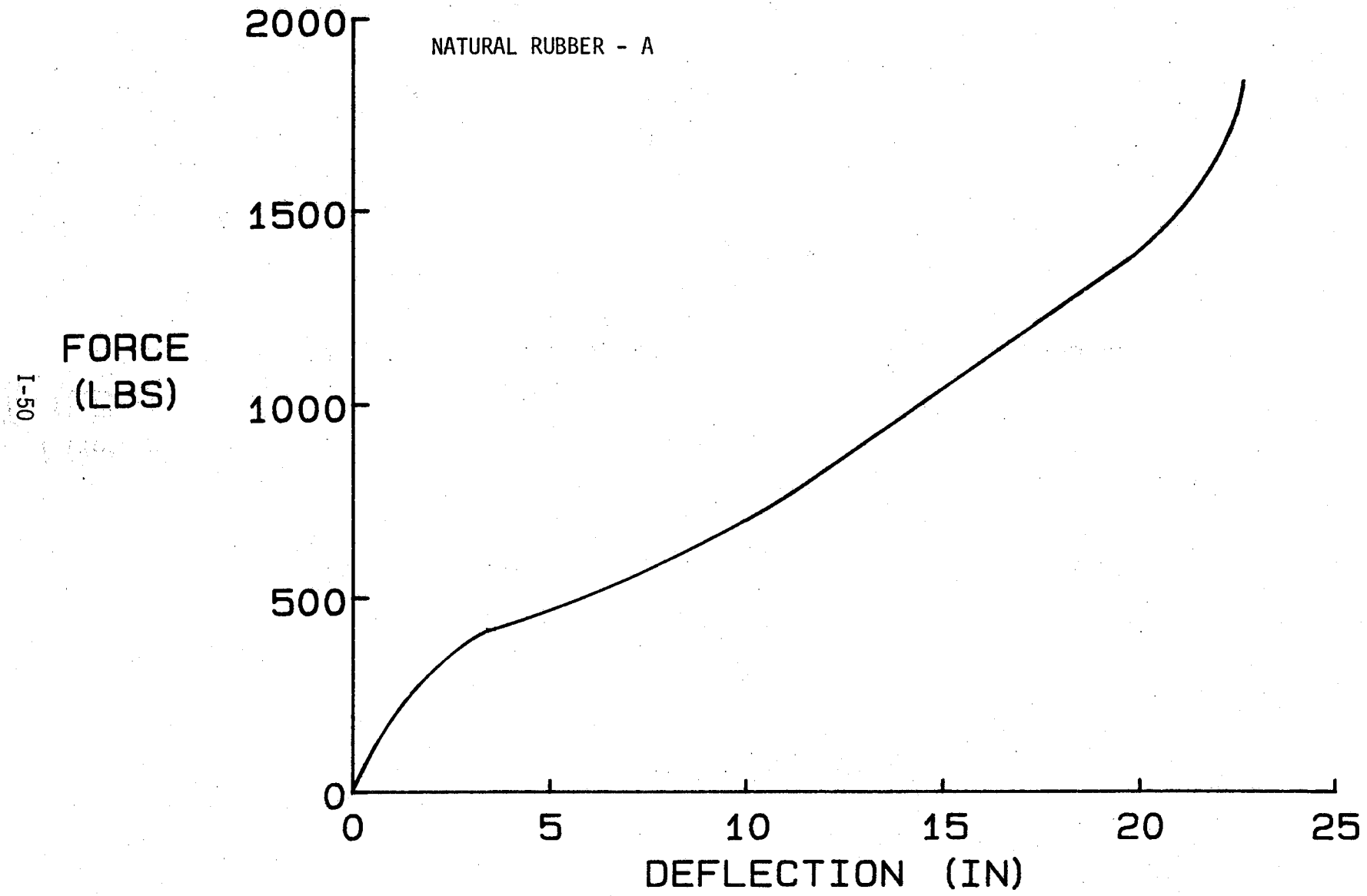

FIGURE - B4

STATIC TEST RESULTS
(SAMPLE: 4.5" X 28.5" X 24")

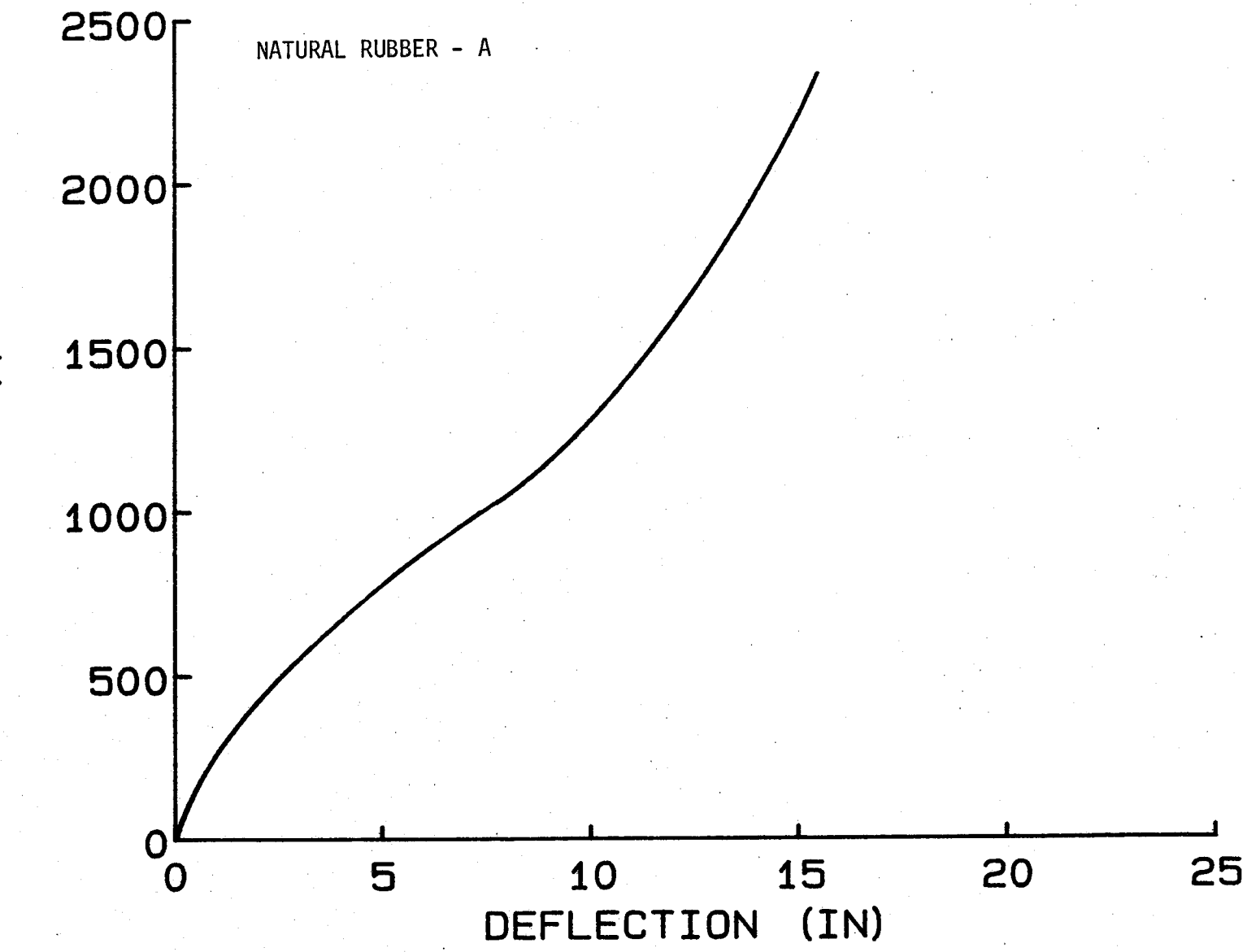

APPENDIX C

FIGURE - C1

DYNAMIC TEST RESULTS

(SAMPLES: .30"-50 , .45"-50 & .60"-50)

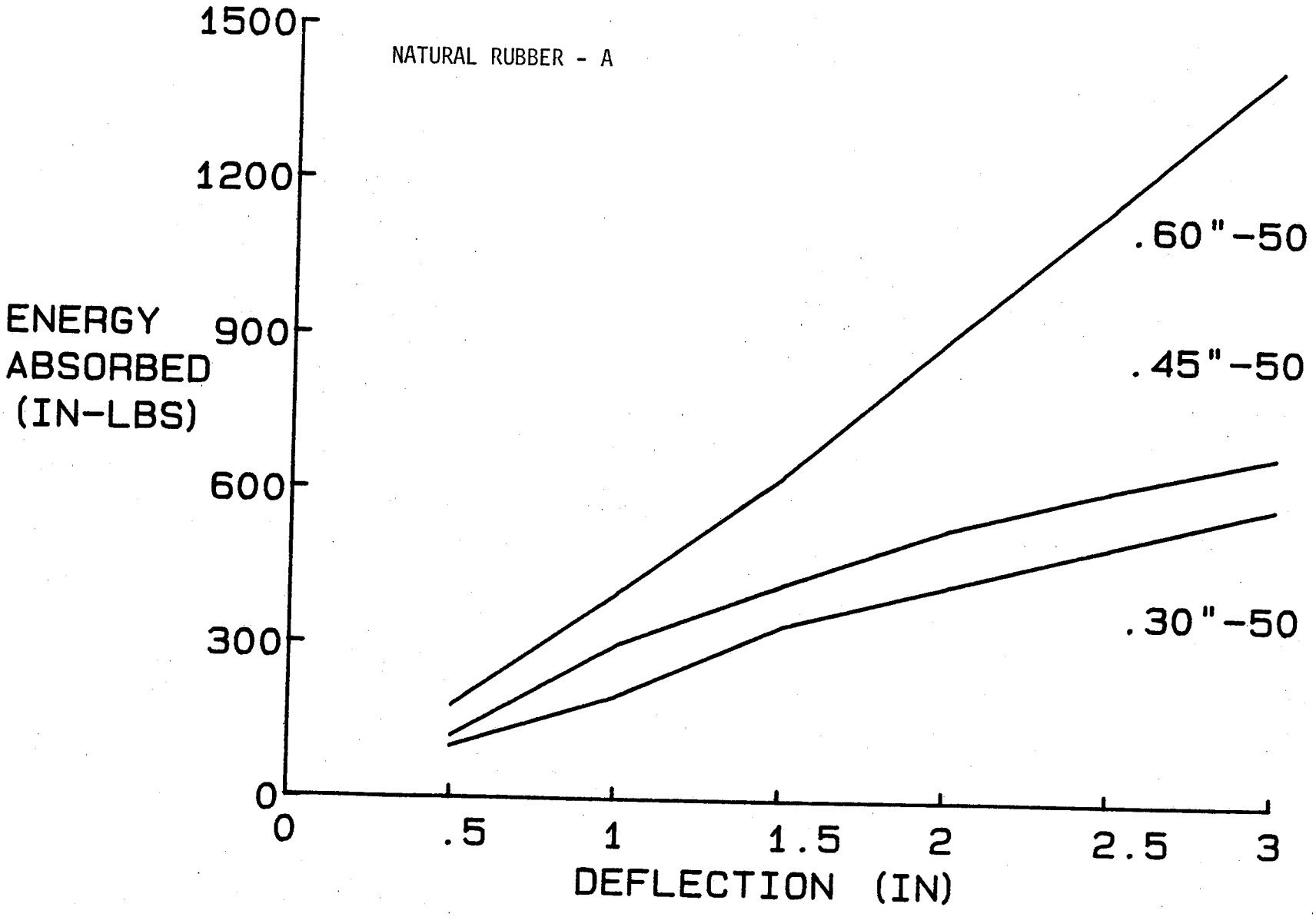

FIGURE - C2

DYNAMIC TEST RESULTS

(SAMPLES: .30"-60 , .45"-60 & .60"-60)

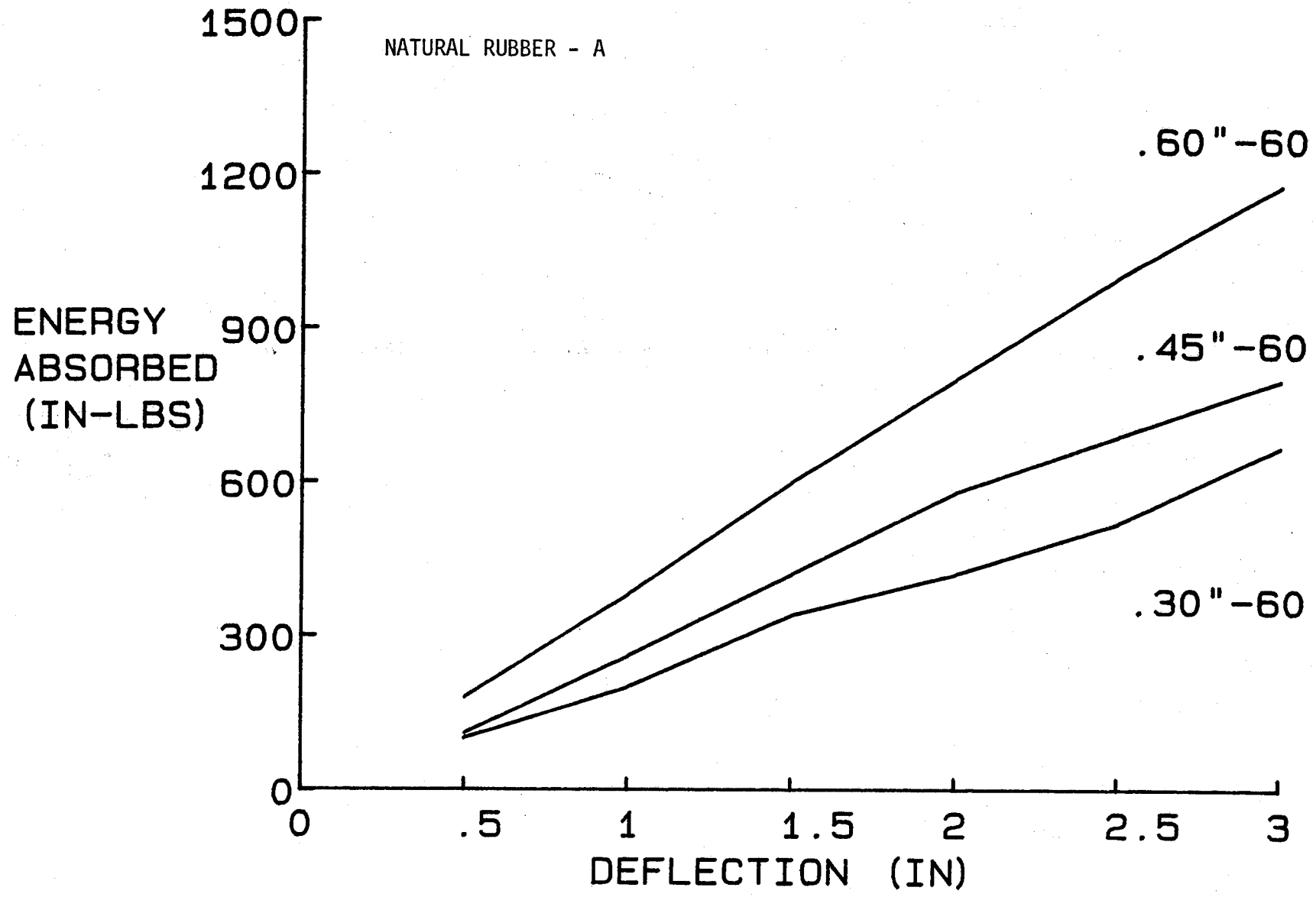

FIGURE - C3

DYNAMIC TEST RESULTS

(SAMPLES: .30"-70 , .45"-70 & .60"-70)

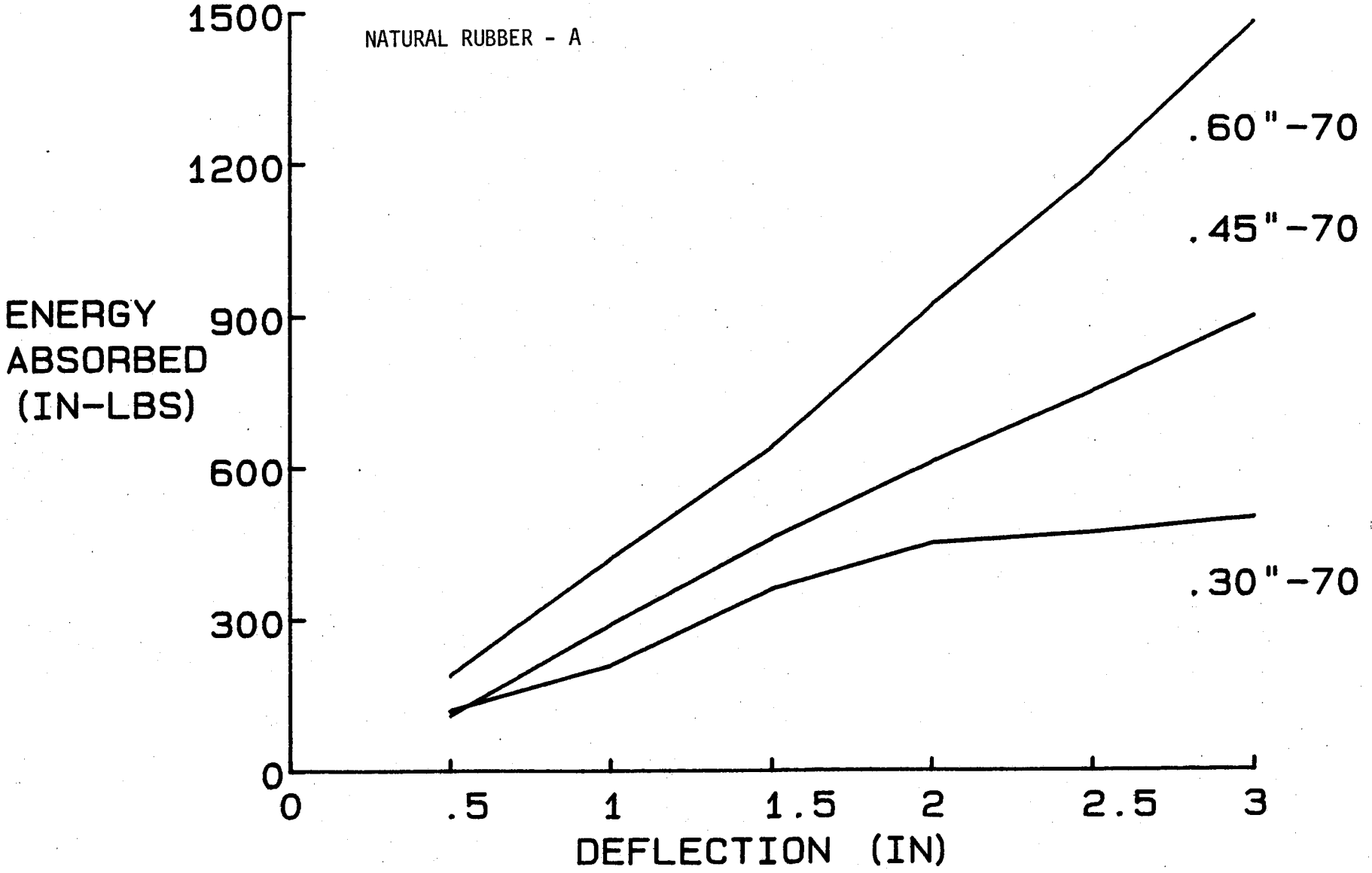

FIGURE - C4

DYNAMIC TEST RESULTS

(SAMPLES: .30"-80 , .45"-80 & .60"-80)

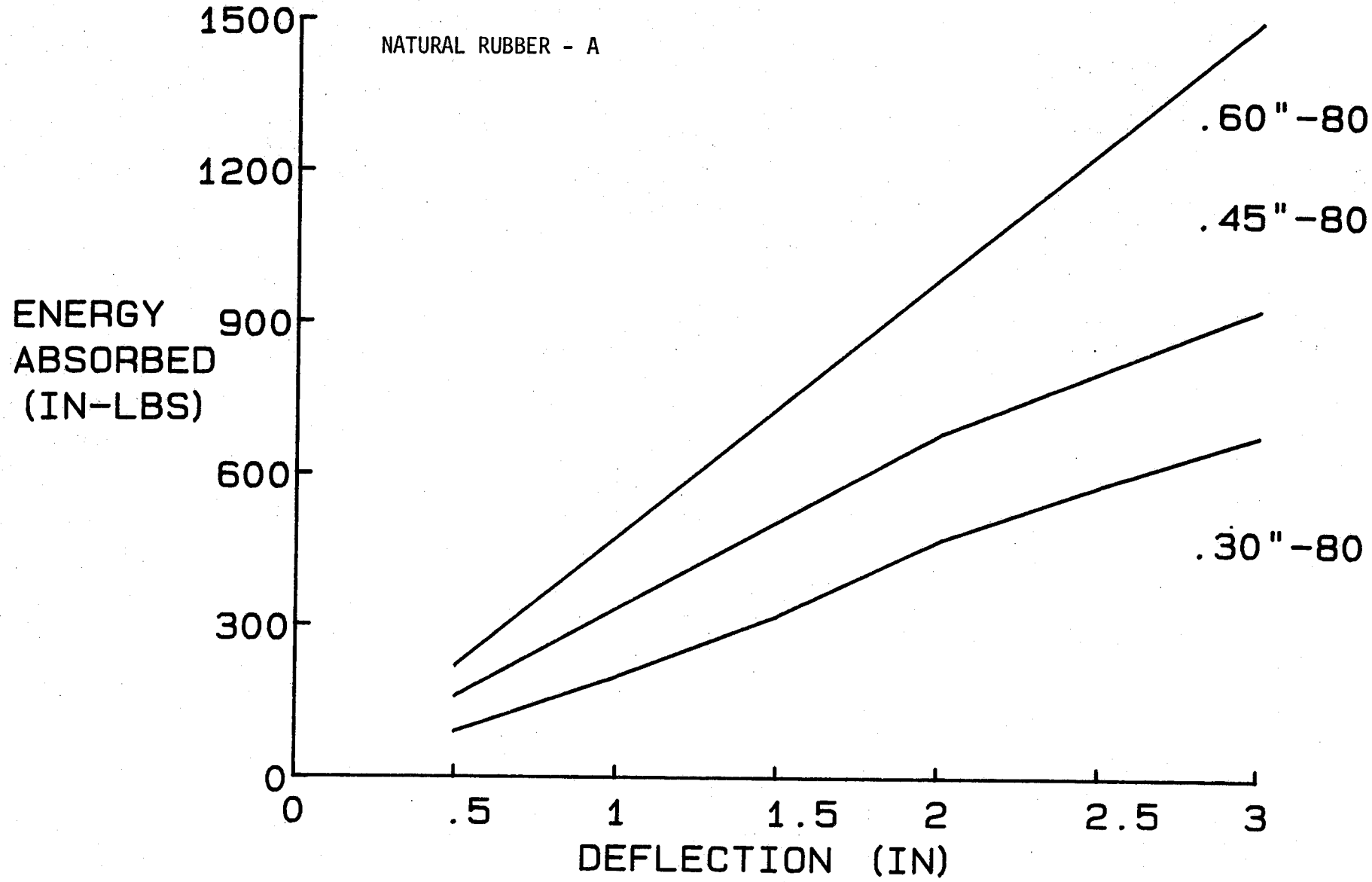

FIGURE - C5

DYNAMIC TEST RESULTS

(SAMPLES: 1.20"-50, 1.20"-60 & 1.20"-85)

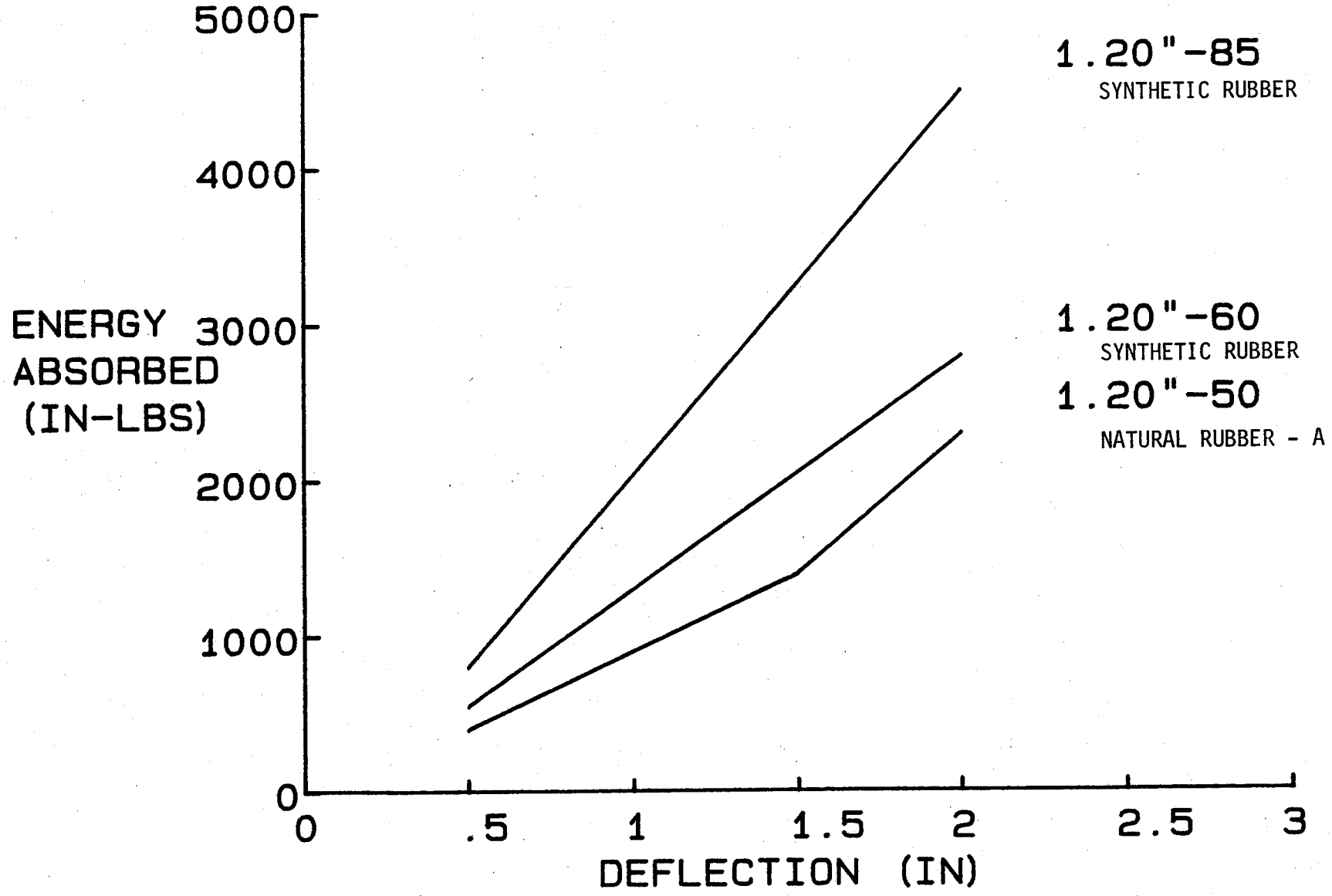

FIGURE - C6

DYNAMIC TEST RESULTS

(SAMPLES: .60"-N , 1.20"-N & 1.20"-80)

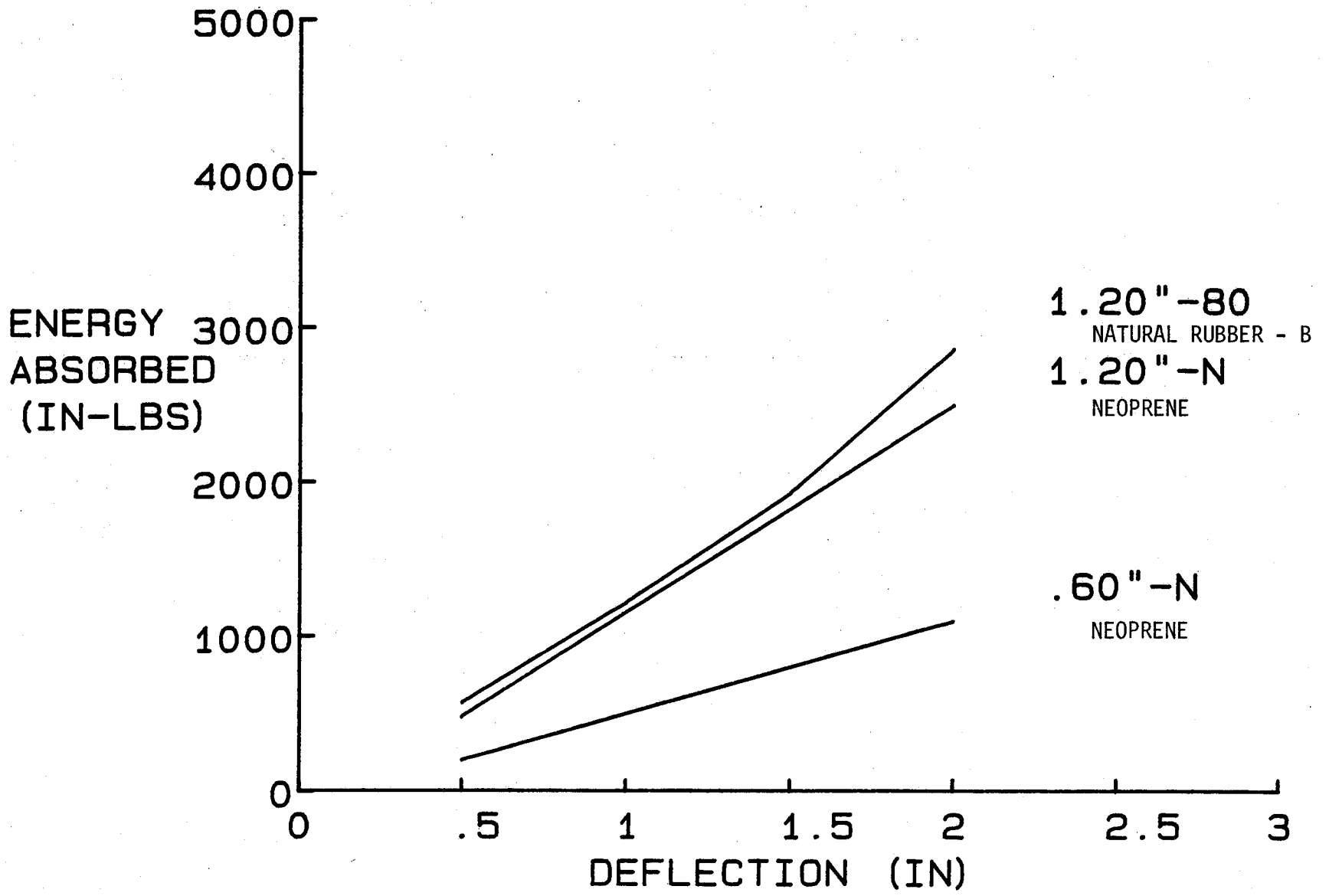

FIGURE - C7

DYNAMIC TEST RESULTS

(SAMPLES: .312"-80 , .437"-80 & .625"-80)

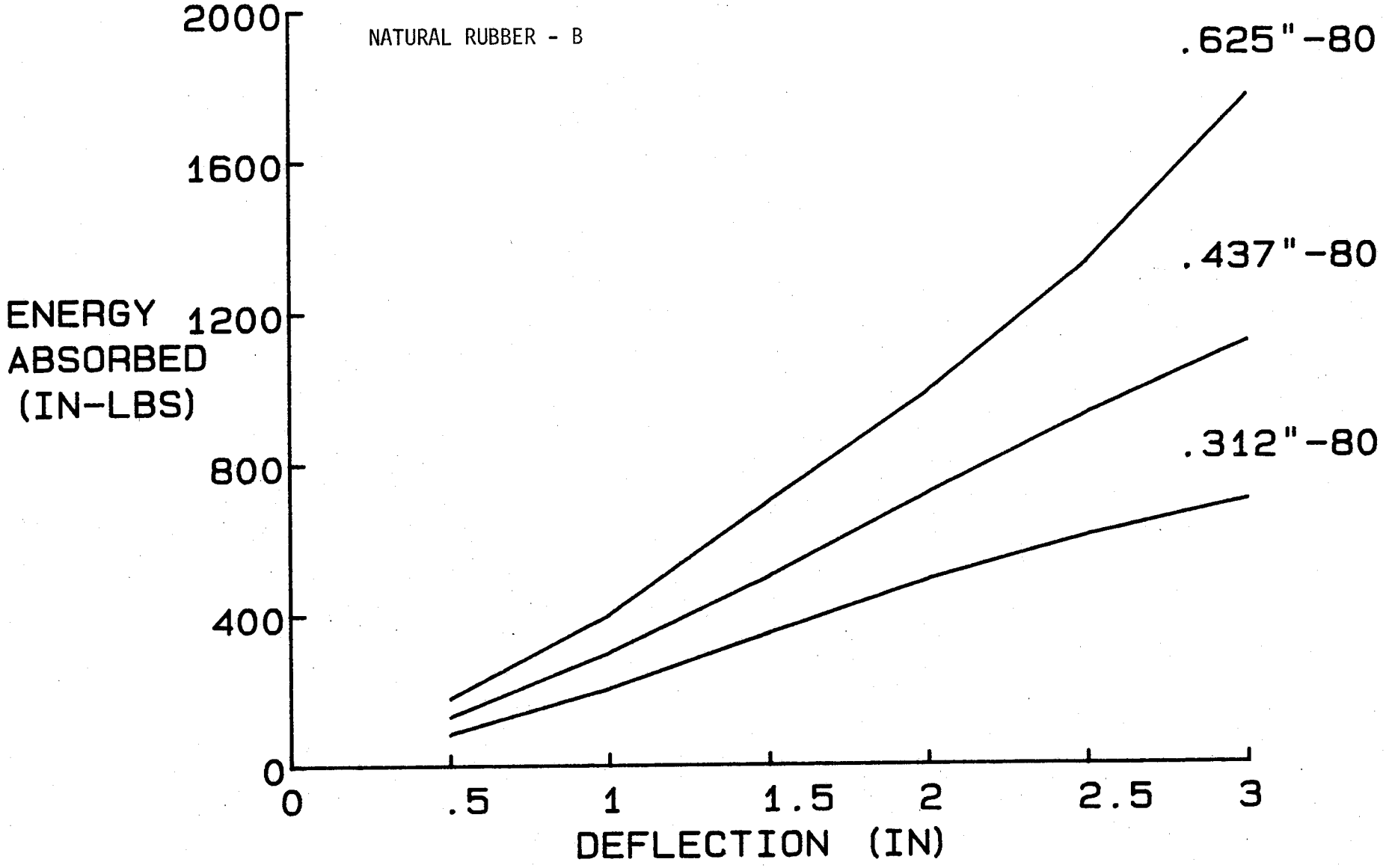

APPENDIX D

MAXWELL MODEL

When the brittleness temperature is below service conditions an elastomer can have both elastic strain and viscous flow. In the simplest situation, known as the Maxwell model, the behavior of the elastomer may be represented by a mass supported by a spring and dashpot acting in parallel as shown.

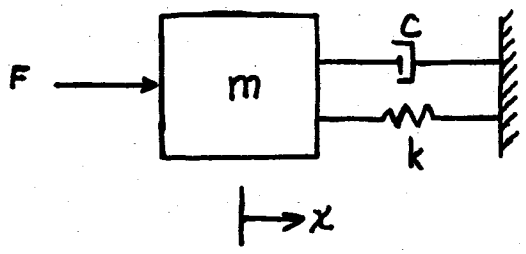

A free body diagram of the mass looks like,

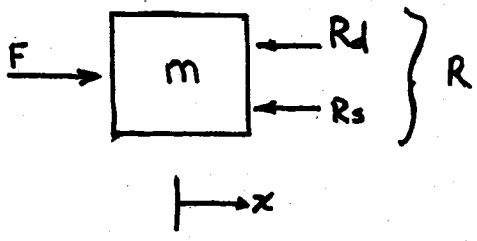

Define R as the total reaction that is resisting the applied force, F,

$$R = Rd + Rs$$

where, $Rd = c\dot{x}$ = the force in the dashpot

$Rs = kx$ = the force in the spring

Summing forces in the horizontal direction for the free body diagram on the preceding page,

EQ-1 $F = kx + cx + mx$

Equation 1 is the governing equation of motion for the Maxwell model. The equation may be integrated over the length of the compression stroke to calculate the amount of work done in compressing the sample.

COMPLEX MODEL

The second model may be derived using a dynamic analysis approach like the Maxwell model, however an energy approach will be used instead. In this model the cylinder is represented by four lumped masses connected by massless rods. A schematic of the model is shown below .

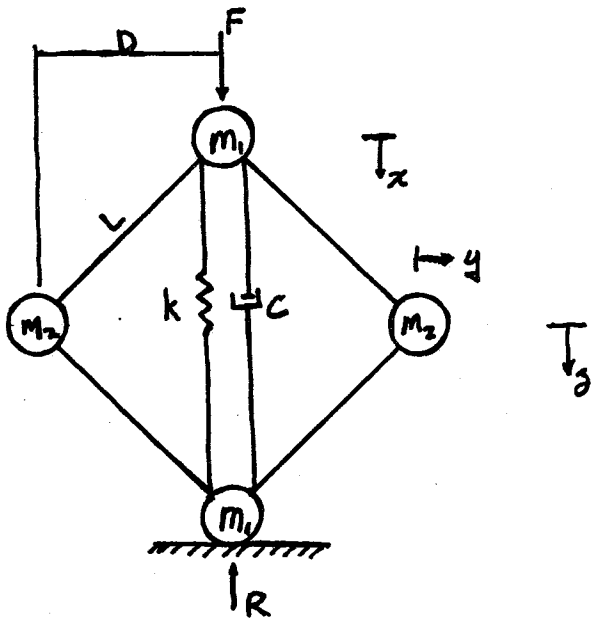

where, F = force applied by the load cell

k = spring constant

c = damping coefficient

R = reaction at the base of the sample

x = vertical distance traveled by the top of the sample

y = vertical distance traveled by m_2

z = horizontal distance traveled by m_2

Since all of the potential energy is stored in the compressed spring, the internal energy of the system may be represented by

$$\text{EQ-2} \qquad V = .5kx^2$$

and the kinetic energy of the system, T, may be calculated by

$$\text{EQ-3} \qquad T = .5m_1 \dot{x} + 2\left(.5m_2 \dot{y}\right) + 2\left(.5m_2 \dot{z}\right)$$

which may be reduced to

$$T = .5m_1 \dot{x}^2 + m_2 \dot{y}^2 + m_2 \dot{z}^2$$

To reduce the equation further assume $y = .5x$ and noting that

$$z = \left[D^2 + x(L^2 - D^2) - .25x^2 \right]^{1/2} - D$$

The total energy of the system, E, may be written in terms of x

$$E = T(x) + V(x)$$

Applying partial differentiation to get to Lagrange's equation of motion (3),

$$\frac{\partial}{\partial t}\left(\frac{\partial T}{\partial \dot{x}}\right) + \frac{\partial V}{\partial x} - \frac{\partial T}{\partial x} = Q_i$$

where, $Q_i = F - cv$

After differentiation, the equation of motion looks like

$$F = \frac{3}{2}m\ddot{x} + \frac{m\ddot{x}}{2}\frac{(d - x/2)^2}{[D^2 + xd - \frac{x^2}{4}]} - \frac{m\dot{x}^2}{4}\left\{\frac{(d - \frac{x}{2})^3}{[D^2 + xd - \frac{x^2}{4}]} + \frac{(d - \frac{x}{2})}{[D^2 + xd - \frac{x^2}{4}]}\right\}$$

$$+ Kx + C\dot{x}$$

where $d = (L^2 - D^2)^{1/2}$

REFERENCES

1. Theory and Practice of Engineering with Rubber, P.K. Freakley and A.R. Payne, Applied Science Publishers LTD, London, 1978.

2. Materials of Engineering, Lawrence H. Van Vlack, Addison-Wesley Publishing Company, Reading,Massachussetts, 1982.

3. Dynamics of Structures, Ray W. Clough and Joseph Benzien, McGraw-Hill Inc., New York,New York, 1975.

4. "Marine Fendering Systems", Uniroyal Inc., Mishawaka, Ind.

APPENDIX II.

ACCELEROMETER TRACES

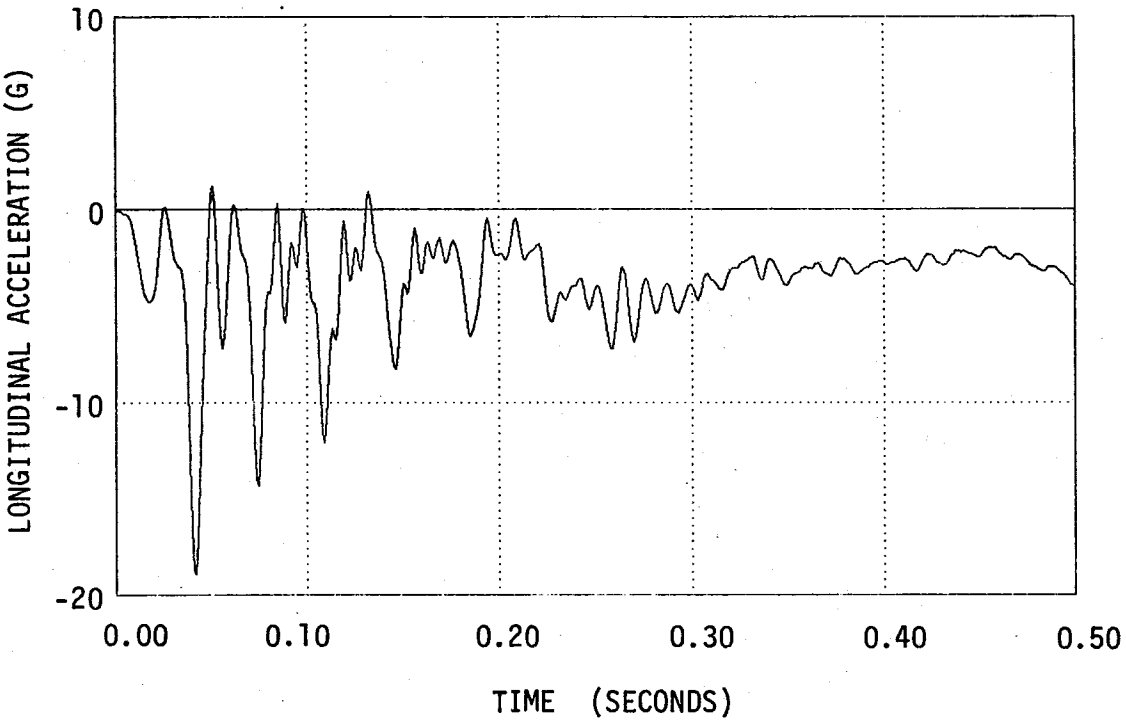

Figure II-1 Vehicle longitudinal accelerometer trace for test 2346-3.

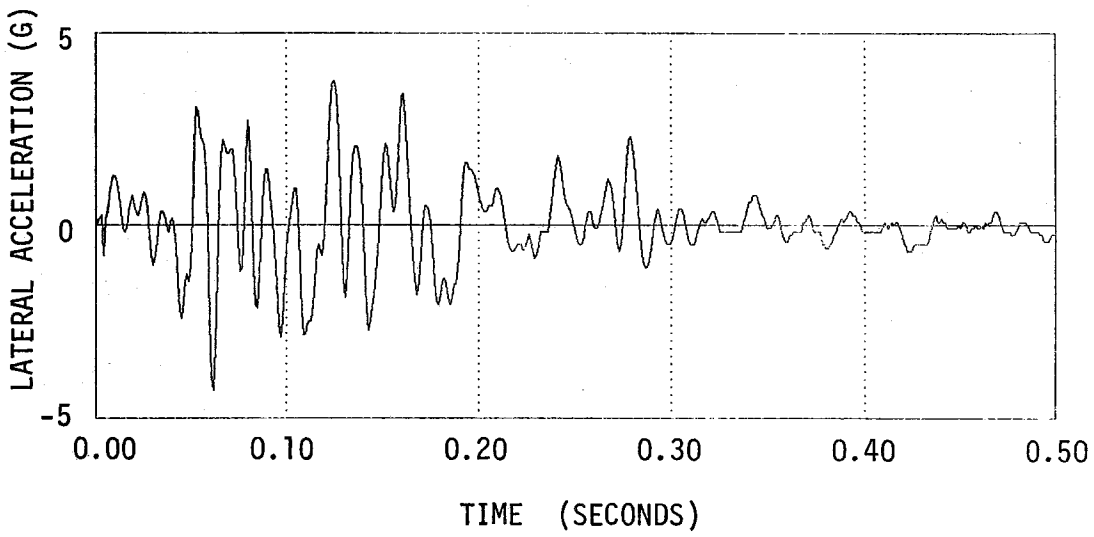

Figure II-2 Vehicle lateral accelerometer trace for test 2346-3.

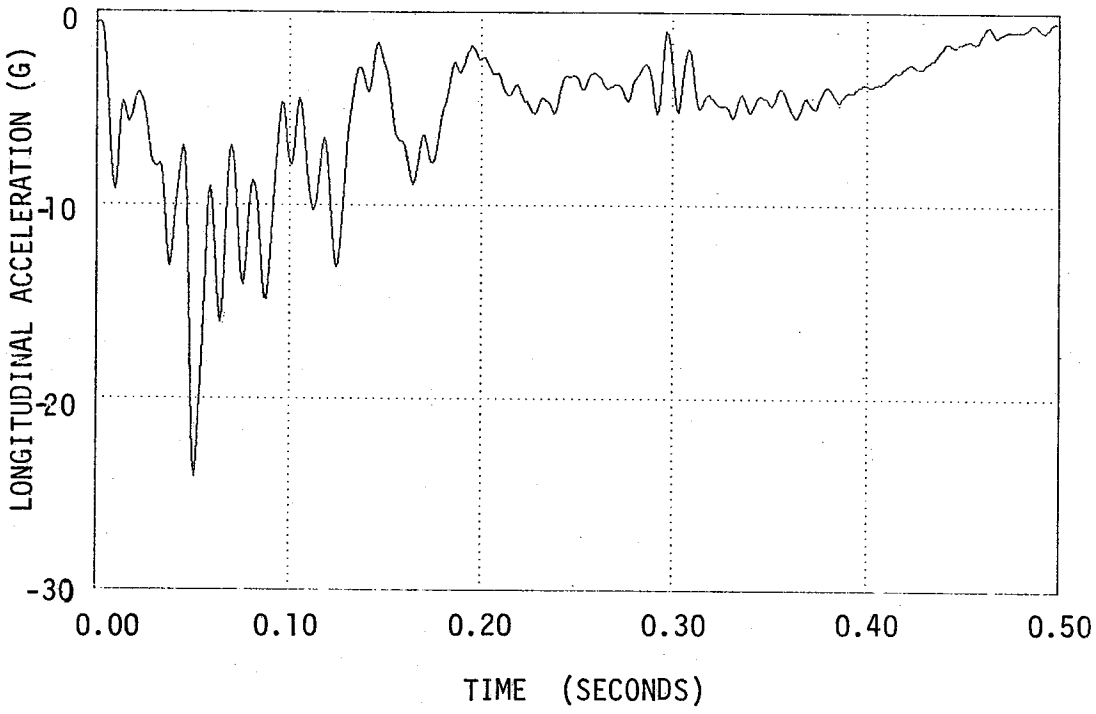

Figure II-3 Vehicle longitudinal accelerometer trace for test 2346-4.

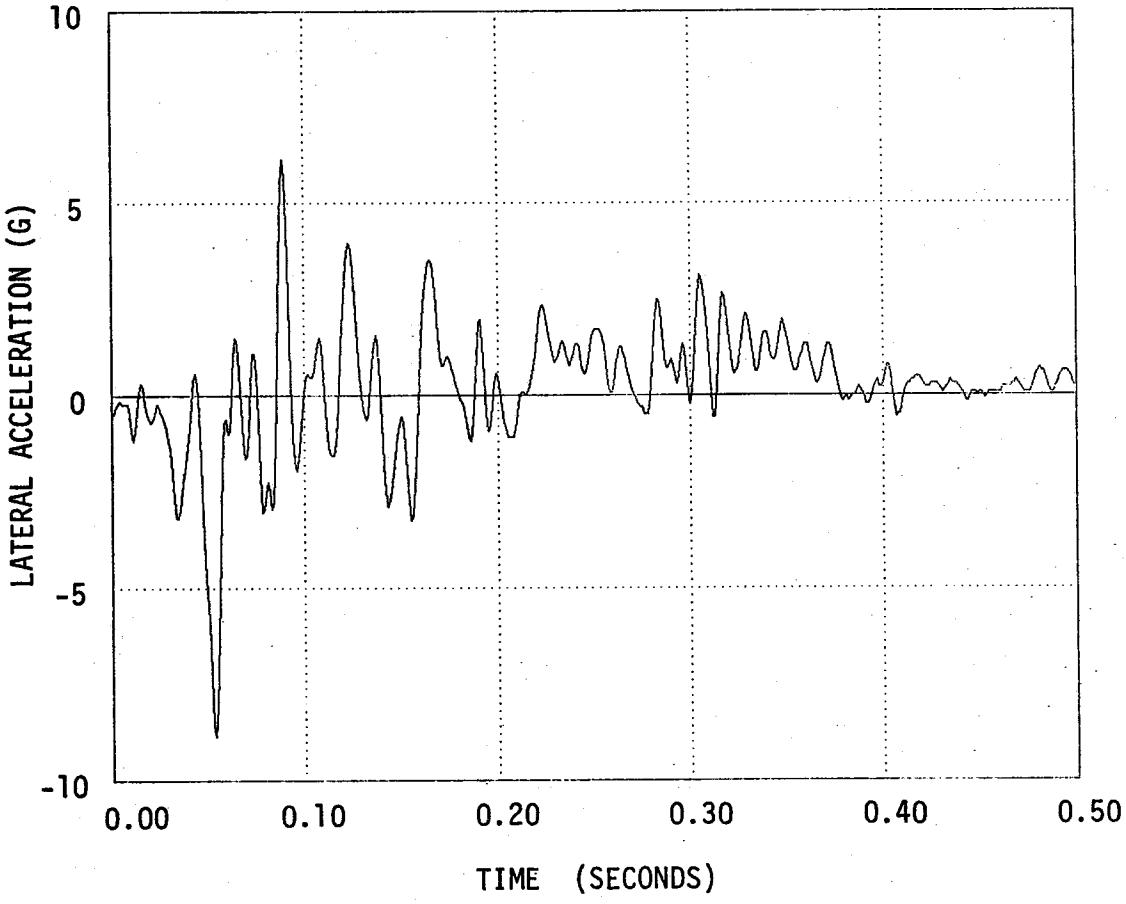

Figure II-4 Vehicle lateral accelerometer trace for test 2346-4.

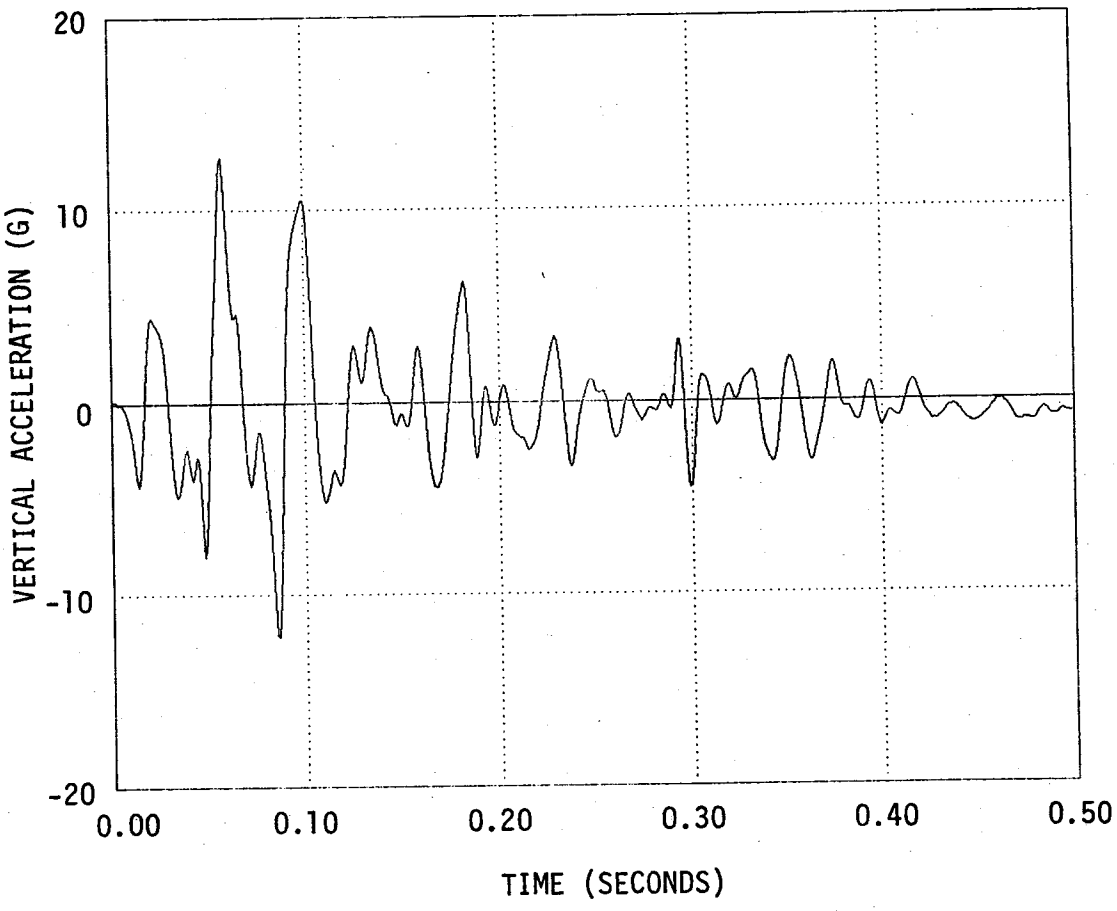

Figure II-5 Vehicle vertical accelerometer trace for test 2346-4.

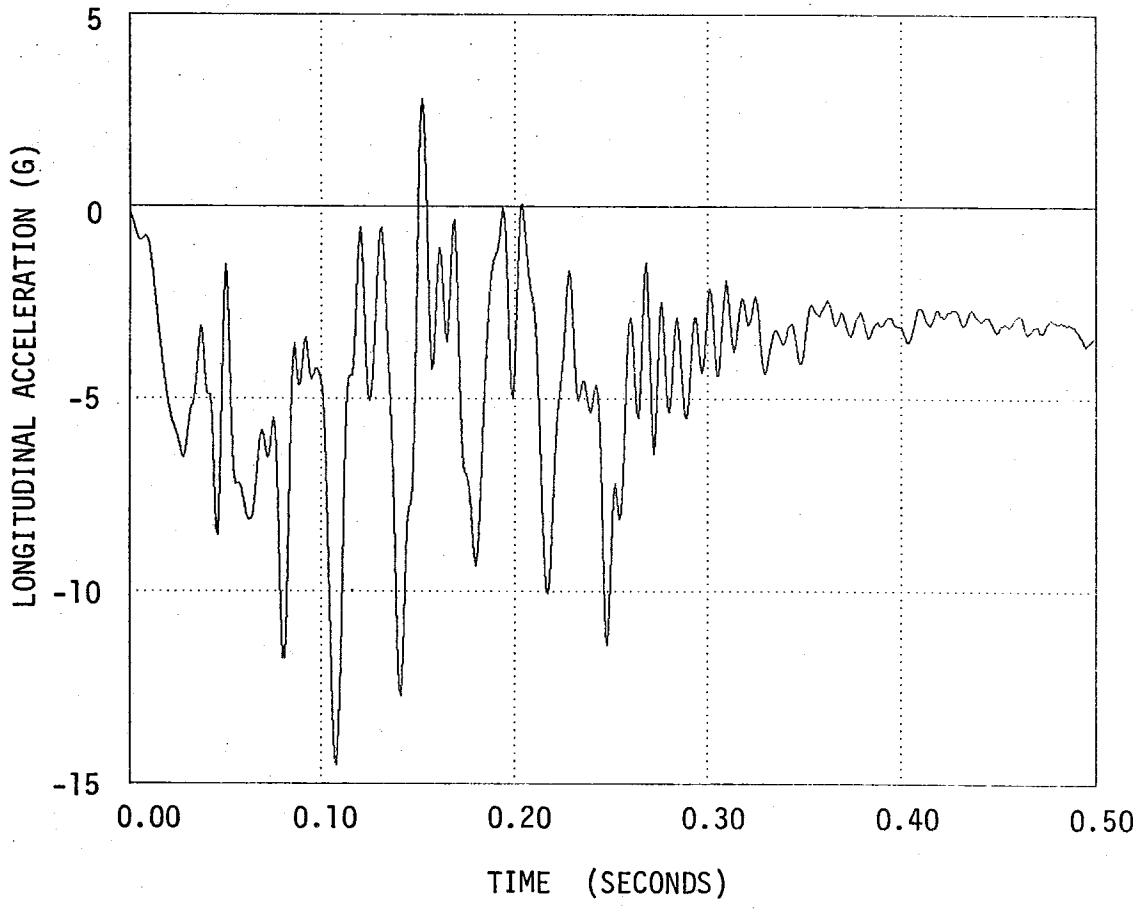

Figure II-6 Vehicle longitudinal accelerometer trace for test 2346-5.

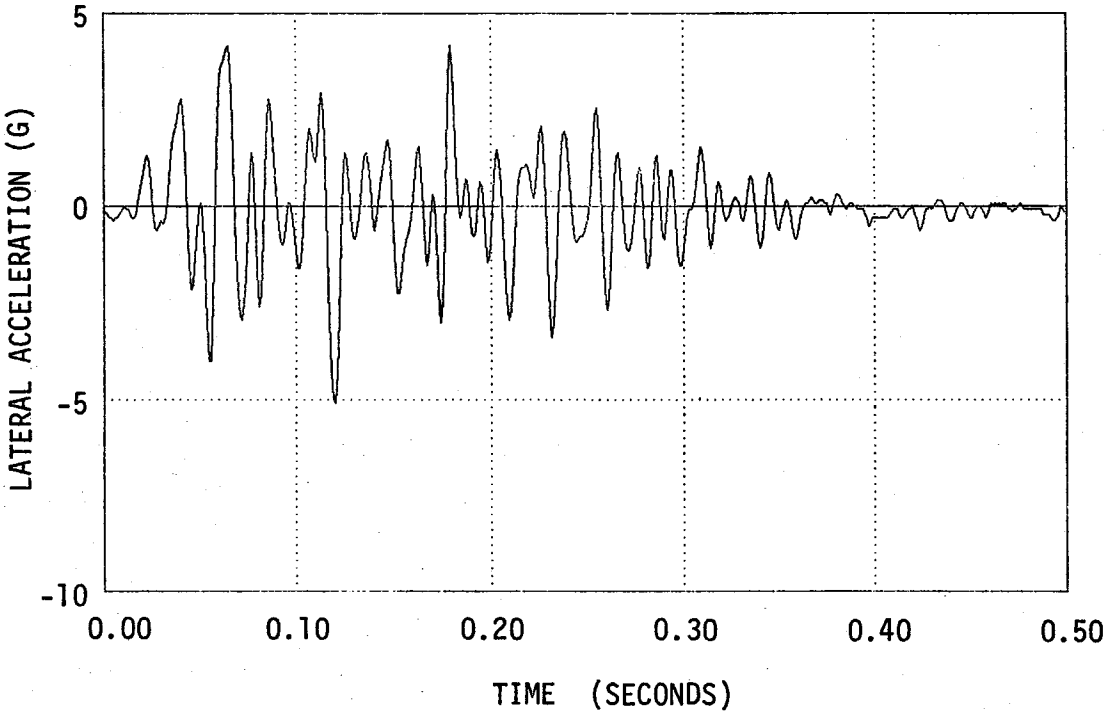

Figure II-7 Vehicle lateral accelerometer trace for test 2346-5.

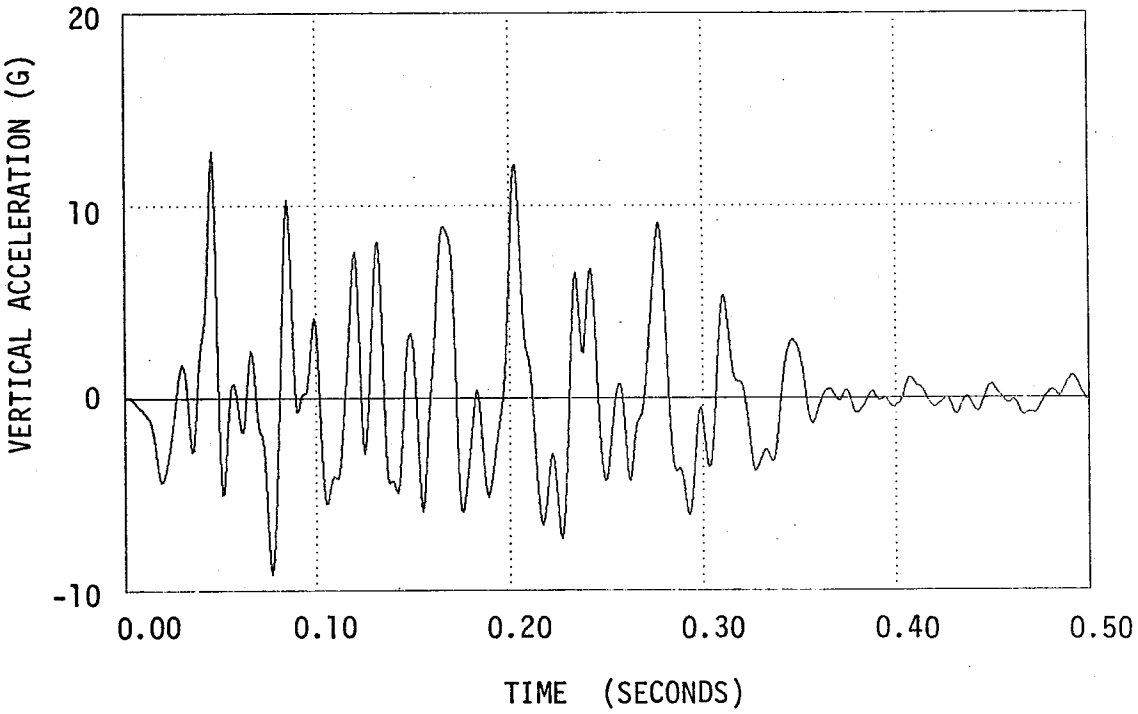

Figure II-8 Vehicle vertical accelerometer trace for test 2346-5.

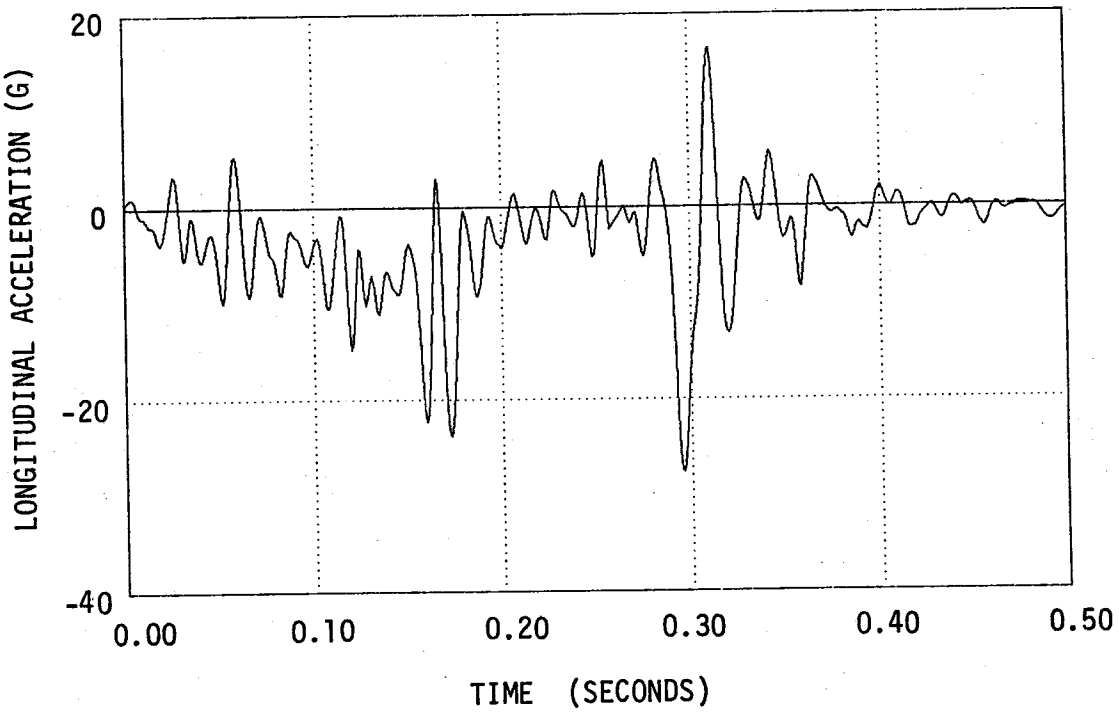

Figure II-9 Vehicle longitudinal accelerometer trace for test 2346-6.

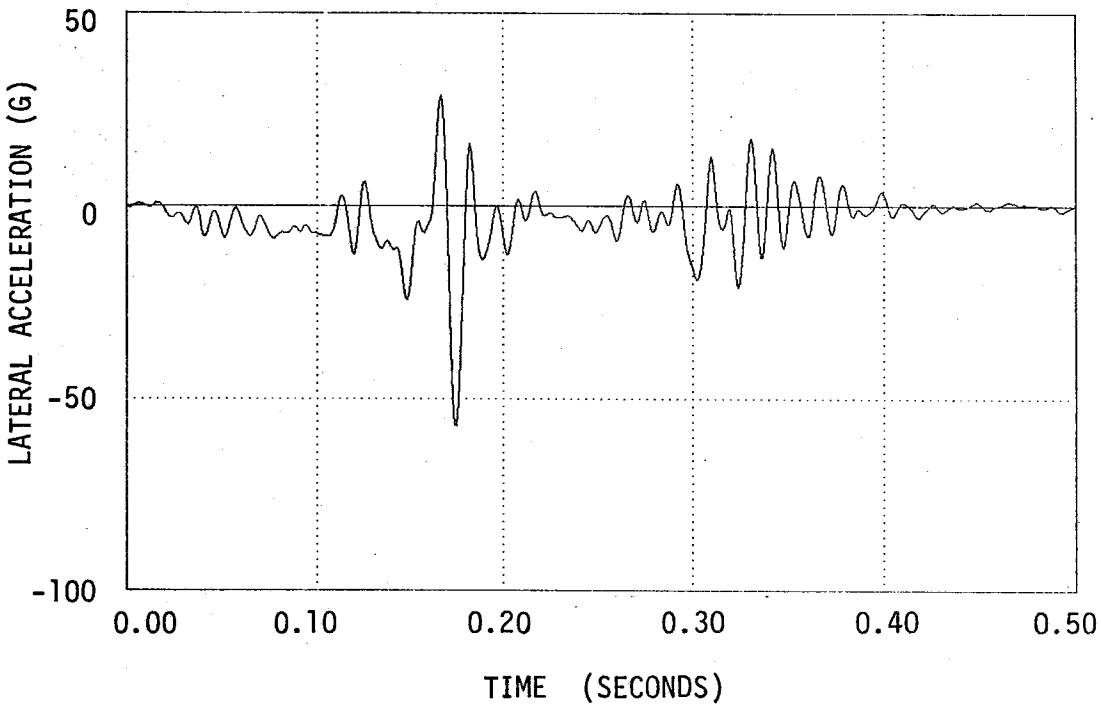

Figure II-10 Vehicle lateral accelerometer trace for test 2346-6.

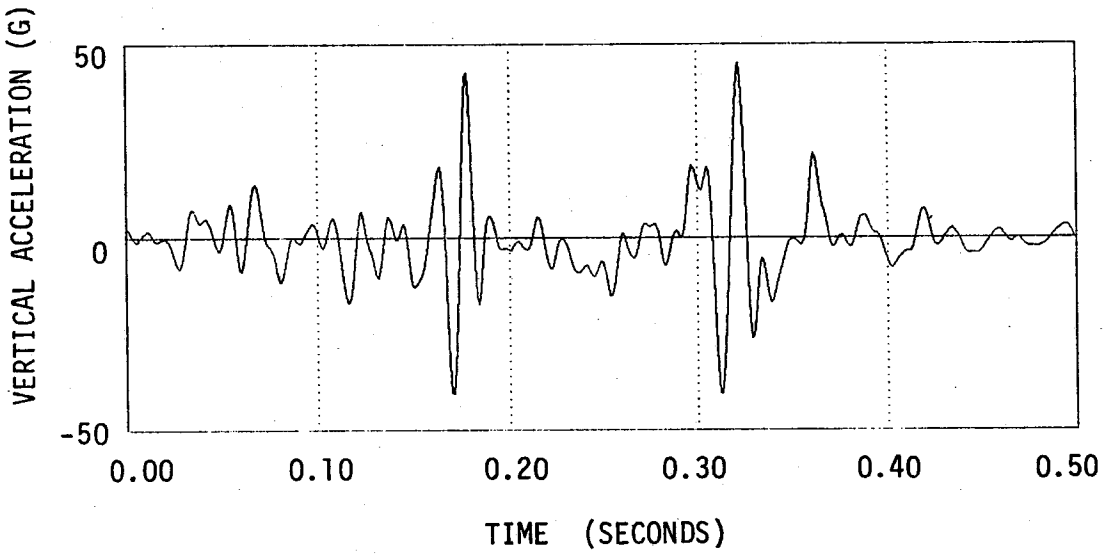

Figure II-11 Vehicle vertical accelerometer trace for test 2346-6.

APPENDIX III.

SEQUENTIAL PHOTOGRAPHS

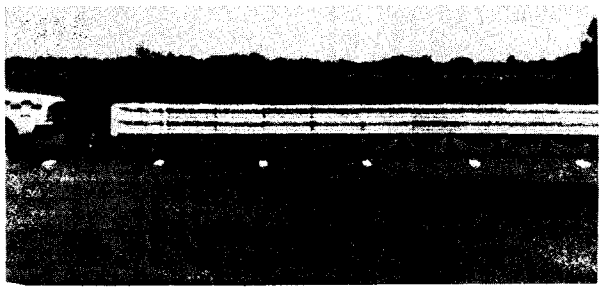

0.000 sec

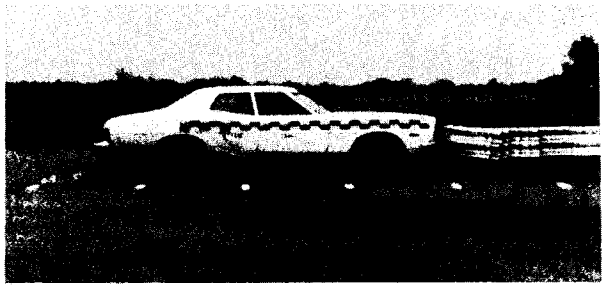

0.343 sec

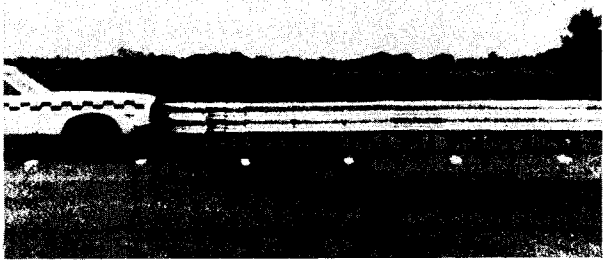

0.086 sec

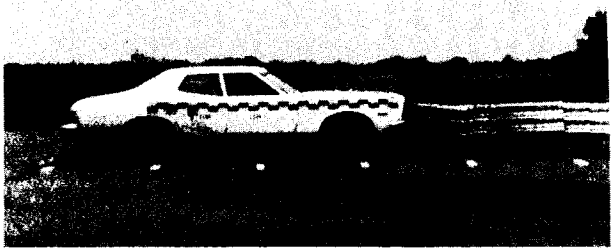

0.429 sec

0.172 sec

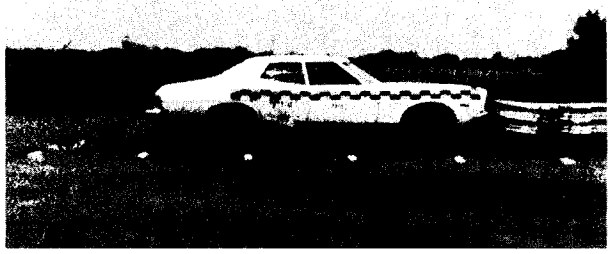

0.515 sec

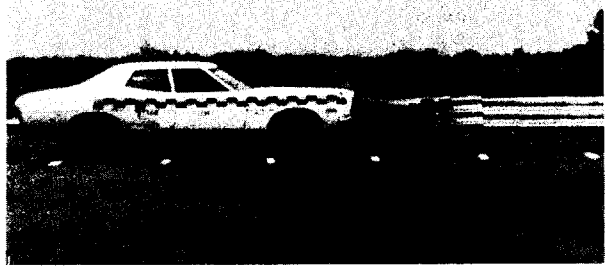

0.257 sec

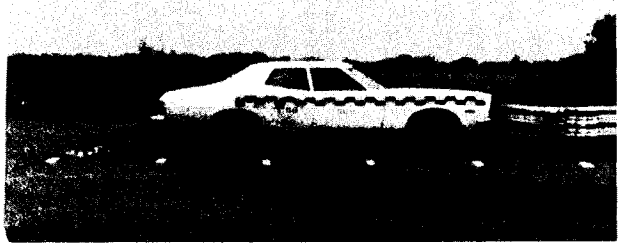

0.598 sec

FIGURE III-1 SEQUENTIAL PHOTOS OF TEST-3

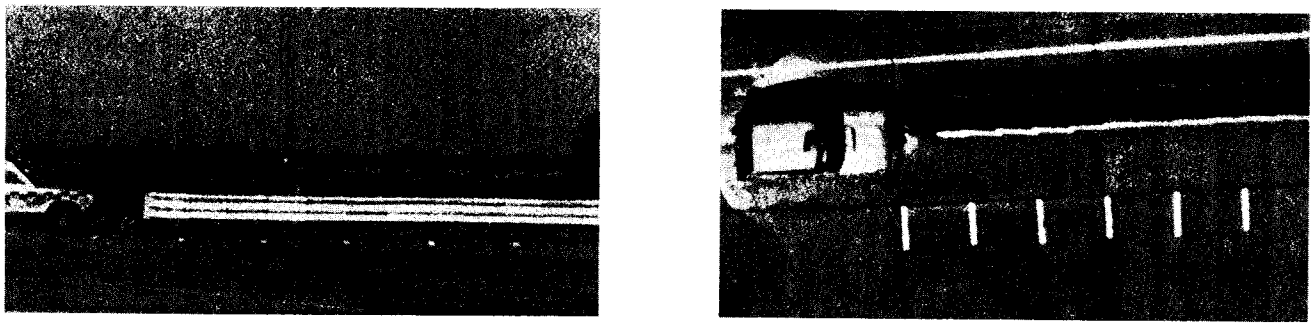

0.000 sec

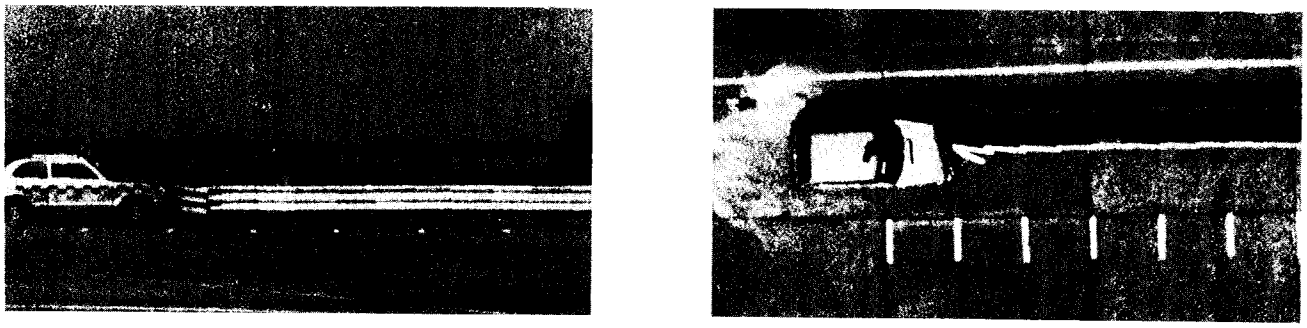

0.065 sec

0.131 sec

0.196 sec

FIGURE III-2 SEQUENTIAL PHOTOS OF TEST-4

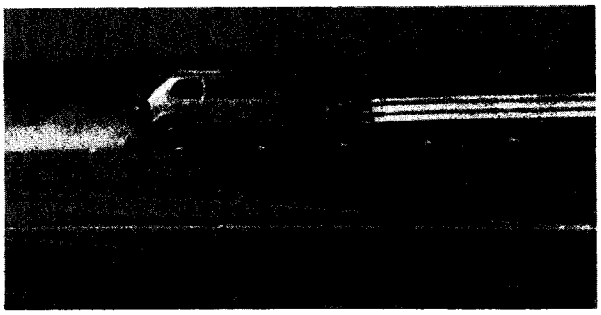
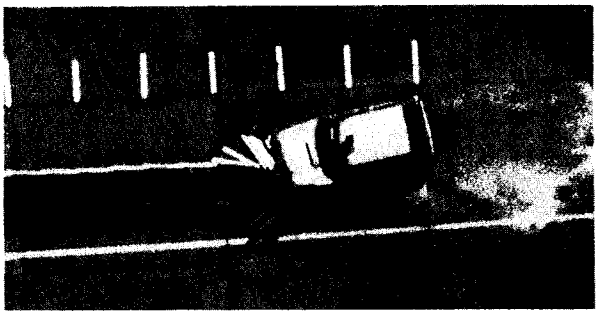

0.262 sec


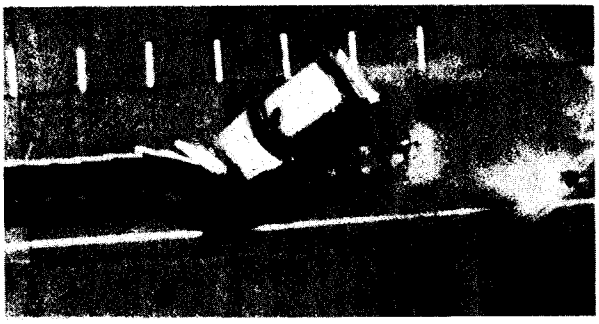

0.390 sec


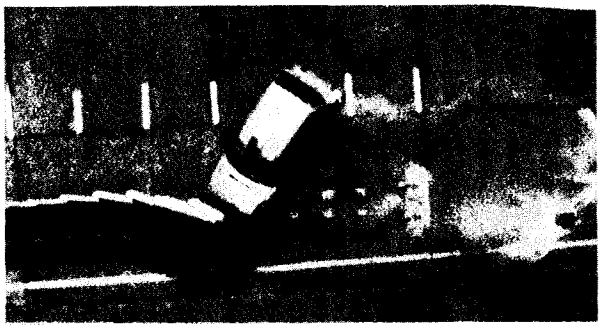

0.521 sec


0.692 sec

FIGURE II-2 SEQUENTIAL PHOTOS OF TEST-4 (CONTINUED)

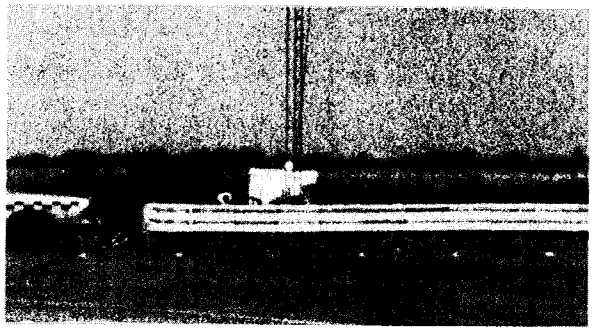

0.000 sec

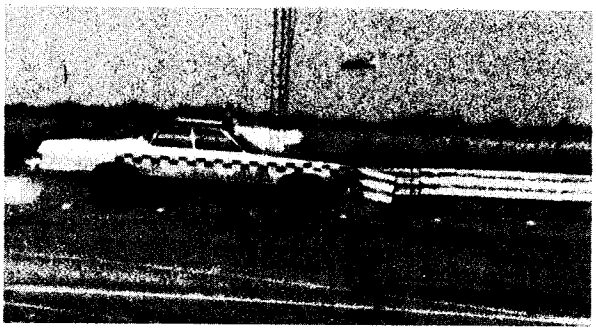

0.252 sec

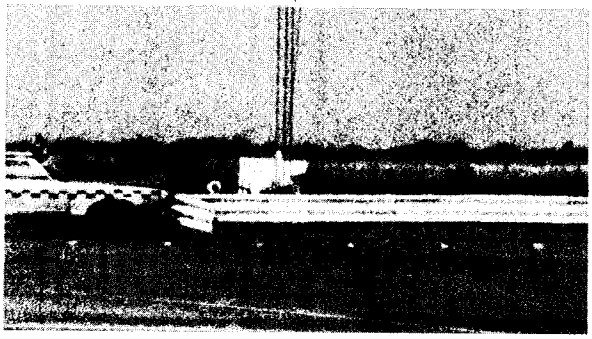

0.063 sec

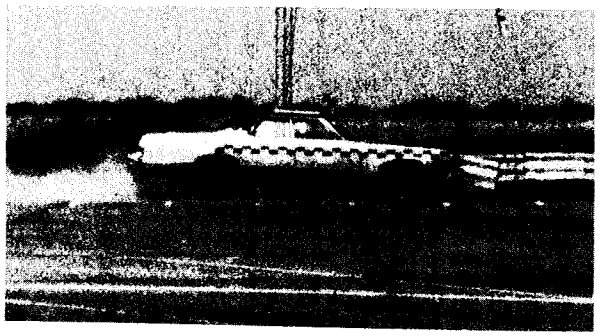

0.405 sec

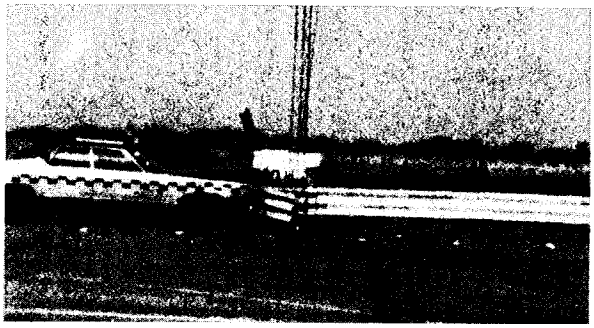

0.126 sec

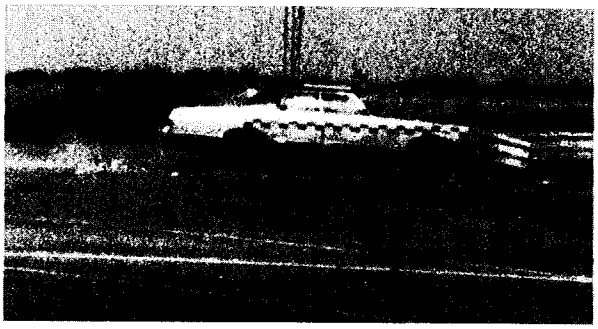

0.558 sec

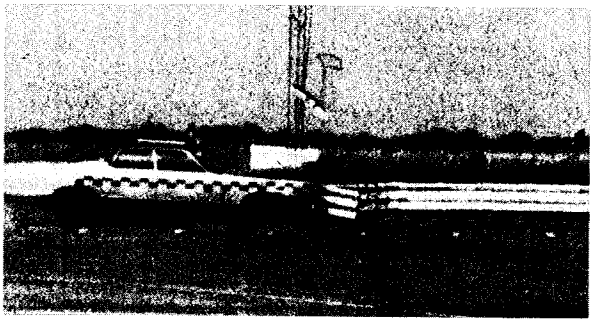

0.189 sec

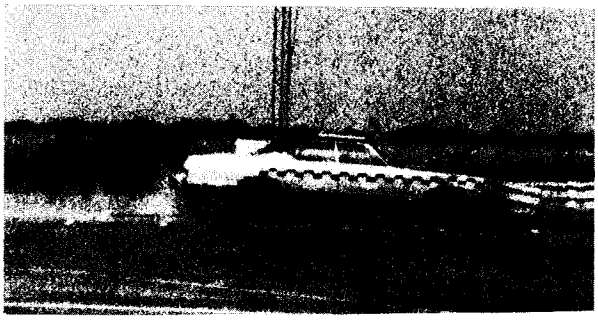

0.712 sec

FIGURE III-3 SEQUENTIAL PHOTOS OF TEST-5

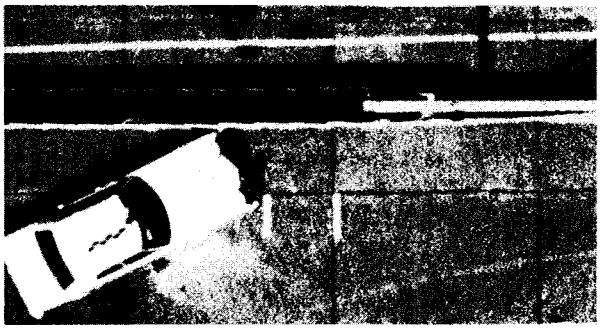

0.000 sec

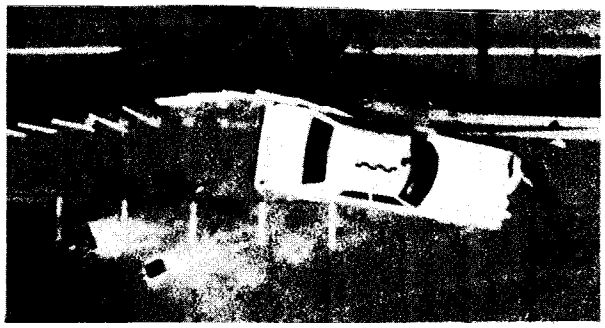

0.267 sec

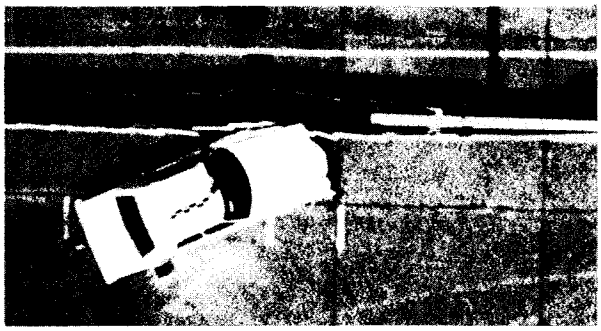

0.067 sec

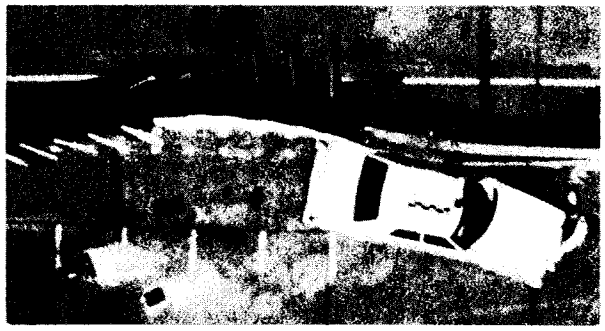

0.334 sec

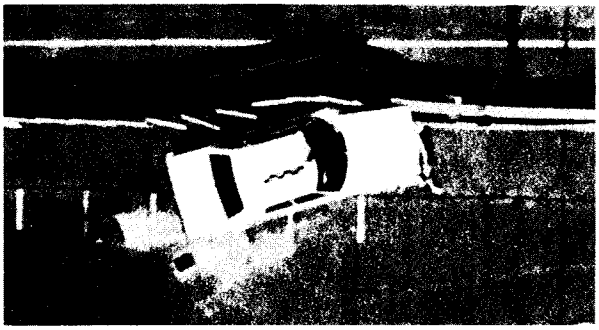

0.134 sec

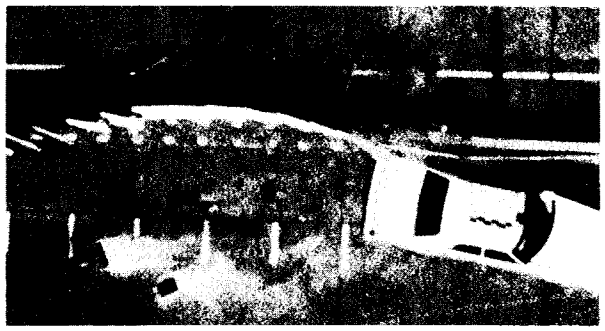

0.407 sec

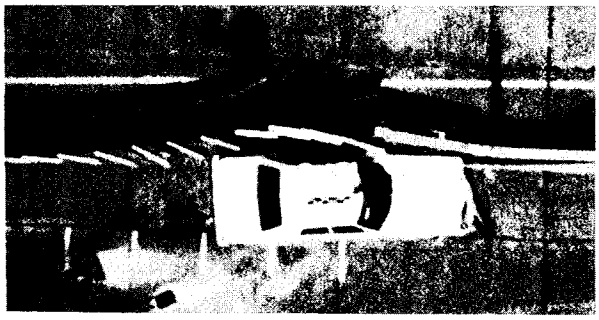

0.201 sec

0.481 sec

FIGURE III-4 SEQUENTIAL PHOTOS OF TEST-6

Appendix IV. Benefit/Cost Model

Appendix IV is a copy of reference 2 and is included as a description of the formulation of the benefit/cost model used in the development of guidelines for the use of concrete barriers on the roadside.

ABSTRACT

In recent years, benefit/cost (B/C) analysis procedures have been widely accepted as a national method for evaluating safety treatment alternatives. Most analysis methods employed to date have significant limitations, overstate the severity of accidents, and are cumbersome to use. An advanced B/C analysis model that incorporates numerous modifications to enhance versatility and improve determination of accident severity is described. Basic encroachment data on which the model is based is presented and the applications and limitations of the model are discussed. An example of the use of the model to develop general barrier use guidelines is also included.

INTRODUCTION

Highway engineers have always faced the difficult problem of determining when and where safety features should be used. Until recently, safety feature use guidelines were based primarily on the relative hazard of the possible alternatives. For example, if a high-speed traversal of a roadside slope was thought to be more hazardous than a similar impact with a roadside barrier, the barrier was deemed to be necessary. No consideration was given to the probability that a high-speed accident would occur. This led highway agencies to invest large sums of money to erect guardrail at sites where there was little or no probability of the occurrence of a severe accident.

When safety improvement programs gained higher priority, safety projects began to compete with construction and other projects for highway agency funds. Therefore, it became necessary to evaluate the relative merits of all projects. A benefit/cost (B/C) analysis procedure for

studying safety improvements was then developed to determine the benefits obtained from each dollar spent on safety improvement (1). The 1977 AASHTO barrier guide presented highway engineers with a "simplified" B/C analysis procedure (2). Accident severities were estimated by highway safety professionals including accident investigators, highway engineers, and researchers. Severities derived in this manner have been found to be representative of high-speed accidents. As a result, all predicted accidents were by default assumed to involve high-impact speeds, and the procedure overstated the severity of many types of accidents. Therefore, the technique frequently led to the use of safety appurtenances at sites where such devices were not warranted. In these cases, accidents involving the safety treatment occur more frequently and are more severe than accidents at similar untreated sites.

Efforts to further refine the B/C analysis technique have led researchers to develop relatively sophisticated algorithms (3,4,5). Although these programs do a better job of properly accounting for all of the costs associated with a safety improvement, the procedures have significant limitations, generally continue to overstate the severity of most accidents that are predicted to occur, and are very difficult to use.

In an effort to resolve some of the problems associated with existing warranting procedures, an advanced B/C analysis algorithm was developed. Major improvements have been made in the algorithm to improve the versatility of the procedure and the determination of the severity associated with predicted accidents. Further, the algorithm has been coded for use with micro-computers to reduce implementation problems.

BENEFIT/COST METHODOLOGY

The benefit/cost methodology compares the benefits derived from a safety improvement to the direct highway agency costs incurred as a result of the improvement. Benefits are measured in terms of reductions in societal costs due to decreases in the number and/or severity of accidents. Direct highway agency costs are comprised of initial, maintenance, and accident repair costs of a proposed improvement. A ratio between the benefits and costs of an improvement is used to determine if the improvement is cost beneficial as shown below:

$$BC_{2-1} = \frac{SC_1 - SC_2}{DC_2 - DC_1} \qquad (1)$$

where:

BC_{2-1} = B/C ratio of alternative 1 compared to alternative 2

SC_i = annualized societal cost of alternative i

DC_i = annualized direct cost of alternative i

For the equation formulated above, alternative 2 is normally considered to be an improvement relative to alternative 1. When the B/C ratio for a safety improvement is below 1.0, the improvement should not normally be implemented. However, budgetary limitations prevent funding of all projects that have a B/C of 1.0 or more. Ideally, a highway agency can use a B/C approach to analyze all proposed projects, including safety improvements, rehabilitation, new construction, etc., to determine the optimum use of available funding.

ACCIDENT PREDICTION MODEL

Most benefits and some costs associated with a safety improvement are directly related to the number and severity of accidents that will occur at the site under consideration. Thus, accident prediction is critical to the analysis of the need for safety improvements. Although some authors have attempted to use accident data to predict accident frequency and severity, to date these efforts have met with limited success due to poor quality and/or small accident data bases. Currently, the best available methods for predicting accident frequency and severity are based on encroachment probability models.

An encroachment probability model is based on the concept that the number of run-off-the-road accidents occurring at a given site can be related to the number of vehicles that inadvertently leave the roadway at that site. Further, it is assumed that the frequency and nature of uncontrolled encroachments can be related to roadway and traffic characteristics. Thus the goal of an encroachment probability model is to relate roadway and traffic characteristics to the expected accident frequency at any site.

The general approach in calculating accident frequency is to determine the region along the roadway, or hazard envelope, within which a vehicle leaving the travelway at a prescribed angle will impact the hazard. A typical hazard envelope is shown in Figure 1. Note that the hazard envelope is divided into three basic ranges. The first encroachment range corresponds with accidents involving the side of the hazard parallel to the roadway and is the same length as the hazard. The second range corresponds to impacts on the corner of the hazard between the two exposed faces and is a function of the effective width of the vehicle. Accident

analysis studies have shown that many vehicles involved in roadside accidents are not tracking (6,7). Therefore the effective vehicle width used in the encroachment algorithm is the average of the vehicle width and length. The third encroachment range corresponds to vehicles impacting the side of the hazard and is a function of the width of the hazard.

As shown in Figure 1, uncontrolled vehicles are assumed to encroach along a straight path. The probability that a vehicle of a particular size will leave the traveled way within a specific encroachment range at a prescribed angle and speed is merely the length of the range in miles times the probability of a vehicle encroaching under the given conditions.

$$P(E_{V,\theta}^{W,2}|E) = P(w)P(E_{V,\theta}|E)(We/\sin\theta)/5280 \qquad (2)$$

where

$P(E_{V,\theta}^{W,2}|E)$ = The probability that a vehicle of size w will encroach at speed v and angle θ into encroachment range 2, given that an encroachment has occurred.

$P(w)$ = The probability that an encroaching vehicle will be of size w.

$P(E_{V,\theta}|E)$ = The probability that an encroaching vehicle will be traveling at speed v and encroaching at angle θ.

We = Effective vehicle width (1/2 vehicle width + 1/2 vehicle length) (ft)

Note that this probability is based on the assumption that vehicles encroach randomly within the area of interest.

When a vehicle leaves the travelway within the hazard envelope, there is some probability that the vehicle will stop or steer back to the

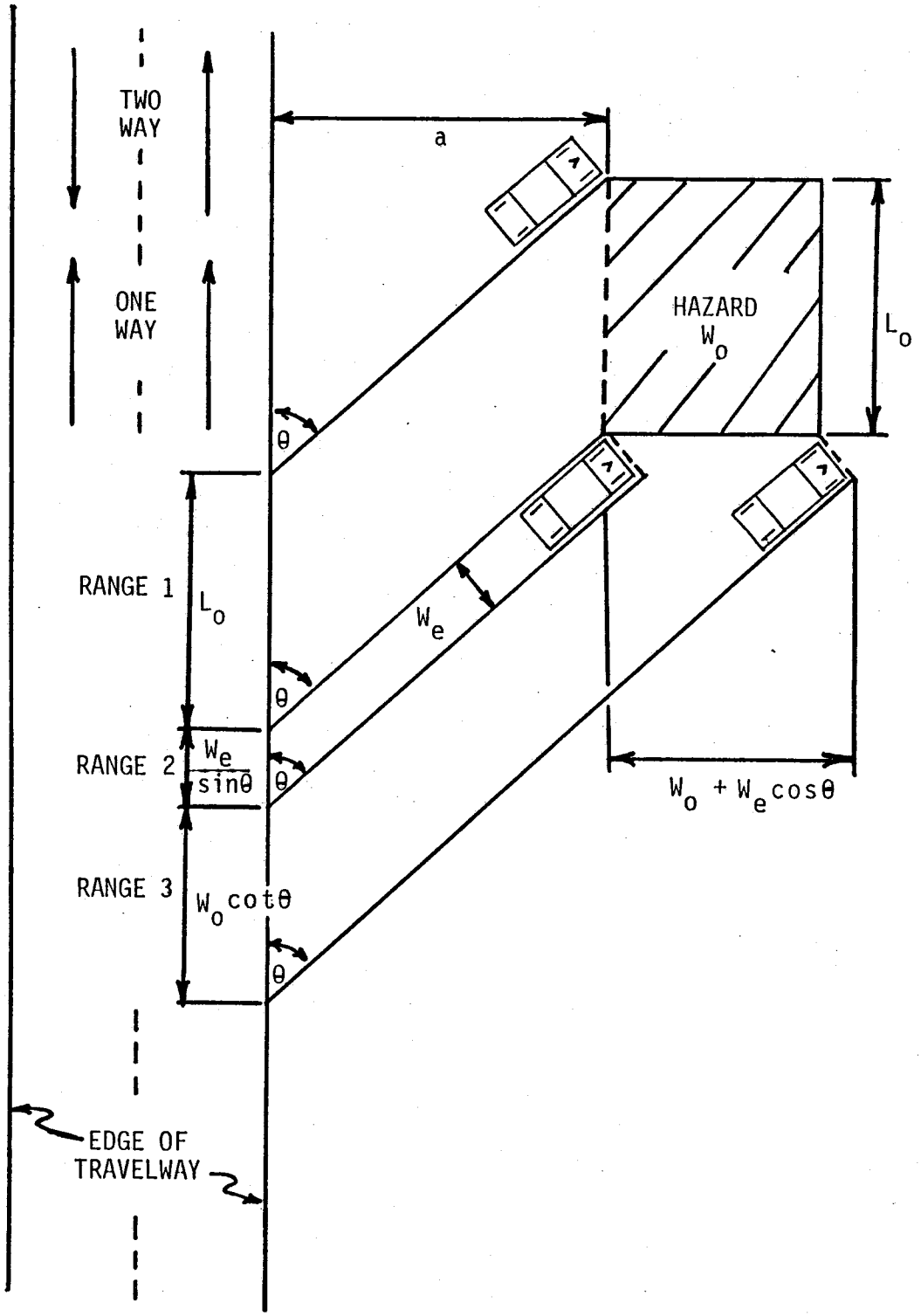

FIGURE 1. HAZARD ENVELOPE FOR SINGLE HAZARD

roadway before impacting the hazard. Therefore, the probability of entering the hazard envelope must be modified by the probability of a vehicle encroaching far enough laterally to reach the obstacle. The probability that an encroaching vehicle will impact the corner of the hazard is

$$P(C_{V,\theta}^{W,2}|E) = P(w)P(E_{v,\theta})(1/5280)(\sec\theta \csc\theta \sum_{j=1}^{N} P(LE>(a+j-1/2))) \quad (3)$$

where

$P(C_{V,\theta}^{W,2}|E)$ = probability that a vehicle of size w encroaching at speed v and angle θ will impact hazard within range 2, given that an encroachment has occurred.

a = distance from travelway to fixed object (ft).

$P(LE>(a+...))$ = probability that the lateral extent of encroachment is greater than or equal to a+...

$N = W_e \times \cos\theta$ (ft)

The probability that an encroaching vehicle will impact with a single hazard is merely the sum of the probabilities of impacts within each encroachment range.

For most circumstances of interest, two or more hazards are present at one location. For these situations the hazard envelopes can overlap and create a complex geometric problem as shown in Figure 2. This figure shows a rectangular hazard shielded by guardrail. Some vehicles encroaching within this region will impact the longitudinal barrier and be redirected, while other accidents will involve vehicles going behind or through the barrier and impacting the protected hazard. Hazard envelopes for multiple hazard locations can be described if the relative locations and the geometry of all hazards are known. Figure 2 shows nine encroachment ranges comparing the overlapping hazard envelopes of the two

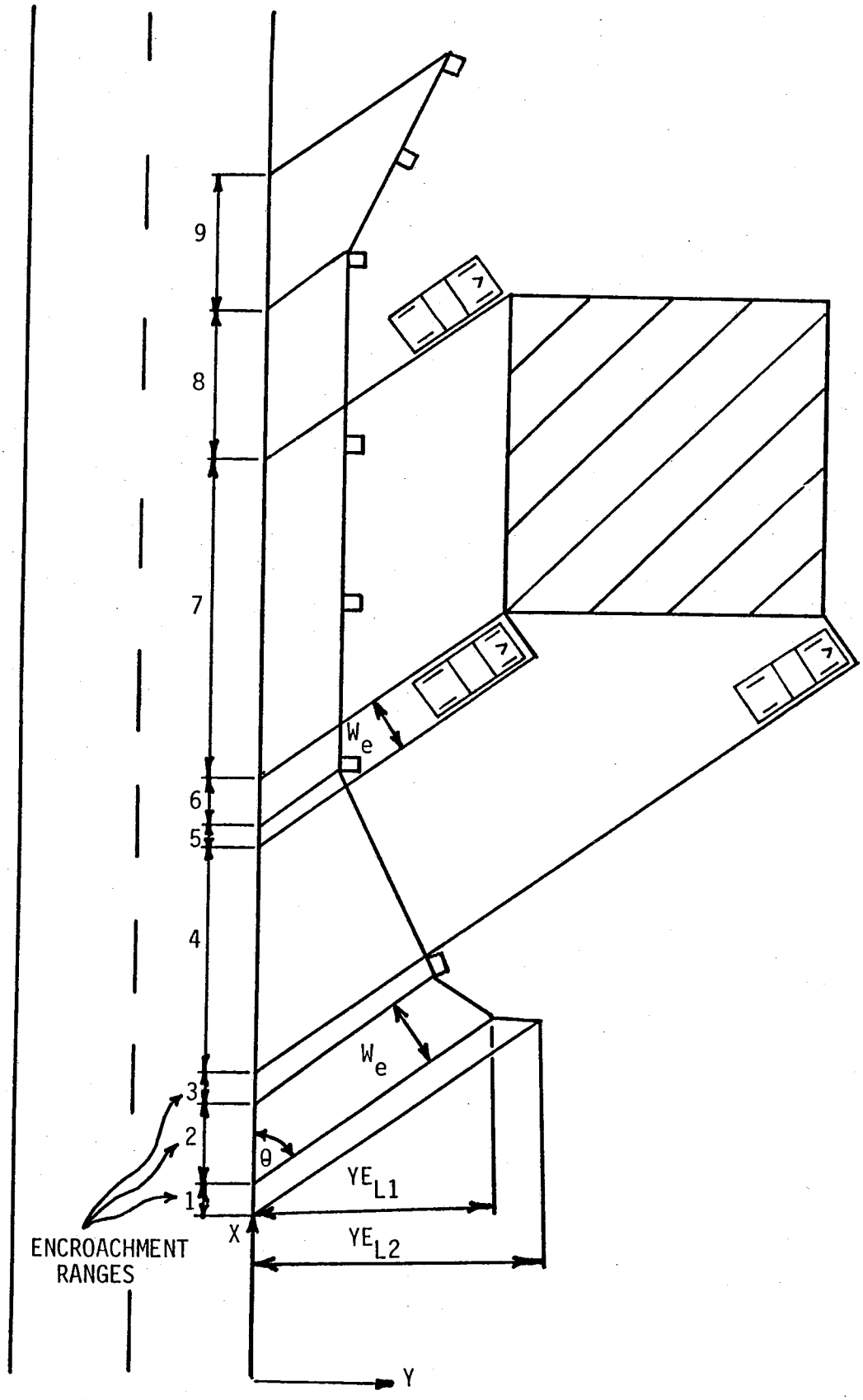

FIGURE 2. HAZARD ENVELOPE FOR MULTIPLE HAZARDS

hazards. Each encroachment range describes a unique combination of hazard faces which an encroaching vehicle would contact. For example, a vehicle with sufficient speed to penetrate the barrier, leaving the roadway within encroachment range 7, would first contact the longitudinal face of the barrier and then the longitudinal face of the hazard.

The encroachment probability model developed under this study uses hazard locations and geometry to determine the limits of all encroachment ranges and the lateral distances to each hazard within the range. The model then calculates the probability of a collision within each encroachment range in a manner analogous to that given in equation 3 as shown below:

$$P(C_{V,\theta}^{W,i} \mid Ev,\theta^{W}) = L_i/5280 \sum_{j=YB_{L_i}}^{YE_{L_i}} \frac{P(LE \geq j)}{\left| YE_{L_i} - YB_{L_i} \right|} \qquad (4)$$

where

$P(C_{V,\theta}^{W,i} \mid Ev,\theta^{W})$ = Probability that a vehicle of size w leaving the roadway at speed v and angle θ will impact the first hazard within encroachment range i given that an encroachment has occurred involving v,s,w, speed v, and angle θ.

L_i = Length of encroachment range i.

YE_{L_i} = Lateral distance from end of encroachment range i to first hazard within the range.

YB_{L_i} = Lateral distance from beginning of encroachment range i to first hazard within the range.

The total accident costs for any site can then be determined by multiplying the collision probability from equation 4 by the encroachment

frequency and the accident cost of the predicted accident and summing overall possible accident types.

$$AAC = \sum_{w} \sum_{v} \sum_{\theta} \sum_{i} P(C^{w,i}_{v,\theta} E^{w}_{v,\theta}) AC^{w,i}_{v,\theta} E_f \qquad (5)$$

where

AAC = Annual accident costs arising from run-off-road traffic accidents within the region of interest ($/yr).

E_f = Uncontrolled encroachment frequency (Enc/mi/yr).

$\sum_{w}$ = Summation over all encroachment vehicle sizes.

$\sum_{v}$ = Summation over all encroachment velocities.

$\sum_{\theta}$ = Summation over all encroachment angles.

$\sum_{i}$ = Summation over all encroachment ranges.

$AC^{w,i}_{v,\theta}$ = Accident costs associated with an accident involving a vehicle of size w, impacting hazard i at speed v and angle θ.

The above equation is based on the probability of the encroaching vehicle impacting the first hazard within encroachment range i. For some predicted accidents, the impacting vehicle will penetrate the first hazard within the encroachment range. For example, longitudinal barriers have a performance level beyond which vehicle restraint cannot be assured. When a vehicle is predicted to penetrate the first hazard within the range, it is assumed that the vehicle will impact the next hazard within the range.

Accident costs shown above were calculated for traffic moving in only one direction. A very similar procedure was developed for use on two-lane, two-way highways. In this application, the accident prediction

algorithm is used twice. The procedure is first used to determine the costs of accidents resulting from vehicles leaving the right side of the roadway. Then accident costs are developed in an analogous procedure for accidents involving vehicles leaving the left side of the roadway. Encroachments from the right side lane have been shown to comprise approximately 65% of all encroachments (6,8). For two-lane roadways, the remaining encroachments must originate from the left side of the travelway.

Encroachment Characteristics

The accident prediction model described above requires a knowledge of certain characteristics of uncontrolled encroachments including frequency, speed, angle, and lateral movement. Very little pure encroachment data is currently available. The largest data base containing pure encroachment information was collected on Canadian highways by Cooper (9). Unlike other efforts (10), this study involved highways with operating speeds in the same range as most U.S. highways today. Therefore findings from Cooper (9) were used to determine both encroachment frequency and lateral movement information. Cooper collected encroachment frequency data on relatively straight, flat sections of roadways in two different classes, four-lane divided and two-lane, two-way. These data included both controlled and uncontrolled encroachments. Accident data have been used to adjust encroachment frequencies from Cooper to eliminate controlled encroachments (11,12). The adjusted encroachment frequency curves are shown in Figure 3. Accident data have also been used to develop encroachment frequency adjustment factors, shown in Table 1, to account for the effects of vertical or horizontal curvature on encroachment frequency (13).

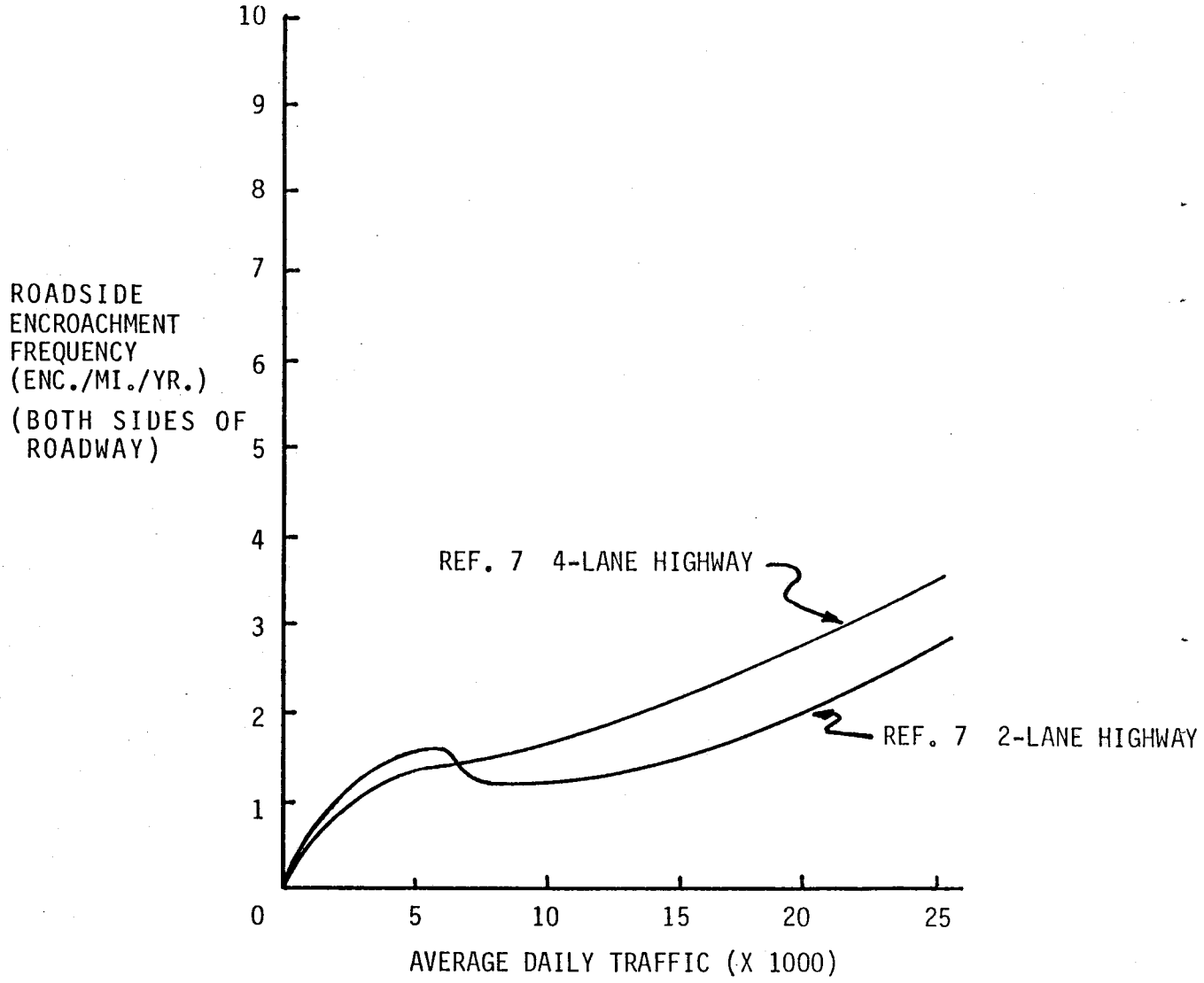

FIGURE 3. ADJUSTED ENCROACHMENT FREQUENCIES FROM REFERENCE 7

TABLE 1. ENCROACHMENT FREQUENCY ADJUSTMENT FACTORS FOR HORIZONTAL AND VERTICAL ALIGNMENT (13)

Roadway Curvature (degrees)	ENCROACHMENT LOCATION WITH RESPECT TO CURVE			
	Inside		Outside	
	Uphill or Moderate Downhill Grade (> - 2%)	Steeper Downhill Grade (≤ - 2%)	Uphill or Moderate Downhill Grade (> - 2%)	Steeper Downhill Grade (≤ - 2%)
0-3	1.00	0.80	1.00	0.80
3.01-6	1.24	2.06	2.76	4.60
> 6	1.98	4.00	4.42	9.00

Cooper also collected lateral extent of encroachment information. Lateral extent of encroachment information from other sources is considered to be unrepresentative of modern accident characteristics since it involved either high-speed traffic (speed limit of 70 mph) (10) or was collected from accident data (8). Distributions of lateral vehicle movement developed from Cooper's data show very few vehicles encroaching less than 10 ft before returning to the roadway. Many of the highways studied had paved or graveled shoulders that tend to hide evidence of encroachments with short lateral extent. Lateral extent of movement data from Cooper has been adjusted by curve fitting the data points beyond 12 ft (the widest shoulder width in the study) to eliminate the effects of paved shoulders. Figure 4 shows both the raw and adjusted lateral extent of movement distributions from reference 9. Note that for very short encroachments, the probability of lateral encroachment is greater than 1. Thus, the curve in Figure 4 serves as an adjustment for the encroachments of short lateral extent that were not detected in the encroachment study.

No pure encroachment data published to date have contained any information regarding encroachment speed. Encroachment velocity and angle are known to be related. Therefore encroachment angle data are believed to be of little value without accompanying speed data. The best available method of estimating combined impact speed and angle distributions is through computer reconstruction of traffic accidents (7,14). Table 2 shows the distribution of freeway encroachment speeds and angles developed from references 7 and 14. Although impact speed distributions developed from accident data are biased toward high impact speeds, accident severities from these distributions are more representative of real-world accidents than severity estimates based solely on high-speed impacts.

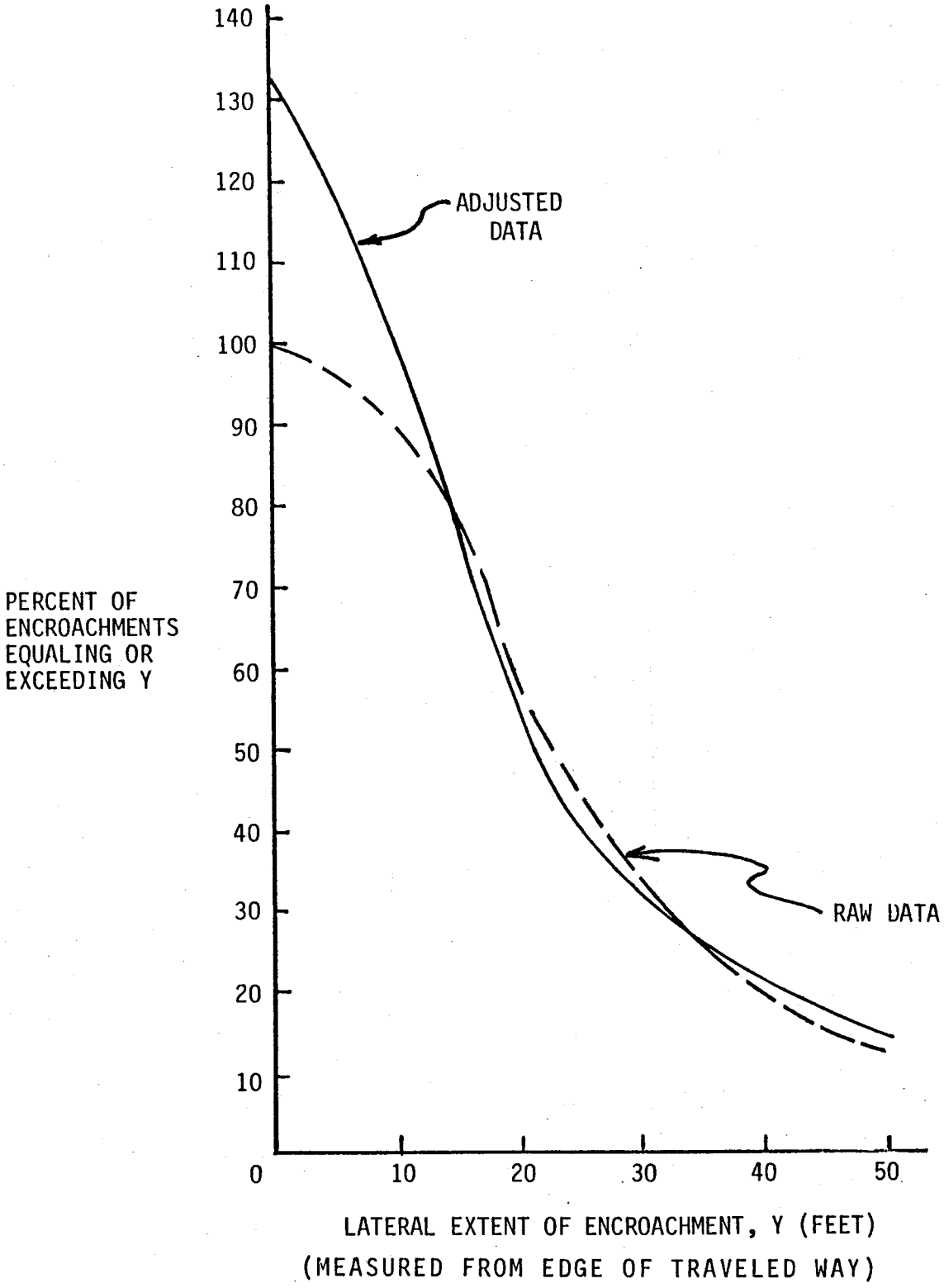

FIGURE 4. ADJUSTED LATERAL ENCROACHMENT DISTRIBUTION FROM REFERENCE 9

TABLE 2. COMBINED IMPACT VELOCITY AND ANGLE DISTRIBUTIONS FROM ACCIDENT STUDIES (9,16)

COMBINED GAMMA FUNCTION PROBABILITIES

Speed (mph)	Angle (degrees) < 5	5-15	15-25	25-35	35-45	> 45	Total
< 20	.0429	.1862	.1163	.0466	.0157	.0067	.414
20-30	.0268	.1163	.0726	.0291	.0098	.0042	.259
30-40	.0168	.0732	.0458	.0183	.0062	.0026	.163
40-50	.0093	.0392	.0245	.0098	.0033	.0014	.088
50-60	.0044	.0191	.0119	.0048	.0016	.0007	.043
> 60	.0035	.0152	.0095	.0038	.0013	.0005	.034
Total	.104	.4490	.2810	.1120	.1790	.016	

Distributions such as the ones shown in Table 2 have been developed for a variety of functional classes of highways. The procedure described herein utilizes the appropriate distribution based on the functional class of highway under consideration.

Although small vehicles have been shown to be overrepresented in reported accident data, it is believed that much of this over-representation is the result of reduced crashworthiness of small mobiles rather than an increased encroachment probability. Little data are currently available to relate encroachment probability to vehicle size. Therefore it has been assumed that encroachment rates are independent of vehicle size and that the probability of an encroaching vehicle being of a particular size is equal to the decimal fraction of vehicles of that size in the traffic stream.

Accident Costs and Performance Levels

Accident costs of primary interest in a benefit/cost analysis are the societal costs resulting from occupant injury and vehicle damage and the direct highway agency costs arising from damage to highway facilities. Societal and direct costs are strongly related to the performance of the highway appurtenance impacted. For example, if a barrier contains and redirects an impacting vehicle, the expected societal costs will normally be well below those of an accident involving barrier penetration. Thus the performance level of a safety device must be defined before accident costs can be determined.

The impact performance of highway appurtenances is generally believed to be limited by the degree of impact loading the device can safely

withstand or attenuate. For barriers, the degree of loading has been shown to be related to the impact severity (IS) as defined below (15,16,17):

$$IS = 1/2\ m(V \sin\theta)^2 \qquad (6)$$

where:

IS = impact severity (ft-lb)

m = vehicle mass ($lb\text{-}sec^2$)

V = vehicle impact velocity (ft/sec)

θ = vehicle impact angle (angle between resultant velocity vector and face of barrier) (deg)

For the benefit/cost algorithm described herein, the performance level for barriers is measured in terms of impact severity. For other devices, such as crash cushions, performance level is measured in terms of total kinetic energy of the impacting vehicle.

Societal costs have traditionally been linked to the severity or probability of injury to vehicle occupants through a severity index scale. This scale was first developed in the mid-1970's (2) and has since been updated to reflect current cost figures (12). Table 3 shows the severity index scale from reference 16.

Crash testing and simulations have been used to estimate impact severities of many common highway hazards in terms of vehicle accelerations and damage. Vehicle accelerations have been linked to occupant injury by comparing damage to crash test vehicles and damage to vehicles involved in traffic accidents (18). Procedures from reference 18 can be used to estimate crash test injury probabilities from measured

TABLE 3. SEVERITY INDEX SCALE

Severity Index	% PDO Accidents*	% Injury Accidents	% Fatal Accidents	Societal Cost per Accident
0	100	0	0	1,600
1	85	15	0	3,450
2	70	30	0	5,500
3	55	45	0	7,500
4	40	59	1	15,800
5	30	65	5	42,400
6	20	68	12	87,900
7	10	60	30	203,000
8	0	40	60	393,000
9	0	21	79	513,000
10	0	5	95	614,000

*PDO refers to those accidents where property damage only is involved.

vehicle accelerations. However, crash testing is normally conducted at speeds near 60 mph. A large gap therefore exists in severity indices data for roadside features at speeds less than 60 mph. In the absence of test data, the researchers have assumed a linear relationship between the severity index, as shown in Table 3, and impact speed. It should be noted that linearity is assumed between severity index and impact speed, not severity per se. As can be seen in Table 3, accident costs increase exponentially as the severity index increases. Figure 5 shows severity indices of W-beam guardrail accidents derived from measured crash test accelerations. Crash test data used in the development of Figure 5 was collected from tests involving full-size, subcompact, and mini-size vehicles. Note that most crash tests involve impact angles of 15 and 25 degrees. Therefore, severity indices for other impact angles must be interpolated and extrapolated from curves shown in Figure 4.

Costs arising from damage to a highway appurtenance are generally believed to be proportional to the degree of impact loading on the appurtenance. References 16 and 17 have shown that IS is approximately proportional to the degree of barrier loading and it follows that barrier repair costs should be roughly proportional to IS. Figure 6 shows repair costs for W-beam guardrail estimated from crash test results. Repair costs of other safety appurtenances are assumed to be roughly proportional to the total kinetic energy of the impacting vehicle. More detailed descriptions of performance level and accident cost determination can be found in reference 5.

Improvements to the Benefit/Cost Model

The benefit/cost model described herein has incorporated most of the improvements found in all previous models. Additional modifications have

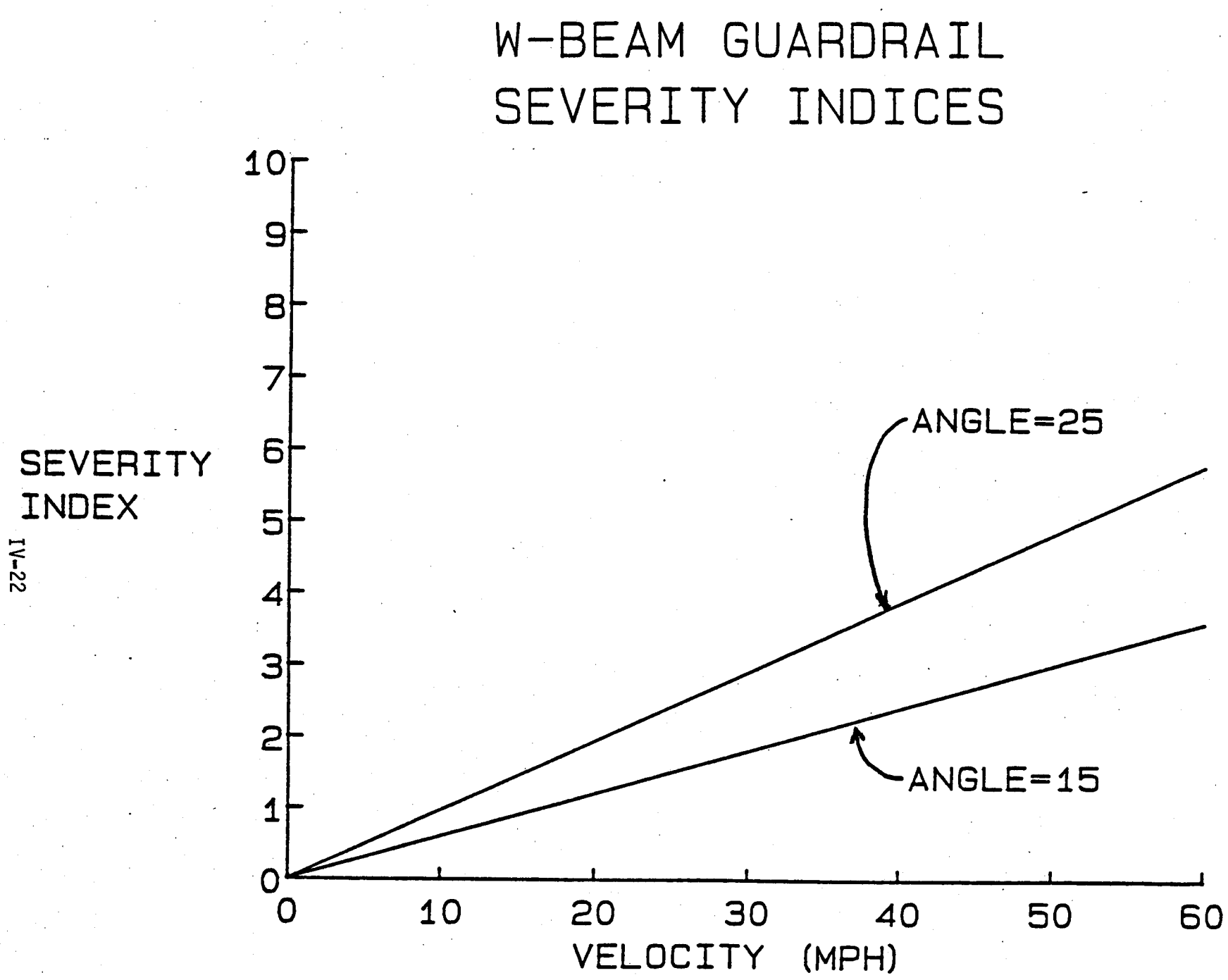

FIGURE 5. W-BEAM GUARDRAIL CRASH TEST SEVERITY INDICES

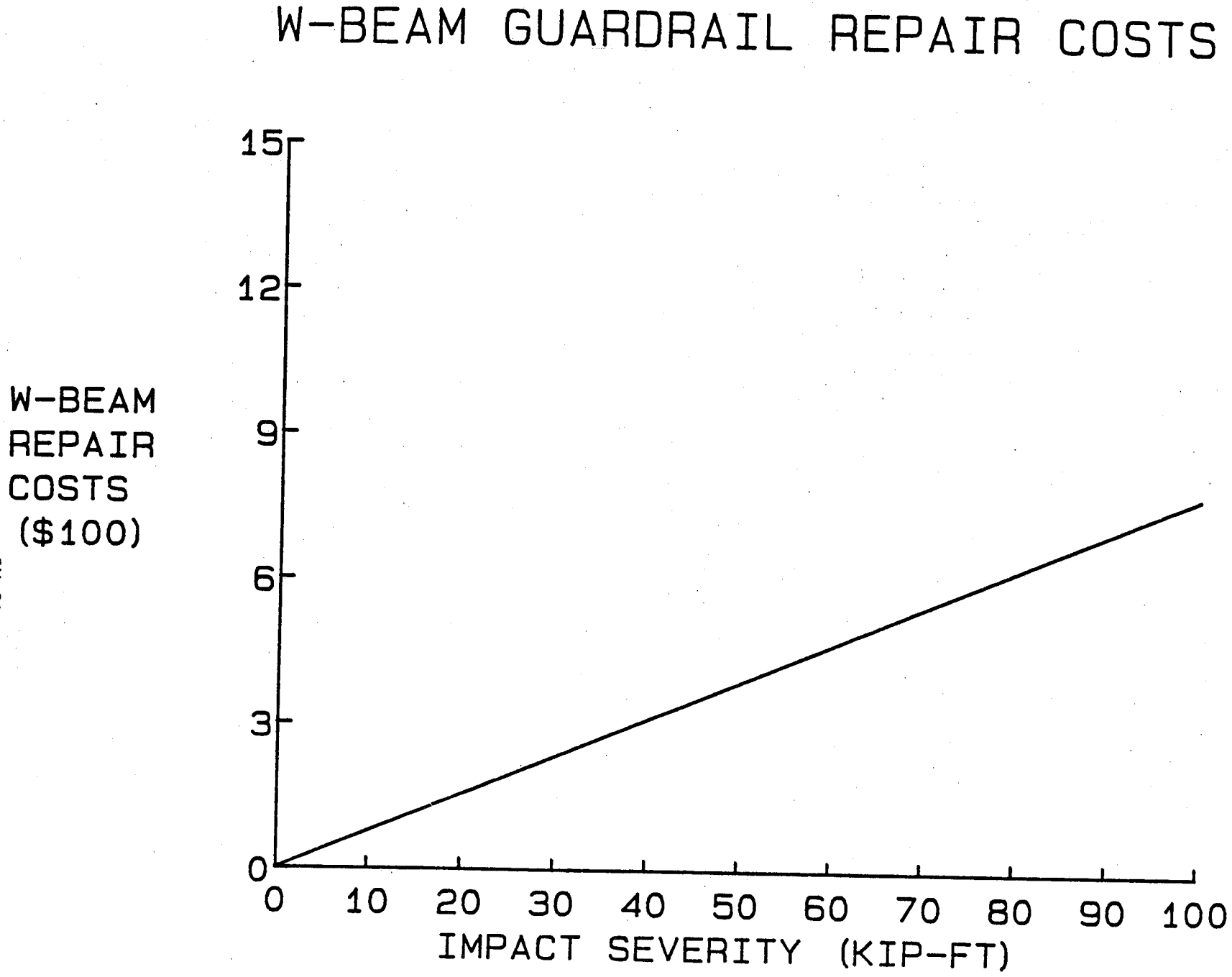

FIGURE 6 W-BEAM GUARDRAIL REPAIR COSTS

been added to improve accuracy and enhance capability of the algorithm including: shielding of one obstacle by another, accident cost and appurtenance repair as a function of accident impact conditions, use of reconstructed accidents to predict impact conditions, and relating appurtenance performance to impact conditions.

Applications and Limitations

The encroachment probability model on which the benefit/cost model is based is general in nature and can therefore be used to study a wide variety of highway conditions. These models are well suited for use in developing general safety treatment guidelines or policies (5).

For example, a common problem faced by many highway engineers is how to safely treat the slope hazard at deep fill sections. In such cases an engineer must determine whether or not to place the slope breakpoint away from the shoulder by increasing the amount of fill material and to use a barrier to shield the slope. Safety treatment alternatives for deep fill sections, shown in Figures 7 and 8, include increasing the available recovery area by moving the slope breakpoint away from the travelway and using W-beam guardrail to shield the slope. Typical cost and severity data for safety treatments of a 20 ft deep fill section are shown below. (Note that for this example the severity of a 60 mph encroachment onto a deep 1-1/2:1 slope is estimated to correspond to a severity index of 8.0. Impact severities for other speeds are estimated based on the assumed linear relationship between impact speed and severity index discussed previously. Further, the severity of impact with steep roadside slopes is assumed to be relative independent of impact angle.)

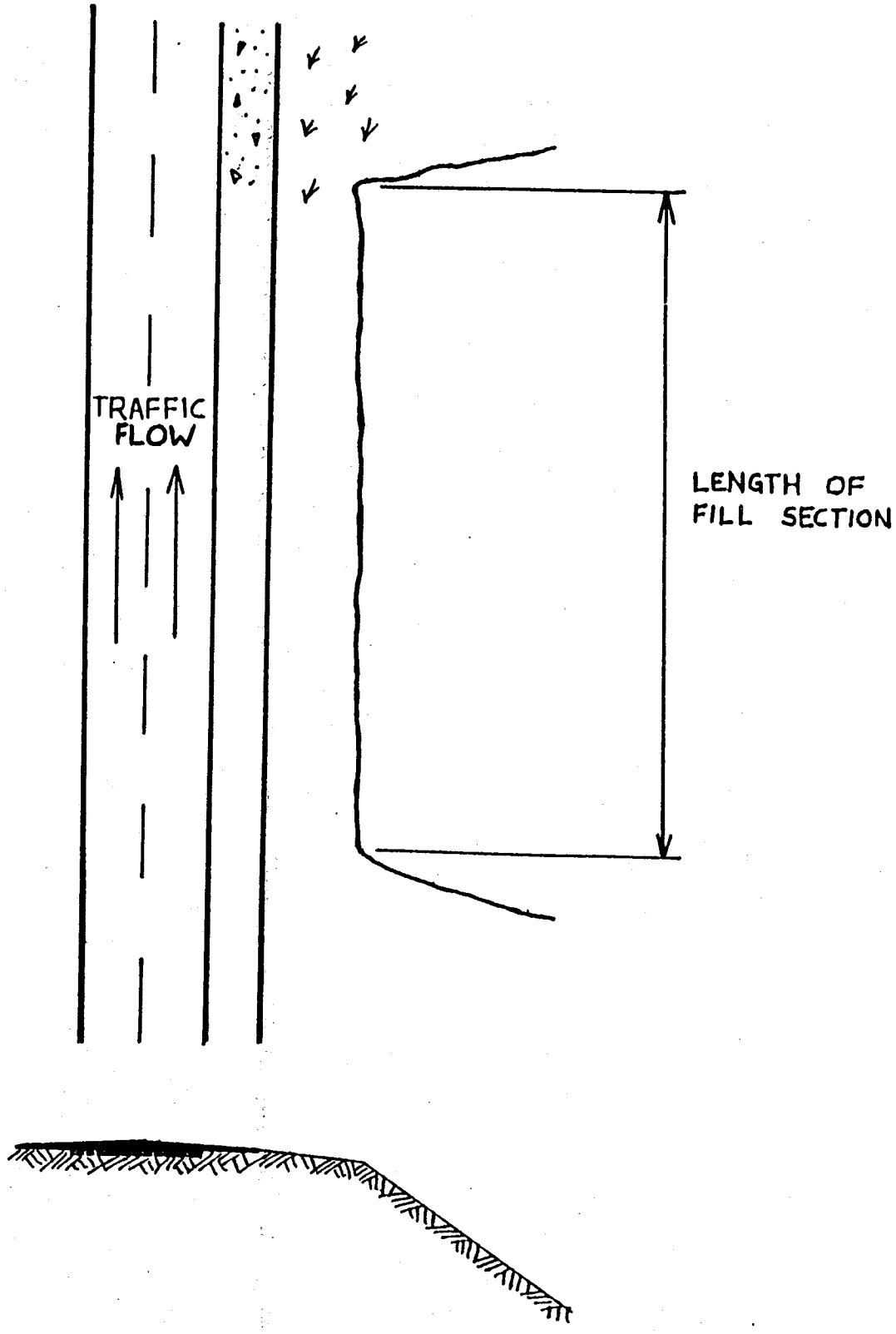

FIGURE 7. TYPICAL BARN ROOF FILL SECTION

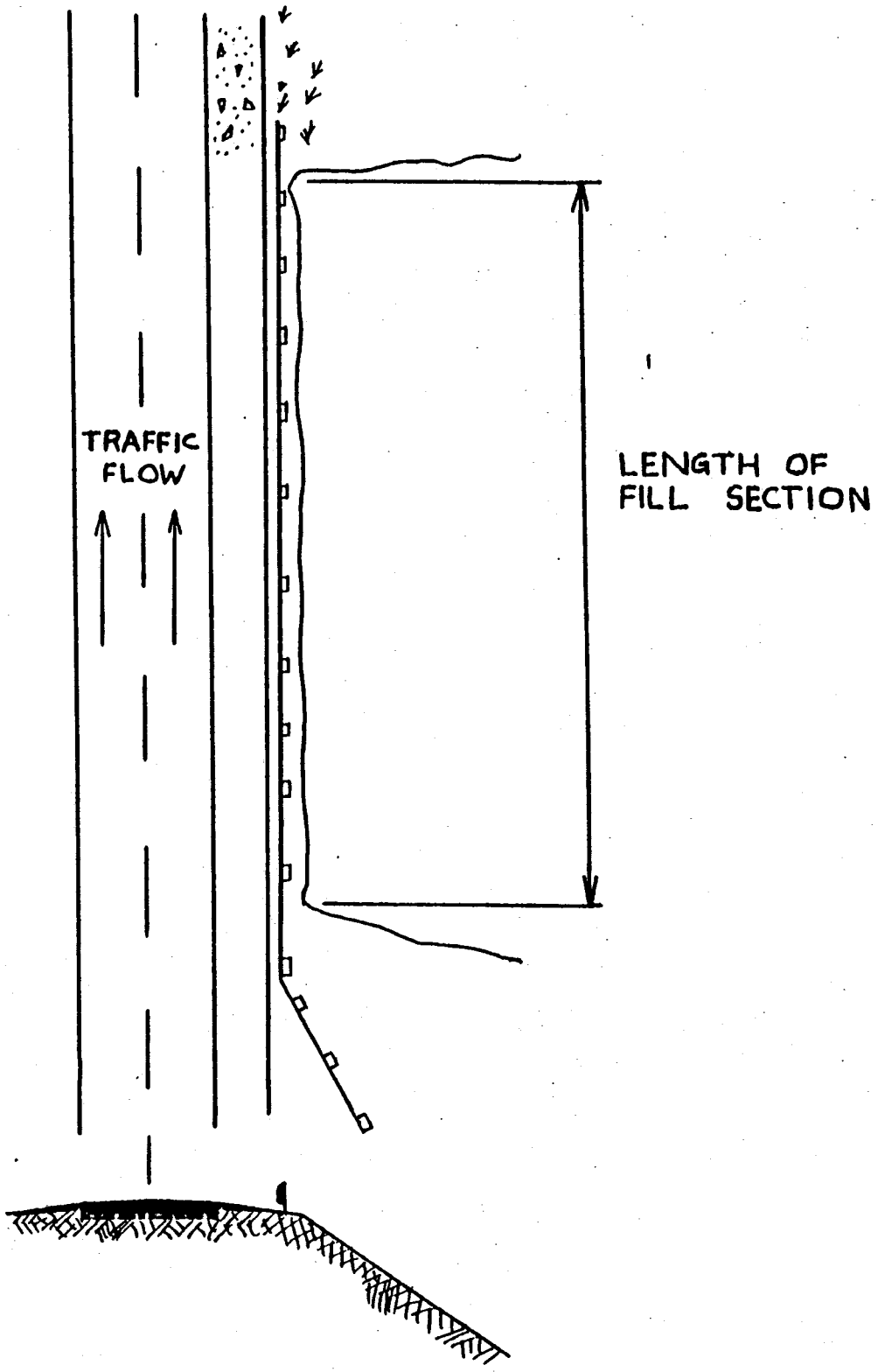

FIGURE 8. TYPICAL GUARDRAIL PLACEMENT ON FILL SECTION

Safety Alternative Costs

W-Beam Barrier	15 $/ft
Repair Costs	7.8 $/ft-kip (IS)
	(See Figure 6)
Performance Level	97 kip-ft
Cost of Additional Fill	5 $/yd (in place)

Accident Severity Indices

W-Beam Barrier

Impacts below PL Figure 5

Impacts above PL SI = 7.0

1.5:1 Slope SI = 0.133 x impact velocity (mph)

Additional input data sources and highway descriptors were assumed to be as follows:

Variable	Assumed Value or Source
Accident Costs	Table 3
Discount Rate	4%
Project Duration	20 years
Roadway Alignment	Straight, flat
Functional Highway Class	Freeway
Type of Highway	Four lane, divided
Encroachment Speeds and Angles	Table 2
Lateral Vehicle Movement	Figure 4

The benefit/cost model was then used to determine the relative benefits and costs for barrier protected and unprotected slopes with the slope

breakpoint offset 3, 15, 30, and 45 ft from the traveled way. The most cost beneficial alternative was determined for a wide variety of fill section lengths and traffic volumes. General guidelines for safety treatment of deep fill sections were then developed as shown in Figure 9.

Another application of the benefit/cost analysis algorithm described herein is in the study of special or new safety appurtenances and unusual sites. General guidelines, such as those shown in Figure 9, cannot be applied to all situations. Further, some safety appurtenances are designed for special sites that cannot be generalized. Highway engineers have expressed a need for a method of studying these special situations whenever they arise. Finally, this algorithm provides for the first time an objective method for determining optimum barrier flare rates and optimum barrier runout lengths in front of fixed hazards.

Limitations

As shown in the foregoing discussion, encroachment models have been developed to study accident frequencies of roadside hazards. These models are not designed to examine other types of accidents such as multiple vehicle accidents. Therefore, this technique cannot be used to study most safety treatments at intersections or to determine warrants for median barrier applications.

Another limitation of encroachment probability models is in the determination of accident severity based on predicted impact conditions. Accident severity is a very important factor in determining the total accident costs of a safety alternative. There is still only a tenuous link between impact conditions and accident severity. Further, accident severities of some hazards, such as dropoffs and roadside slopes, are very

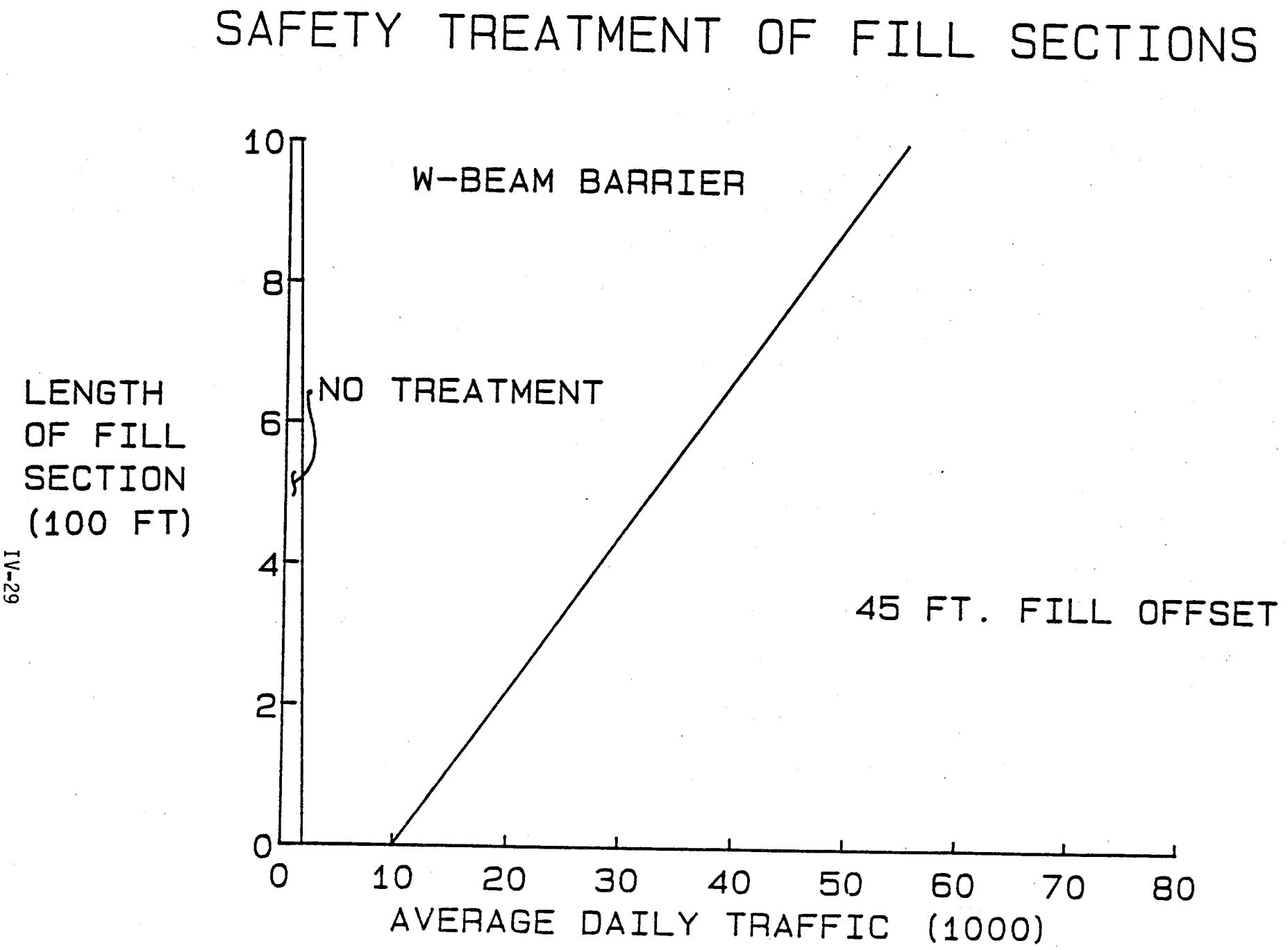

FIGURE 9. GUIDELINES FOR SAFETY TREATMENT OF FILL SECTION 20 FT DEEP

difficult to quantify. Thus, the model has a limited value in the analysis of problems in which the severity of potential accidents cannot be estimated.

Conclusions

The benefit/cost procedures described herein represent a significant improvement over existing procedures in the accuracy and versatility of analysis of the need for safety improvements. The technique is based on the best accident, encroachment, and impact severity information currently available. When better data become available, it should be incorporated into the procedures. The computer model can be used to develop general roadside safety appurtenance use guidelines. FHWA has adopted the model for developing barrier use guidelines for the update to the 1977 Barrier Guide.

Microcomputer versions of this program should allow practicing highway engineers to apply these procedures without the difficulty associated with most other methods. Therefore this benefit/cost model should allow more potential safety improvement projects to be analyzed in terms of the expected benefits and costs, thereby resulting in a more efficient application of available highway improvement dollars.

References

1. "Development of Design Criteria for Safer Luminaire Supports," NCHRP Report 77, 1969.
2. "AASHTO Guide for Selecting, Locating, and Designing Traffic Barriers," American Association of State Highway and Transportation Officials, 1977.
3. Calcote, L. R., "Development of a Cost-Effectiveness Model for Guardrail Selection," Final Report on DOT Contract No. FH-11-9927, Nov. 1977.
4. McCoy, P. T., Hsueh, R. T., and Post, E. R., "Methodology for Evaluation of Safety Improvement Alternatives for Utility Poles," Transportation Research Record 796, Transportation Research Board, 1981.
5. Ross, H. E., Jr., and Sicking, D. L., "Guidelines for Use of Temporary Barriers in Work Zones," Final Report on DOT Contract No. FH-11-9927, Nov. 1984.
6. Lampela, A. A. and Yang, A. H., "Analysis of Guardrail Accidents in Michigan," Michigan Department of State Highways and Transportation, Report TSD-243-74, July 1974.
7. Mak, King K. and Mason, Robert L., "Accident Analysis - Breakaway and Nonbreakaway Poles Including Sign and Light Standards Along Highways," Vol. II: Technical Report, Final Report on Contract DOT-HS-5-01266, Southwest Research Institute, Aug. 1980.
8. Perchonok, K., et al., "Hazardous Effects of Highway Features and Roadside Objects," Vol. 2, FHWA Report No. FHWA-RD-78-202, Sept. 1978.

9. Cooper, P., "Analysis of Roadside Encroachments - Single Vehicle Run-Off-Road Accident Data Analysis for Five Provinces," B.C. Research, Mar. 1980.

10. Hutchinson, J. W. and Kennedy, T. W., "Medians of Divided Highways - Frequency and Nature of Vehicle Encroachments," Engineering Experiment Station Bulletin 487, University of Illinois, June 1966.

11. Moskowitz, K. and Schaefer, W. E., "Barrier Report," California Highways and Public Works, Vol. 40, Nos. 9-10, Sept.-Oct. 1961.

12. McFarland, William F. and Rollins, J. B., "Cost-Effectiveness Techniques for Highway Safety," Final Report on Contract DTFH61-80-C-00080, Federal Highway Administration, Nov. 1982.

13. Wright, Paul H. and Robertson, Leon S., "Priorities for Roadside Hazard Modification: A Study of 300 Fatal Roadside Object Crashes," Institute of Transportation Engineers, Traffic Engineering, Vol. 46, No. 8, Aug. 1976.

14. Mak, K. K. and Calcote, L. R., "Accident Analysis of Highway Narrow Bridge Sites," Report No. FHWA-RD-82/140, Federal Highway Administration, Washington, D.C., 1983.

15. Michie, Jarvis D., "Recommended Procedures for the Safety Performance Evaluation of Highway Appurtenances," NCHRP Report 230, National Cooperative Highway Research Program, Transportation Research Board, 1981.

16. Bronstad, M. E. and Michie, J. D., "Multiple-Service-Level Highway Bridge Railing Selection Procedures," NCHRP Report 239, National Cooperative Highway Research Program, Transportation Research Board, 1981.

17. Ivey, D. L., Buth, C. E., et al., "Portable Barriers for Construction and Maintenance Zones -- Analysis and Re-Design of Current Systems," Interim Report of Tasks 1 and 2, Contract DOT-FH-11-9458, Texas Transportation Institute, Texas A&M University, July 1983.

18. Olson, R. M., et al., "Bridge Rail Design Factors, Trends, and Guidelines," NCHRP Report 149, 1974.